2023

Development of Holographic Recording Material for Fabrication of Solar Concentrators for Micro Satellites

Brian Rogers
Technological University Dublin, brian.rogers@tudublin.ie

Development of Holographic Recording Material for Fabrication of Solar Concentrators for Micro Satellites

Brian Rogers B.Sc

A thesis submitted for the degree of Doctor of Philosophy to

Technological University Dublin

Supervisors: Dr. Suzanne Martin, Prof. Izabela Naydenova

Centre for Industrial and Engineering Optics

School of Physics, Clinical and Optometric Sciences

Technological University Dublin

2023

Abstract

Holographic solar concentration has been a topic of increasing interest over recent years because of the lightweight and physically compact nature of holograms, which gives them an advantage over other, conventional concentration methods. As holographic recording materials develop further, their characteristics prove to meet the demands required of them to make more effective holographic solar concentrators. The development of photovoltaics in tandem with holographic materials has led to a host of solar concentrating device designs that take advantage of the unique properties of diffractive optics. Compared to refractive optics, holographic devices are more lightweight and compact. This makes holographic devices a good candidate for use in space based applications where weight reduction is a major cost saving measure.

This work presents the development of holographic recording materials for use in holographic solar concentrators. Improvements to materials refractive index modulation (RIM), the development of more environmentally robust recording materials, methods of improving stable performance of the recorded devices, and the characterisation of high RIM materials is presented in this work. In the initial phase of the work the RIM of an acrylamide based photopolymer was improved by 45 % to a value of 4.5×10^{-3} enabling a significant increase in angular working range for devices. Next, focussing on a material with the potential for use in an extreme environment, the RIM of an environmentally robust photosensitive sol gel was increased from 1.4×10^{-3} to 3.3×10^{-3}. Modelling of holographic gratings was then carried out to aid in practical holographic lens and holographic concentration device design. Holographic concentrators were tested in solar simulators with photovoltaic (PV) cells in order to

compare the performance of devices recorded in two high RIM materials, and to provide some insight into the nature of these devices in a practical environment.

This work has resulted in significant improvements to the RIM of photopolymer and sol gel materials have made them better candidates as holographic solar concentrators; the modelling, fabrication and testing of holographic lenses have given insights into the design choices surrounding holographic solar concentrators.

Declaration

I certify that this thesis which I now submit for examination for the award of **Doctor of Philosophy** is entirely my own work and has not been taken from the work of others, save and to the extent that such work has been cited and acknowledged within the text of my work.

This thesis was prepared according to the regulations for graduate study by research of Technological University Dublin and has not been submitted in whole or in part for another award in any other third level institution. The work reported on in this thesis conforms to the principles and requirements of the TU Dublin's guidelines for ethics in research.

TU Dublin has permission to keep, lend or copy this thesis in whole or in part, on condition that any such use of the material of the thesis be duly acknowledged.

Candidate: **Brian Rogers**

Signature _____ Date _____

Acknowledgments

First and foremost I would like to thank my supervisors Prof. Izabela Naydenova and Dr. Suzanne Martin for their support and guidance throughout my time with them.

I would also like say that it has been a pleasure to work with all the students and staff who have come and gone through the Centre for Industrial and Engineering Optics; an especially big thank you to Dr. Tatsiana Mikulchyk for all of the help and productive chats over the years.

I'm thankful for all the staff of the FOCAS Research Institute for providing the facilities that made this work possible.

Finally I would like to thank all my family and friends for their encouragement during my time in TU Dublin.

Table of Contents

Table of Figures

List of Tables

List of Abbreviations:

RIM – Refractive index modulation

PV – Photovoltaic

HOE – Holographic optical element

PVA – Polyvinyl alcohol

AA – Acrylamide

BA – N,N' methylenebisacrylamide

TEA – Triethanolamine

MDEA – Methyldiethanolamine

DMEA – Dimethylethanolamine

CAB - Cellulose acetate butyrate

MDTOA - 7-methylene-1,5-dithiacyclooctan-3-yl acetate

PETMP - Pentaerythritol tetrakis(3-mercaptopropionate)

Nomenclature/ Units:

l/mm – Lines per millimetre

Λ – Spatial period

λ - Wavelength

θ_1 – Incident beam 1

θ_2 – Incident beam 2

θ_s – Slant angle

θ_b – Bragg angle

η – Diffraction efficiency

ξ – Deviation from Bragg condition

V – Modulation parameter

k – Grating vector

T – Thickness

n_1 – Refractive index modulation

n_0 – Average refractive index

Q – The Q criterion

P – The Rho criterion

1 Introduction:

The changing economics of spaceflight has made it more available and affordable than ever before for public and private entities to endeavour on space missions. Costs of rocket launches have been slowly decreasing over time, with a recent sudden decline in costs with the introduction of reusable rockets (Figure 1-1).

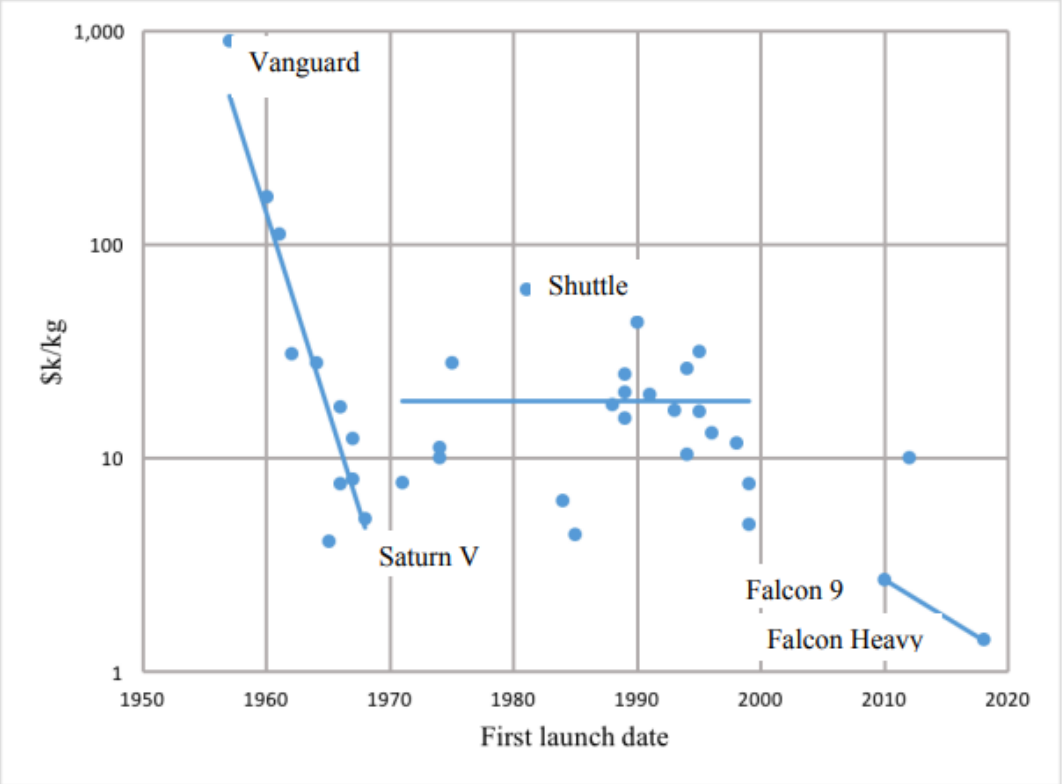

Figure 1-1: Rocket launch cost per kg over time [1]

The above figure shows that cost per kg for a payload has been significantly reduced since the birth of spaceflight, reaching as low as 1.4 thousand dollars per kg with the Falcon Heavy. [1]

Compounding this affordability is the microsatellite, a smaller and comparatively lightweight satellite (10-100 kg) [2], several of which may be launched to earth orbit

with a single rocket launch, with the record recently set in January 2021 by SpaceX of 143 satellites in a single launch.

Microsatellites vary greatly in their individual design and can rely on a host of methods to power their missions depending on their application [3]. Most microsatellites rely on PV cells for power; these cells can make up much of the available surface on the microsatellite (depending on design) reducing the space available for equipment or sensors on the satellite [4]. Improving PV cell efficiencies with a combination of new PV cell technologies and novel methods of solar concentration and solar tracking could reduce the required area needed for PV cells.

The earliest satellite missions relied on relatively low efficiency silicone solar cells with efficiencies in the region of 10-15 %. These were intended to power low energy devices in the range of 5 mW. Development of solar cell technology over time has increased efficiencies to the region of 30 % using triple junction gallium arsenide solar cells. This increase in efficiency coupled with the development of deployable solar cell arrays has made it possible for satellites to output in excess of 20 kW. [5]

Every microsatellite is different, specifically designed with a particular use/mission in mind with various degrees of complexity [6]. This complexity extends to their power generation systems, from PV cell type to solar tracking ability. This expands the range of possibilities for the development of solar concentrating technologies, from spectrum splitting holographic devices [7, 8], traditional reflective concentrators [9], to wavelength matched luminescent waveguides [10] to name but a few.

The work of this thesis focuses on the development of novel holographic solar concentrating methods and materials for space power; identifying desirable qualities for holographic solar concentrators, developing the required material properties to achieve

these qualities, recognising the technology's limitations and identifying possible solutions.

The following chapters identify several solar concentrating technologies designed for microsatellites, with a particular focus on holographic concentration. Holographic concentrators are lightweight, with high efficiency making them appropriate for use on microsatellites [11]. The next chapter will look at the presently available solar power and solar concentrating technologies for space and terrestrial applications as well as relevant recording materials and the theory behind holographic gratings.

1.1 Chapter Summary:

1. Project motivation/ introduction:

A brief description of the state of the aerospace industry and the developments in PV cell and solar concentrating technology.

2. Literature review:

An overview of the state of the art solar concentrating methods and solar tracking systems across multiple fields in the context of space based PV power. An introduction to various holographic methods used in solar concentrating and tracking systems is presented. An overview of the holographic recording materials available, examinations of their various mechanisms and properties. Their ability to perform well in the context of space based solar concentration is considered.

The fundamental theory behind the function of holographic gratings, their various classifications and the mathematics behind their function is explored.

3. Modelling:

Holographic gratings are modelled in the context of solar concentration. The conditions

required to minimise angular selectivity and maintain high diffraction efficiency are examined.

4. Photopolymer improvements:

Refractive index modulation and recording time improvements through chemical changes are quantified in an acrylamide based photopolymer.

5. Sol-gel:

Novel methods of recording, chemical changes and post processing techniques improve the refractive index modulation and recording time of a photosensitive sol gel material. Insights into the recording mechanism are inferred from characterisation of the material.

6. High RIM:

A high refractive index modulation photopolymer is characterised and a low angular selectivity lens is produced in this material. The lens is compared with a more angularly selective lens in a solar simulator.

7. Device proof of concept:

Preliminary work on a holographic chromatic dispersion correction device is presented and theoretical modelling of a concentrating device demonstrates its potential uses.

8. Conclusions:

A Summary of the work of the project, dissemination of work.

1.2 References:

[1] “The Recent Large Reduction in Space Launch Cost - NASA Technical Reports Server (NTRS).” *NASA*, NASA, https://ntrs.nasa.gov/citations/20200001093.

[2] Serra, Lluc Palerm, et al. “[PDF] Microsatellites and Microlaunchers: The Tandem That Will Disrupt the Satellite Industry: Semantic Scholar.” *[PDF] MICROSATELLITES AND MICROLAUNCHERS: THE TANDEM THAT WILL DISRUPT THE SATELLITE INDUSTRY | Semantic Scholar*, 1 Jan. 1970, https://www.semanticscholar.org/paper/MICROSATELLITES-AND-MICROLAUNCHERS%3A-THE-TANDEM-THAT-Serra-Barrera/4bb8d234f68354e54353d006b816e4127a3eb3dd.

[3] Zahl, Harold A., and Hans K. Ziegler. “Power Sources for Satellites and Space Vehicles.” *Solar Energy*, vol. 4, no. 1, 1960, pp. 32–38., https://doi.org/10.1016/0038-092x(60)90047-5.

[4] Tanaka, M., et al. “Microstrip Antenna with Solar Cells for Microsatellites.” *Electronics Letters*, vol. 31, no. 1, 1995, pp. 5–6., https://doi.org/10.1049/el:19950010.

[5] Work Performed under the Planetary Science Program Support Task “Solar Power Technologies for Future Planetary Science Missions” Strategic Missions and Advanced Concepts Office, Solar System Exploration Directorate, Jet Propulsion Laboratory, for Planetary Science Division, Science Mission Directorate, NASA, December 2017

[6] Robertus, Triharjanto. “System Designs of Microsatellites: A Review of Two Schools of Thoughts.” *Satellite Systems - Design, Modeling, Simulation and Analysis*, 2021, https://doi.org/10.5772/intechopen.92659.

[7] Darbe, Sunita, et al. “Simulation and Partial Prototyping of an Eight-Junction Holographic Spectrum-Splitting Photovoltaic Module.” *Energy Science & Engineering*, vol. 7, no. 6, 2019, pp. 2572–2584., https://doi.org/10.1002/ese3.445.

[8] Chrysler, Benjamin D., and Raymond K. Kostuk. “Volume Hologram Replication System for Spectrum-Splitting Photovoltaic Applications.” *Applied Optics*, vol. 57, no. 30, 2018, p. 8887., https://doi.org/10.1364/ao.57.008887.

[9] Warmann, Emily C., et al. “An Ultralight Concentrator Photovoltaic System for Space Solar Power Harvesting.” *Acta Astronautica*, vol. 170, 2020, pp. 443–451., https://doi.org/10.1016/j.actaastro.2019.12.032.

[10] Needell, David R., et al. “Ultralight Luminescent Solar Concentrators for Space Solar Power Systems.” *2019 IEEE 46th Photovoltaic Specialists Conference (PVSC)*, 2019, https://doi.org/10.1109/pvsc40753.2019.8981161.

[11] Collados, M. Victoria, et al. “Holographic Solar Energy Systems: The Role of Optical Elements.” *Renewable and Sustainable Energy Reviews*, vol. 59, 2016, pp. 130–140., https://doi.org/10.1016/j.rser.2015.12.260.

2 Literature Review:

In this chapter the state-of-the-art developments in holographic solar concentrators are reviewed. Improvements to modern solar cells, solar tracking technology and how holographic concentrators interact with these systems are examined.

The materials chosen to record holographic devices are examined; their qualities and suitability studied in the context of solar concentration.

Finally the theory behind holographic gratings is presented, and the theoretical limitations of certain gratings discussed.

2.1 Introduction:

One of the first applications of PV cell technology was in the aerospace industry, a solution to powering satellites out of reach in the depths of space. Since their inception, continual improvements to the efficiency of PV cells have been made. One of the technologies at the forefront of the industry is gallium arsenide based solar cells, boasting a wide range of spectral absorption.

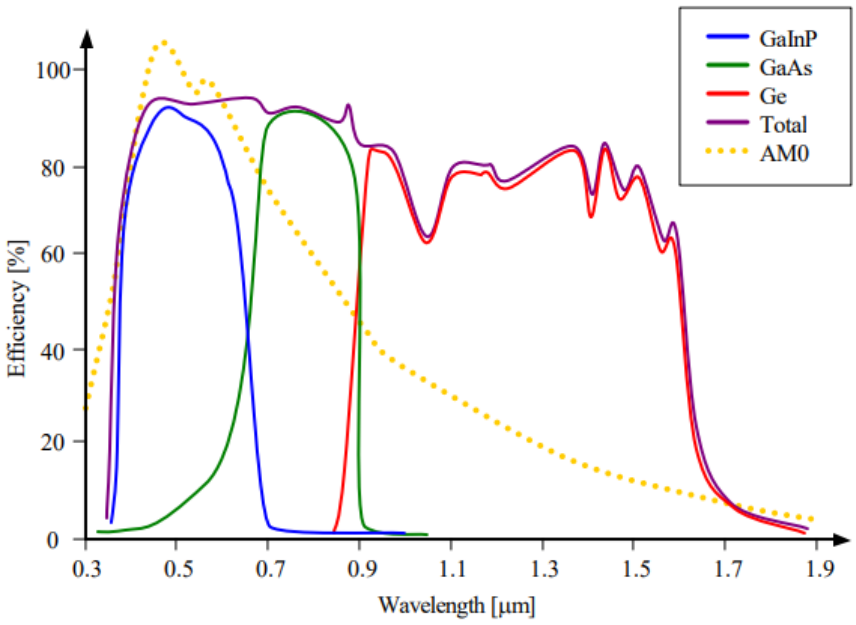

Figure 2-1: Example of triple junction solar cell absorption spectrum [1]

The example in *figure 2-1* shows the range of wavelengths these cells can efficiently absorb [1]. Knowing the absorption range can influence the design of holographic concentrators for these cells. Some designs take the wavelength selective nature of gallium arsenide cells and holograms, and turn it to their advantage, as shown in the figure below.

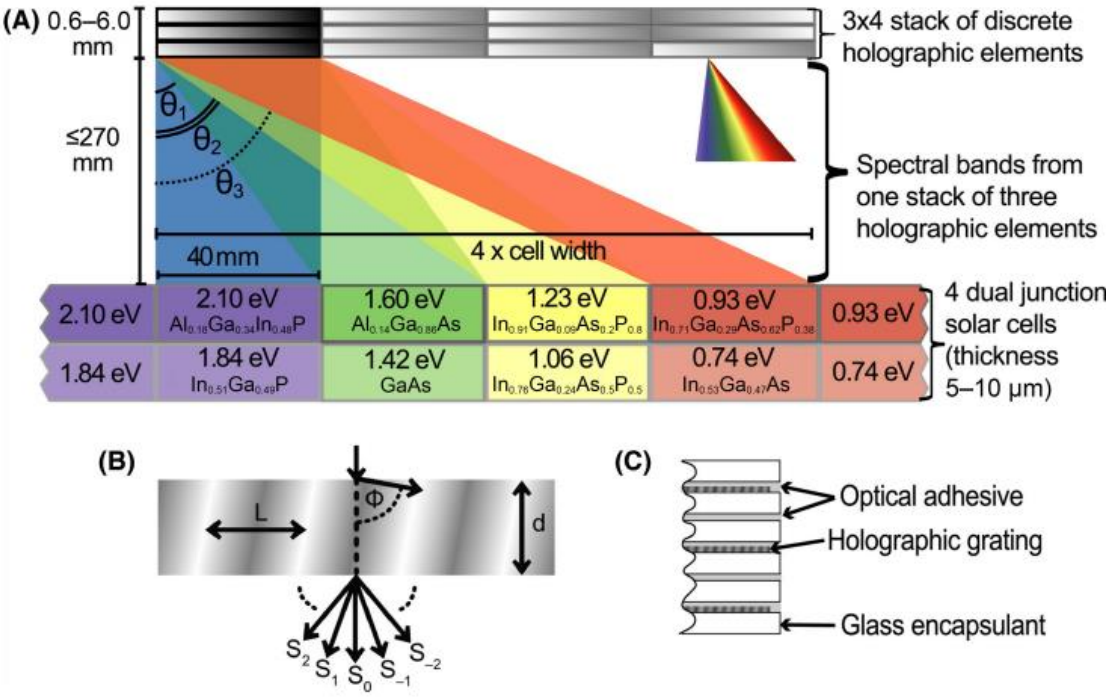

Figure 2-2: Holographic concentrator coupled with wavelength selective gallium arsenide cells [2]

This approach of stacked gratings in different positions introduces crosstalk problems, with some wavelengths of light not hitting their intended target. This is one of the many challenges of holographic solar concentration [2]. This is but one of many devices proposed to address the challenges associated with solar concentration on extra-terrestrial devices. This section will examine some of the solutions, holographic and otherwise, proposed to meet the requirements of space-based solar concentrators; namely lightweight, high efficiency and low angular selectivity devices.

Before examining the details of holographic concentration, devices and holographic solar tracking, alternate methods of solar capture are investigated with a focus on space-based applications.

2.2 Concentration methods:

Many methods of solar concentration can be employed to increase the intensity of sunlight such as traditional methods like mirrors and glass lenses, however employing these methods in extra-terrestrial applications can prove challenging.

2.2.1 Traditional solar concentrator:

Traditional concentrators such as Fresnel lenses, which one might consider for solar concentration, are not without their disadvantages. The sensitivity to thermal variations causing deformations to the lens or changes to the refractive index rendering the lens ineffective highlights the need for robust materials for extra-terrestrial applications. Temperature can vary in space with different severity depending on the orbit of the spacecraft and the dimensions of the spacecraft itself; any concentrator designed to work in these conditions should be designed with the specific mission of the satellite in mind. [3, 4]

Some designs utilise traditional concentrating methods such as concave mirrors to achieve high concentration ratios. Warmann et al present a lightweight solar concentrator which utilises a series of concave mirrors that act to concentrate light onto solar cells with reduced area. The materials proposed make the most of the reflected visible spectrum while also cooling the solar cells acting as a heat sink. The presented design suffers from being angularly selective and the reflective material still requires significant development before it can be used in such thin layers. [5]

2.2.2 Luminescent solar concentrators:

Typical luminescent solar concentrators operate by absorbing and downshifting photons which get trapped and directed to a PV cell through an optical waveguide. These concentrators have no angular selectivity and so can operate effectively at all angles of solar irradiance; however, losses at the surface due to Fresnel reflections affect device efficiencies. Needell et al detail a lightweight luminescent concentrator intended for use in space-based applications. The device's emission was wavelength matched to the absorption spectrum of Gallium arsenide based solar cells using a combination of luminescent materials. [6][7]

Luminescent solar concentrators face multiple challenges as device efficiency is reduced through multiple mechanisms. Emitted light can be outside the angular capture range of the waveguide, emitted light can be re-absorbed and incident light can go unabsorbed through the concentrator, to name a few [7]. Solutions to these losses are tackled in many ways, from the addition of wavelength selective mirrors to reduce top escape losses, [8] to up converting photon luminescence relying on mirrors instead of waveguides [9].

2.3 Holographic Solar tracking:

Many solar energy collection systems use solar trackers to maintain the highest possible efficiencies. These systems vary in complexity from single axis to dual axis tracking, using active, passive and chronological techniques and extend from terrestrial to space applications. [10] In the context of space applications and microsatellites there is no singular system which will work efficiently for every orbit and dimension of microsatellite, each mission will have its own specific conditions for which a solar tracking system will be specifically designed [11,12].

These tracking systems can be aided and simplified using holographic concentrators.

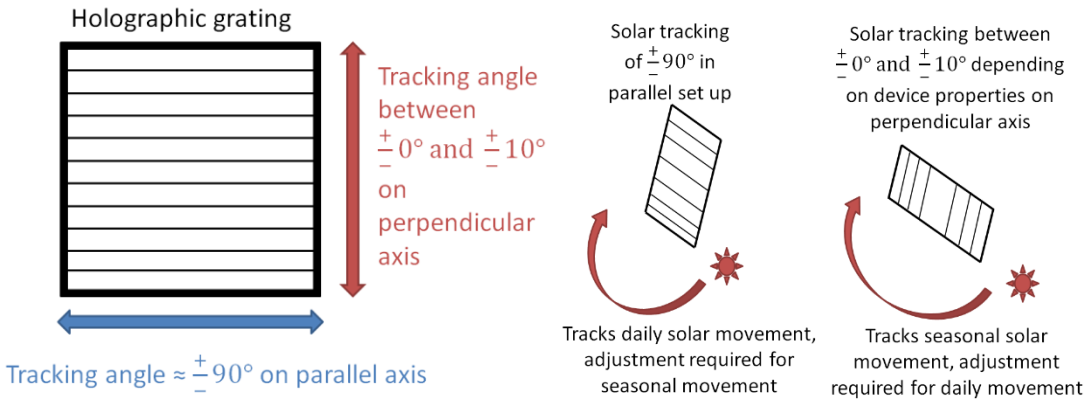

Figure 2-3:Illustration of holographic light tracking based on hologram orientation

Typical volume transmission holograms have an axis of high and an axis of low angular selectivity as shown in *figure 2-3.* This can be exploited for solar concentrating systems where they can effectively act as passive tracking systems [13].

2.4 Holographic Concentrating devices:

Holographic concentrators come in many forms and device configurations, with many taking advantage of the unique properties holograms have to offer. These various devices, their properties and uses as solar concentrators are investigated.

2.4.1 Non – concentrating holograms:

Non concentrating transmission holograms can be used to redirect light to a solar cell where it would otherwise not strike the cell. This system illustrates the importance of hologram orientation when considering its position in a solar collecting system seen in *figure 2-4.*

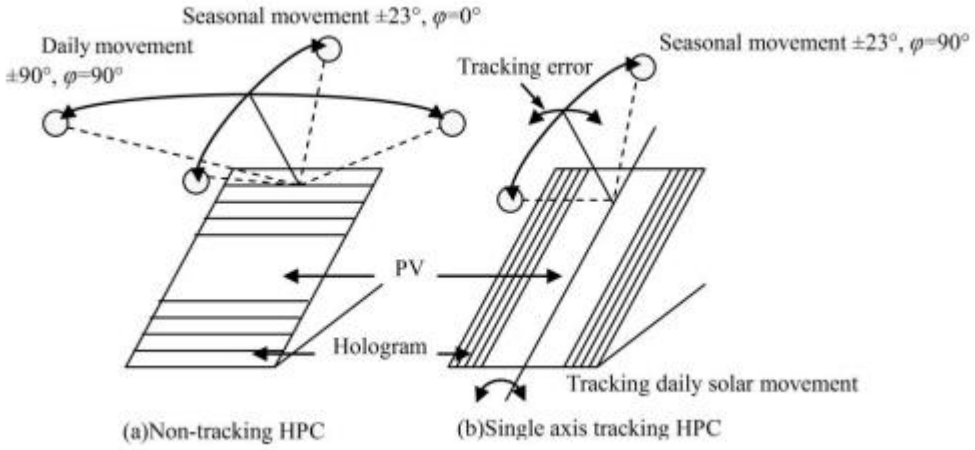

Figure 2-4:Solar tracking holographic device for solar concentration [13]

This system makes use of non-concentrating transmission holograms to redirect light to a solar cell. A smaller area solar cell is used but the amount of useful light falling on the cell remains the same as a larger cell with no redirecting holograms. This reduces costs by replacing the more costly solar cell with transmission holograms [13]. These systems come with some limitations. The axis of low angular selectivity can track the sun's daily movement and is able to concentrate light at all times of day. The recording axis (axis perpendicular to grating lines) however is much more angularly selective and so adjustments to the system must be made throughout the year to maximise efficiency. Minimising the angular selectivity on the recording axis is important as this will reduce the adjustments that need to be made for seasonal tracking of the sun. It will also reduce the precision required to put the hologram in line with the sun.

2.4.2 Single holographic concentrators:

This example uses a cylindrical holographic lens to concentrate light onto a solar cell, illustrated in *figure 2-5*.

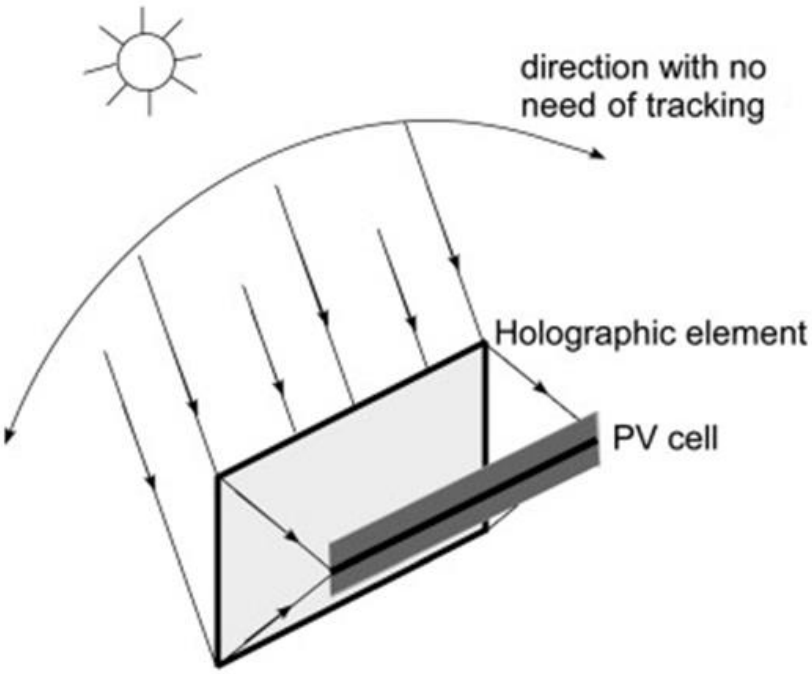

Figure 2-5:Building integrated holographic solar concentrator [14]

This device was made with building integration in mind and is designed to be installed along the building's sun facing walls. The axis of low angular selectivity is orientated in such a way that daily tracking of the sun is not required. [14]

2.4.3 Spectrum splitting devices:

As shown already with the holographic devices integrated with a series of gallium arsenide cells optimised for specific bandgaps, the chromatic dispersion associated with holograms can be exploited to optimise system efficiency [2]. These systems can take many shapes, one such system is presented by Benjamin et al that exploits the chromatic selectivity of holograms while also recording a holographic lens. *Figure 2-6* shows how the system concentrates relevant wavelengths to specific solar cells.

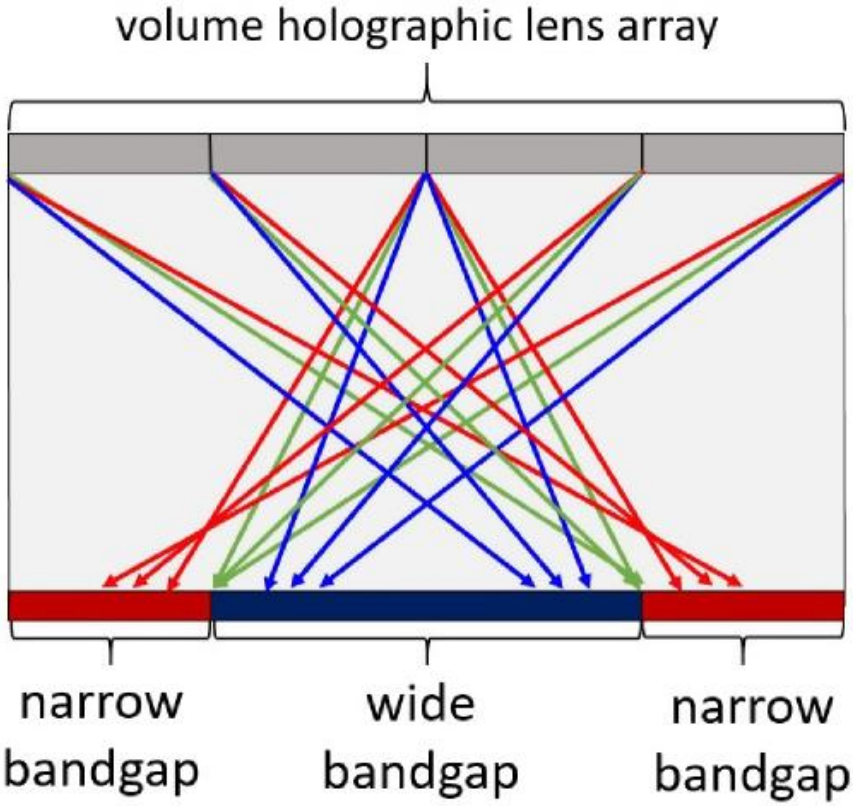

Figure 2-6: Chromatically selective solar concentrating system [15]

This system makes use of cylindrical lenses to concentrate light; each wavelength is diffracted at a different angle making it possible to concentrate the relevant wavelength onto a solar cell optimised for that bandgap. [15]

2.4.4 Stacked gratings:

Systems with multiple stacked holographic elements can also be used to increase the range of functional angles. This is illustrated in *figure 2-7*.

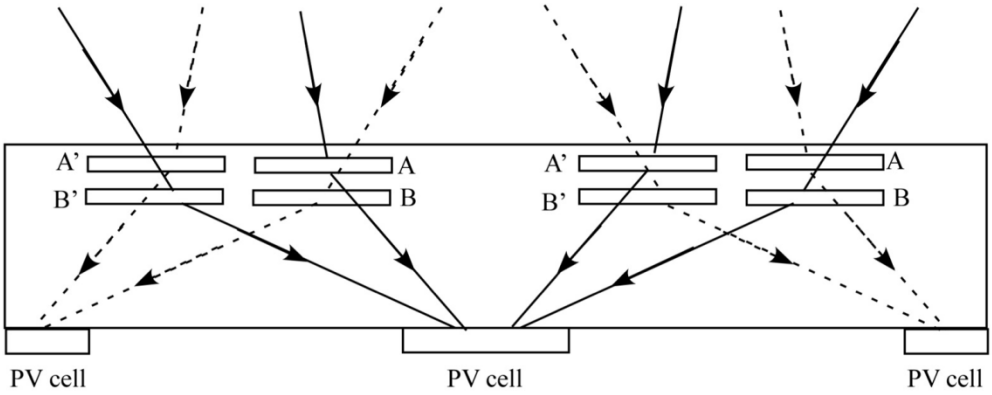

Figure 2-7: Stacked holographic gratings with decreased angular selectivity for solar concentration [16]

Here we see each layer of hologram diffracting most efficiently at different angles of incidence. Systems like this reduce the amount of solar tracking required. [16]

2.4.5 Multiplexing:

Some systems use multiplexed gratings where multiple holograms are recorded in the same volume of the layer. This can be exploited in solar concentration to produce devices with low angular selectivity in thicker layers. There are several methods to multiplex holograms. In angular multiplexing the angle between the two recording beams is fixed while the recording material is rotated relative to the beams [17].

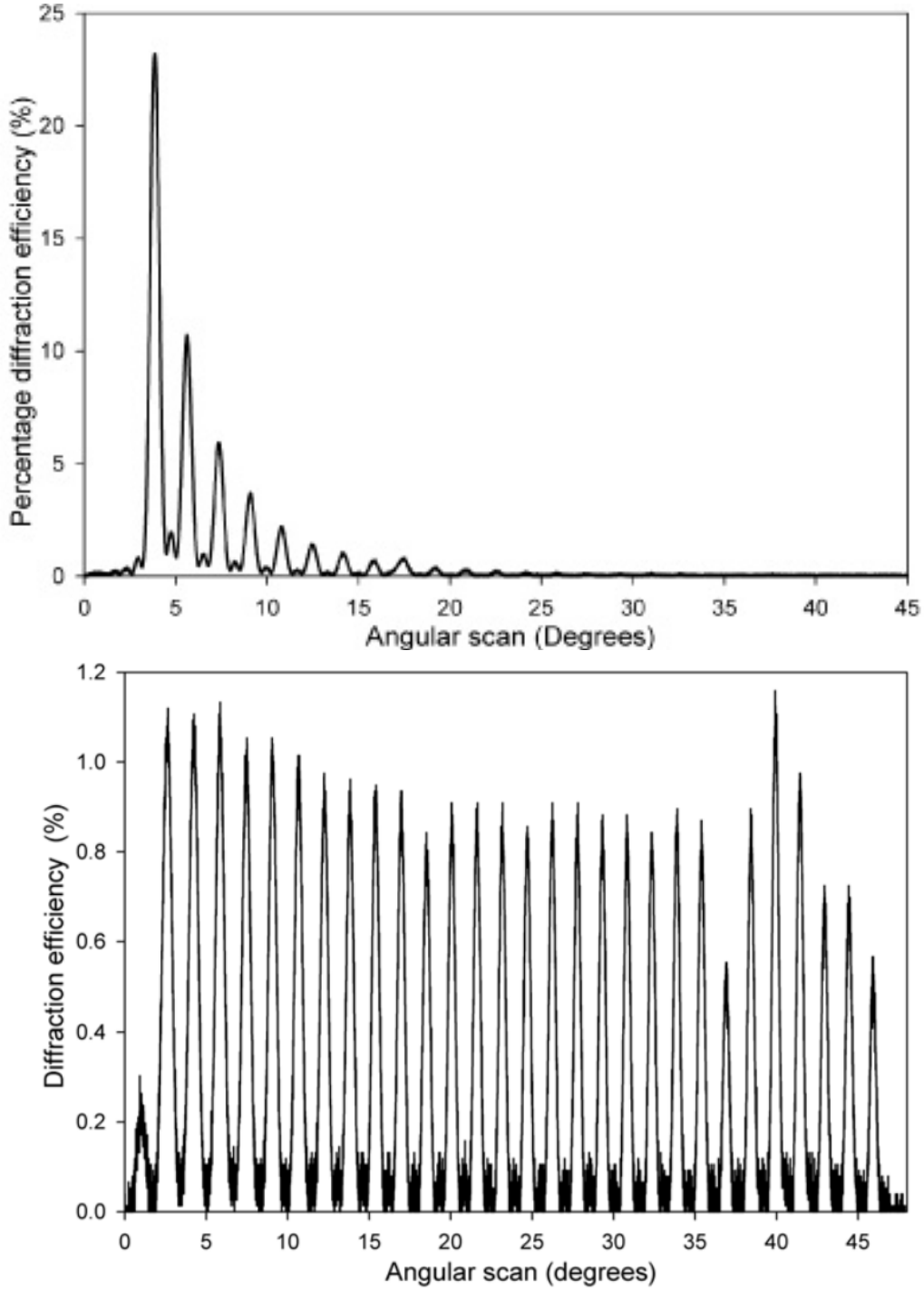

Figure 2-8: Dependence of diffraction efficiency response on probe angle and equalised diffraction efficiency in multiplexed gratings [17]

While solar collection is not the focus of this paper it is clear how the wider range of effective angles could potentially be used for solar concentrating systems without solar tracking. Spatial multiplexing involves recording multiple holograms across several spatial frequencies, changing the angles between the recording beams while keeping the

sample at a fixed position [18]. To make this method viable for solar concentration, the selection of specific spatial frequencies and tuning the exposure schedule for equalised diffraction efficiencies can make a low angular selectivity device with high diffraction efficiency. In this paper different exposure schedules are used to record the multiplexed gratings.

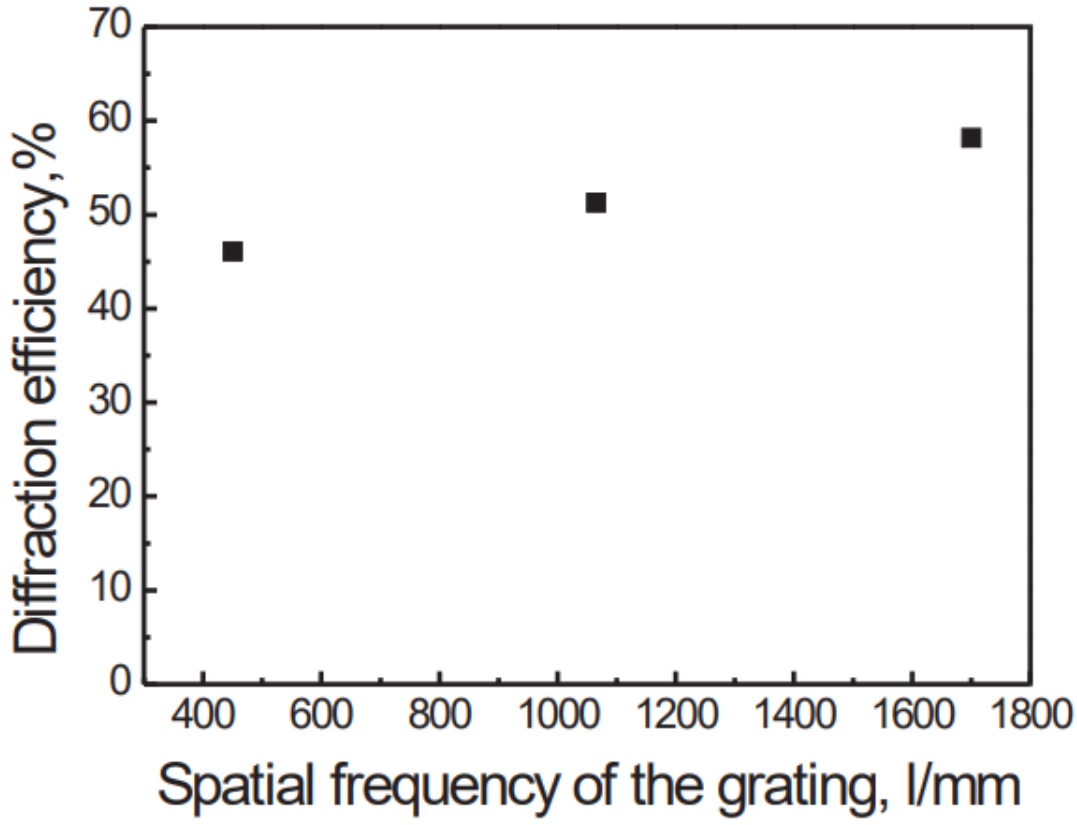

Figure 2-9: Diffraction efficiency of multiplexed device when probed at the Bragg angle of each recorded spatial frequency [19]

The photopolymer used in this paper was able to achieve diffraction efficiencies between 45 and 60% when using particular exposure energies for each spatial frequency [19].

2.4.6 Parallel gratings:

Another concentrating device is explored by Bianco et al. In this study, 3 holographic lenses were used, placed side by side, each operating across a separate set of angles in order to reduce the devices overall angular selectivity range. This device's large range of operational angles was intended to provide passive solar tracking as illustrated below [20].

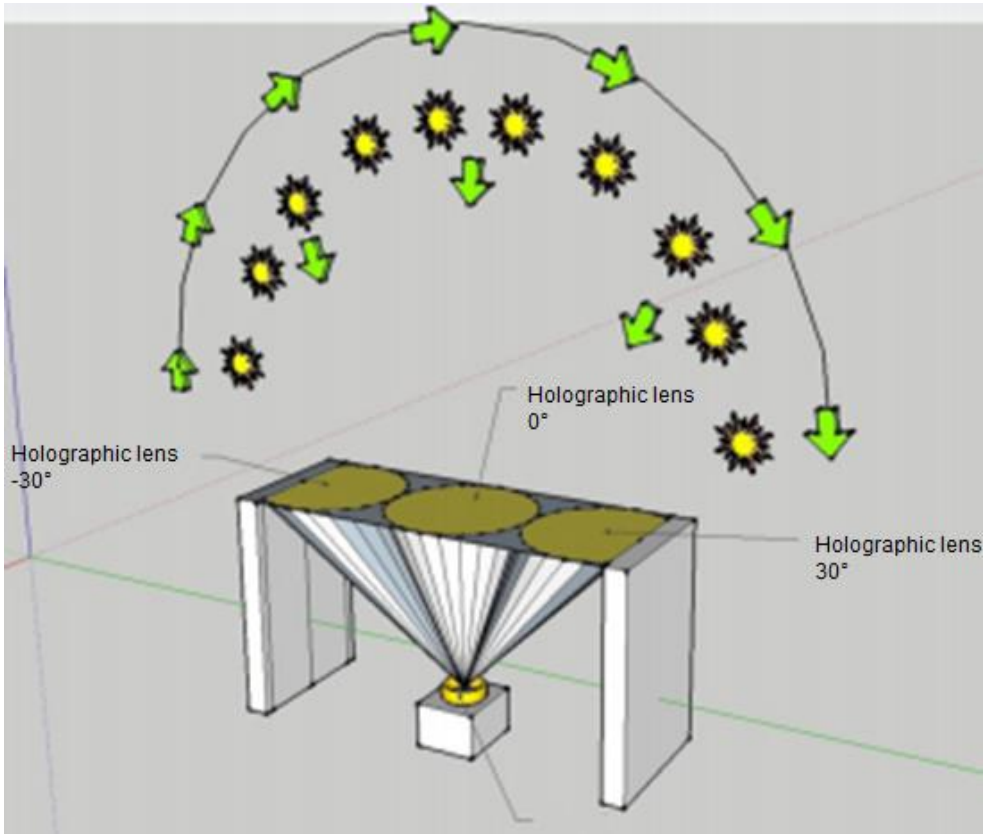

Figure 2-10: Illustration of solar concentrating device [20]

The properties of concentrating holograms will differ depending on the exact context of their use. The examples provided here show different methods and devices that can be used to concentrate solar energy; a variety of approaches can be taken depending on the demands of the device.

2.4.7 Device conclusion:

Following is a summary of the HOEs dealt with in this chapter.

Table 2-1: HOE device summary and potential adaptations and improvements for use in microsatellites.

Device	Summary	Potential Improvements for microsatellites
Non concentrating HOE	Reduce costs by replacing expensive PV cells with cheaper simple holographic transmission grating.	Greater angular selectivity to stop seasonal fall of in efficiency without solar tracking.
Cylindrical concentrator	Not angularly selective in one plane, can be tuned to be more or less wavelength selective depending on light tracking needs.	Using higher concentration ratios in the lens could be used for more compact devices.
Stacked HOEs	Multiple stacked HOEs can be used do enhance device functionality; this can be manipulated to decrease angular selectivity or increase wavelength selectivity depending on the device.	There is potential to remove the need for solar tracking with a limited number of devices by decreasing an individual HOE's angular selectivity.
Spectrum splitting device	Spectrum splitting devices can be used to focus particular wavelengths onto solar cells optimised for those wavelengths.	Incorporating reflection holograms can be used to remove any unwanted wavelengths from falling on solar cells.
Multiplexed device	Recording multiple holograms in a single volume can produce holographic devices capable of diffracting at high efficiencies at multiple probe angles.	A combination of multiplexed and stacked HOEs could be used to make a low angular selective and potentially wavelength filtering device.

A number of techniques are outlined here, each with their own unique qualities. Angular selectivity, concentration ratios and wavelength selectivity can be enhanced or reduced based on device design; and appropriate techniques can be selected for a given microsatellite, no single solution is necessarily best for solar concentration. Devices that use a single hologram have the advantage of taking up less space than their stacked or parallel grating counterparts, however improvements to these devices require material development. Stacked gratings can increase their efficiency and reduce selectivity by continually adding more gratings, however this solution requires more physical space which is not necessarily always available on microsatellites. A common feature to note between all devices is the importance of a low angular selectivity for the purpose of solar tracking.

The next section will examine the holographic recording materials that can be used to record these devices, their qualities examined under the lens of solar concentration applications.

2.5 Review of holographic recording materials

Numerous holographic recording materials exist, each with their own advantages and disadvantages. This section presents an overview of some materials and their properties.

2.5.1 Photopolymer:

Photopolymers have been explored for many applications as media for holographic recording [21]. As their improvement continues it is becoming clear that their properties are well suited to the development of a variety of different devices including holographic data storage [17], wavefront sensors [22], humidity, gas and temperature sensors [23-25], and as solar concentrating optics. [26].

Some of the advantageous properties of photopolymers include long shelf life, high diffraction efficiency and self-development. High refractive index modulation is an

important characteristic for many holographic devices, especially when optimising the diffraction efficiency of devices recorded in thinner layers. For example, holographic optical elements (HOEs) requiring a large angle of operation such as those designed for solar concentration and light dispersion. This is because reducing layer thickness increases angular acceptance [20]. In the opposite case, in holographic data storage applications, thicker devices are preferred since the high angular selectivity makes it possible to achieve higher data density [17].

There are many systems through which photopolymers achieve a refractive index modulation, presented here are some examples of these systems in different photopolymers.

Photopolymers have several chemical components that work in tandem allowing it to react with light. It works by polymerising a monomer in areas of high light intensity. This polymerisation causes a localised change in refractive index. This reaction is achieved through a multi-step system involving several components. The key components are a monomer, initiator, dye, plasticiser and binder. The process begins with the dye absorbing a photon and transferring to an excited state. The excited state dye will react with an initiator molecule, changing it to a free radical. The free radical initiator will then react with a monomer, forming a monomer radical. The monomer radical will react with more monomer molecules causing a chain reaction. As the monomer polymerises in areas of high light intensity denser polymer chains are formed and their refractivity is changed, thus locally changing the refractive index. In addition, a monomer concentration gradient is created. This drives diffusion of monomer molecules from areas of high monomer concentration (low light intensity) to low monomer concentration (high light intensity). This mass transport causes additional

change in refractive index across the photopolymer which allows diffraction to occur. This process is visualised in the figure below.

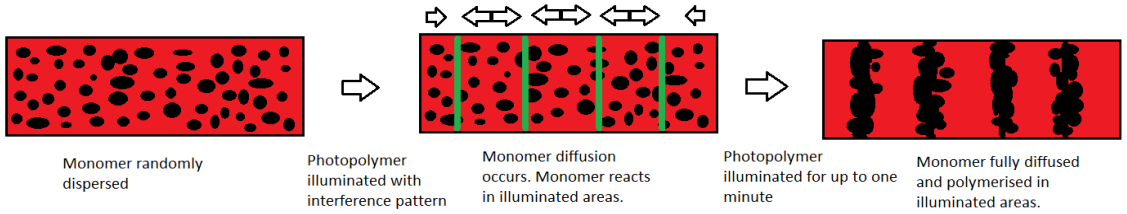

Figure 2-11: Polymerisation of photopolymer during holographic recording.

In highly permeable photopolymer systems [27] a third process has been observed – a diffusion of mobile oligomers from areas illuminated by high intensity to low intensity areas. This process has a negative effect on the final refractive index modulation and causes limited diffraction efficiency at very high spatial frequency of recording. The initiating/sensitising system facilitating the photopolymerisation process has been a subject of much study [28]

Multiple methods of materials' sensitisation and initiation of polymerisation reaction exist. Systems involving the interaction of a dye molecule with an initiator in order to produce a free radical capable of interacting with a monomer are an example of one such system [29, 30]. Some molecules can act as both dye and initiator which can change reaction rates between initiator and monomer [31]. The rate of fabrication of HOEs is an important factor when considering the mass production of photopolymer based holographic devices. Higher production rates and lower costs are some of the main advantages of faster initiation and recording. Altering the initiator system can have an effect on the recording time. It has been previously observed that different initiators are capable of changing the bleaching rate of photopolymers implying different reaction rates [30]. Guoqiang et al. found that methyldiethanolamine (MDEA) had the fastest

bleaching time of a number of initiators, among TEA and 1,4-Diazabicyclo[2.2.2]octane (DABCO). In dye sensitised photopolymers based on free radical chain polymerisation, the creation of a free radical is often a process relying on the interaction of at least two molecules, the absorbing dye and the initiator. Thus the size of these molecules is expected to be important factor in the rate of radical generation.

A photopolymer material developed by Covestro offers a similar reaction mechanism with the main difference being the formation of the photopolymer matrix. This material is commercially available. The matrix is formed through a thermal process where matrix precursors are cross linked [32].

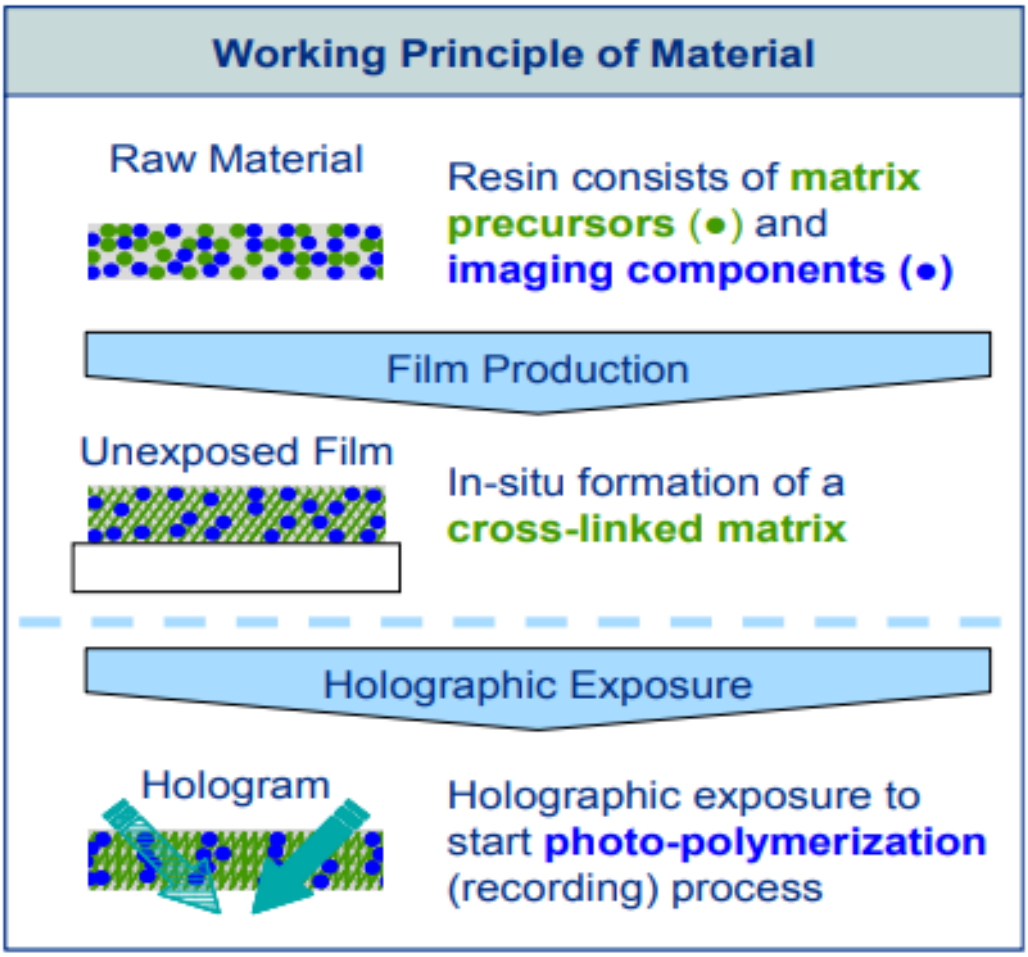

Figure 2-12: Recording mechanism of Covestros photopolymer [32]

After the formation of the matrix, the holographic recording process is the same as the process outlined already.

Another photopolymer system is cationic ring opening photopolymer; this reaction uses a sensitising dye to interact with an acid generator producing a proton. This proton will further react with cyclic monomers, opening them and linking them in a polymer chain. This photopolymer material offers low shrinkage, and has been suggested as suitable for holographic data storage [33], but low shrinkage is also an attractive feature for applications such as wavefront sensing [22] where precise reconstruction of a wavefront is useful.

Some photopolymers have the advantage of needing no post processing after recording. This means the grating formation can be monitored in real time, allowing for fine tuning of the recording process for each device. However, other photopolymer materials rely on thermal post treatment processes that can improve refractive index modulation. Although this can be a disadvantage it is also possible, with knowledge of the average RIM achieved in these materials, to design devices such as solar concentrators by fine tuning the thickness and spatial frequency so that a certain diffraction efficiency value will be met.

Depending on the photopolymer used, the refractive index modulation can range from 0.002-0.034. [32] [34]

2.5.2 Silver halide emulsions:

Silver halide was a popular choice of recording material in the past for holography and was the subject of much study. They continue to produce high quality visual reflection holograms; however they have largely been replaced by self-processing materials.

The chief mechanism of recording in silver halide involves the conversion of silver halide grains to silver through light exposure. A post process removes the unconverted silver halide grains leaving only the converted silver behind to form a holographic recording. One of the main advantages silver halide offers is its large refractive index modulation in the order of 0.02. This large refractive index modulation makes it possible to achieve low angular selective holograms with large diffraction efficiencies. The post processing makes it impossible to monitor in real time and precise device formation can be difficult. Silver halide for holography has a long history and is summarised well in this book [35].

2.5.3 Dichromated gelatine:

The formation of holograms in dichromated gel involves the oxidation of Cr^{6+} to Cr^{3+} through a multistep process requiring light exposure. The Cr^{3+} will interact with gelatine molecules and thus cross linking them. This cross linking hardens the gelatine, creating the refractive index modulation with values up to 0.08. Unfortunately, two wet processes are required before and after light exposure making it a time-consuming process. When considering the similar refractive index modulation to photopolymer dichromated gelatine is a poor choice for a holographic concentrator as it has the added burden of the wet processes. [35, 36]

2.5.4 Sol gel:

Sol-gel chemistry is a well-developed synthetic approach to fabricating new functional materials for applications in diverse areas such as medicine, pharmacy, mechanics, electronics, chemistry and others [37][38].

Photsensitive sol-gels are materials used for holographic recording. Synthesised using sol-gel chemistry, they have high optical quality, low scatter, and scratch and water resistance. Sol-gel can be permanently optically patterned (thousands of lines/mm)

using a relatively low intensity light source (typically a few mW/cm^2). This material has the potential to provide a holographic recording material with improved dimensional stability, robustness and capacity for making layers with thickness in the range from tens to hundreds of micrometres [39**,** 40].

One subsection of photosensitive sol-gel represents a water–resistant photopolymerisable hybrid organic-inorganic sol-gel which belongs to Class II hybrid materials according to the classification proposed in [41]. These materials have covalent bonds between the organic and the inorganic species and provides improved dimensional stability and robustness. Dry photosensitive sol-gel layers achieved after thermal curing represent a xerogel consisting of nanoparticles made from MAPTMS with pores filled with transition metal inorganic complexes ((MAA:ZPO):ZCO) [42]. These nanoparticles are further cross-linked by APTES ((3-Aminopropyl)triethoxysilane). The stability of the xerogel, its robustness, and the fine control over the pour size gives the photosensitive sol-gel some distinct advantages over traditional photopolymer materials. Class II sol gels report a refractive index modulation in the order of 0.003 [43].

Class one materials use an inorganic sol gel matrix as a binder for their reactive organic components. The stability of the sol gel, its robustness, and the fine control over the pour size gives class one materials some distinct advantages over traditional photopolymer. Typically, the chemical reactions involved in this class of material are van der Waals, hydrogen and ionic reactions [39]. Some materials of this class report a refractive index modulation as high as 0.015 [40].

2.5.5 Photopolymerisation mechanism in class II materials:

In the following section the photopolymerisation mechanism in class II sol-gel is described since this material was a subject of further investigations and improvement of

this thesis. The photopolymerisation mechanism for holographic patterning of the photosensitive sol-gel Class II is based on a free radical polymerisation process as follows. (1) Initiation: Under laser-irradiation, the photoinitiator molecule (Irgacure 784) dissociates into free radicals that initiate further free radicals on the methacrylate groups (MAPTMS and MAA). (2) Propagation: The radicals produced on the methacrylate groups undergo polymerisation with neighboring methacrylate groups, leading to the formation of rigidly structured nanoparticle-based species in illuminated areas and as a result a local change in the refractive index. If the illuminating light is appropriately patterned this will lead to the creation of a diffraction grating. (3) Termination: A recombination reaction between two activated methacrylate groups (radicals) stops the polymerisation process [42, 43].

2.5.6 Materials conclusion:

Table 2-2:Table of parameters:

	Physically Robust/ environmentally stable	RIM	No Chemical Post Processing	High Dynamic range
Photopolymer	☒	0.03	☑	☑
Silver Halide Emulsions	☑	0.02	☒	☑
Dichromated Gelatine	☒	0.08	☒	☑
Sol Gel (class 2)	☑	0.003	☑	☑

Improvements to holographic recording materials have enabled the design and fabrication of a number of light redirecting devices, including solar concentrators for PV cells [44]. *Figure 2-13* illustrates the key improvements to materials and device

characteristics that could lead to improved qualities in holographic solar concentrating devices.

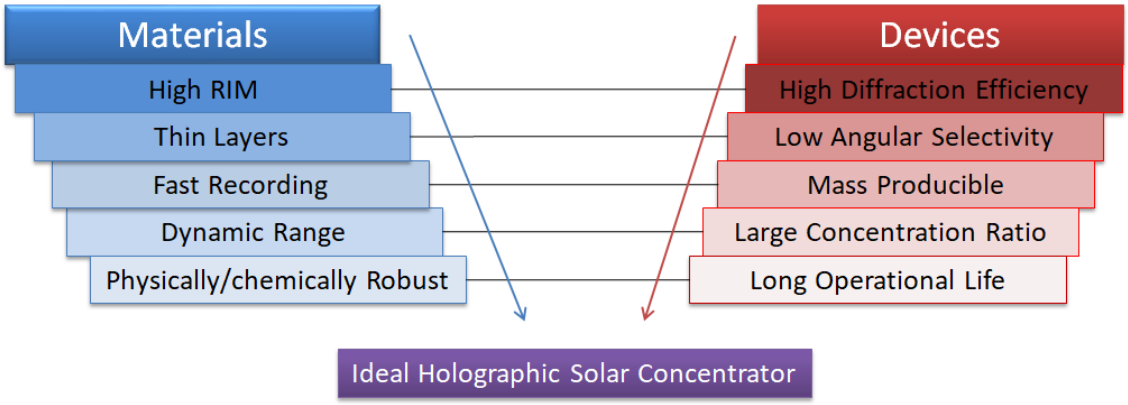

Figure 2-13: Material properties and corresponding device characteristics

An ideal holographic concentrator should be able to operate at a wide range of angles at close to 100 % efficiency. Improving the value of RIM to higher values will enable thinner, less angularly selective devices with high efficiencies.

This work will explore various techniques of chemically and physically manipulating holographic recording materials as well as the characterisation of novel materials with the aim of producing positive characteristics in the scope of holographic concentration.

In order to further understand what qualities are important for solar concentrators a breakdown of the fundamental principles of holograms and diffraction gratings is required. The next section looks at the basic theory of holography, classification of gratings, their limitations and the mathematics behind their function.

2.6 Basics of holography:

The simplest holograms are created by recording the interference pattern made by two planar wavefronts. The interference pattern will induce local physical changes in the recording material creating a difference in the material properties between areas where

constructive and destructive interference have occurred. In phase holograms this takes the form of a refractive index modulation. Once an interference pattern is recorded, a diffractive structure results and a single wavefront matching one of the two wavefronts used at the recording stage will be able to reconstruct the other. *Figure 2-14* illustrates a scenario in which two wavefronts with identical wavelengths (λ) interfere within a recording material. Each wavefront approaches the normal of the material at different angles (θ_1, θ_2) for the purpose of illustrating grating slant (θ_s), where the angle of the interference fringes is not perpendicular to the normal of the material. These fringes extend through the volume of the material at a thickness (*T*) and with spacing (Λ).

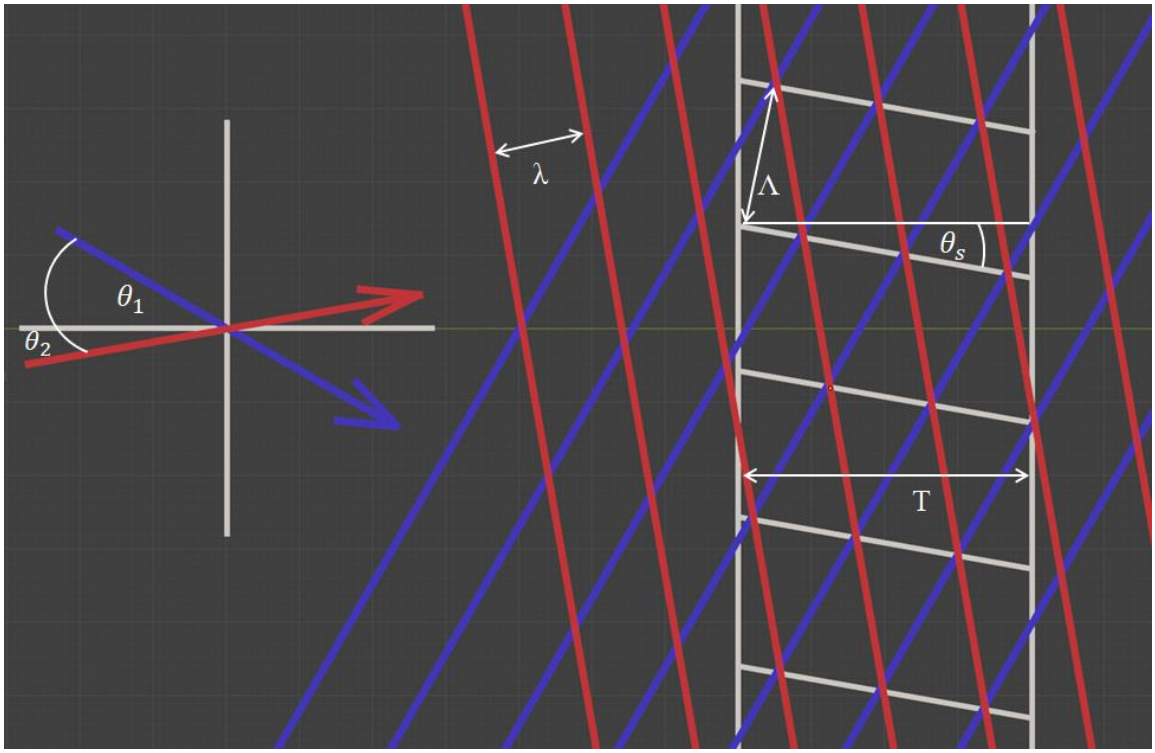

Figure 2-14: Illustration of the interference pattern generated by the interaction of two planer wavefronts inside a recording material.

There are several criteria that must be met for successful holographic reconstruction, however these conditions are dependent on the type of hologram being recorded of which there are several.

2.6.1. Plane (thin) holograms:

One of the first holograms a physics student is likely to encounter is the thin hologram. A more precise definition will be introduced later, but for now a thin hologram can be seen as one where constructive interference of the diffracted beam occurs at multiple angles. This is illustrated below where a planar wavefront approaches a thin holographic grating. When the wave encounters the grating it can be considered to be creating several point sources at a fixed distance apart (that of the fringe spacing Λ). As the wave spreads from these point sources they will constructively interfere at some angles.

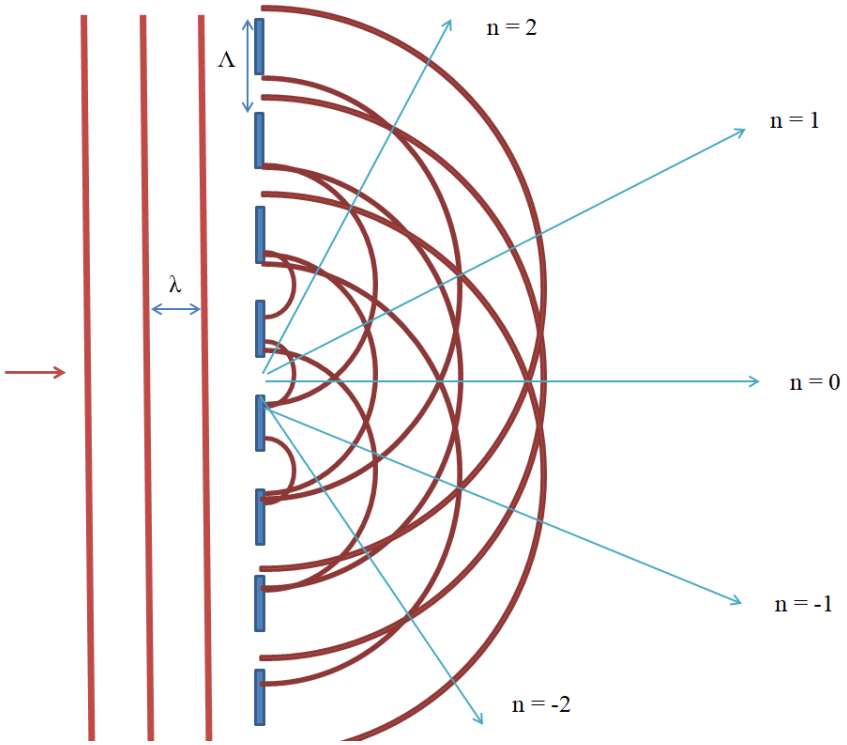

Figure 2-15: Illustration of a plane holographic grating.

The condition for constructive interference is given by equation 2.1.

$$n\lambda = \Lambda \sin\theta \quad (2.1)$$

Where λ is the wavelength of light, Λ is the fringe spacing, θ is the angle at which constructive interference occurs, and n is the diffraction order. The diffraction order is an integer number designating the paths of constructive interference. [45, 46].

2.6.2 Volume (thick) holograms:

A thick hologram is one in which only a single diffraction order exists and a theoretical diffraction efficiency of 100% is possible. Diffraction efficiency is the efficiency at which a diffraction grating converts the energy of the reference beam to the object beam. A representation of a thick holographic grating is shown in the following figure. An arbitrary slant is introduced to the fringes.

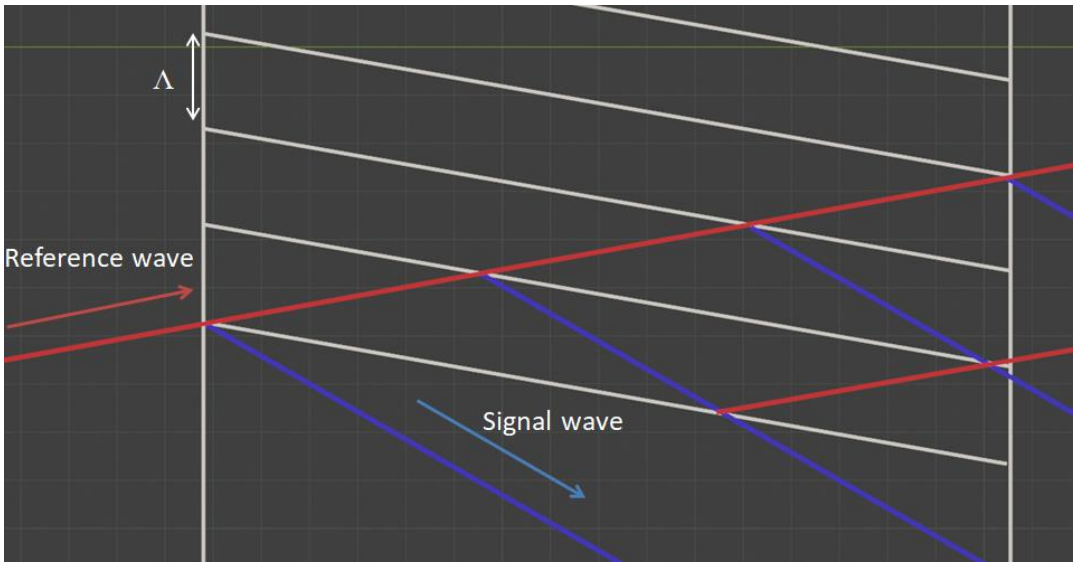

Figure 2-16: Illustration of a reference wave passing through a volume hologram and being converted to a signal wave.

When probed at the correct angle (Bragg angle) the reference wave will be partially converted to the signal wave as it passes through each fringe. The signal wave must be in phase with the other converted signal waves and so that constructive interference can occur between each wave [47].

2.6.3 Reflection holograms:

Reflection holograms can be seen in many common items such as bank notes and identification cards. The reference and signal wave are both on a single side of the hologram. *Figure 2-16* illustrates a reference wave being converted to a signal wave as it passes through the grating.

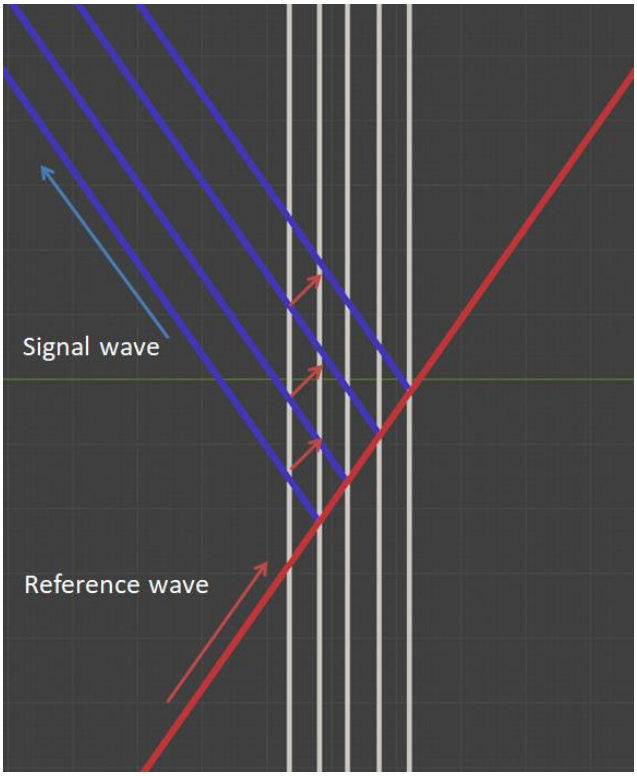

Figure 2-17: Illustration of a reference wave being converted to a signal wave in a reflection hologram.

2.6.4 Coupled wave theory – Fulfilling the Bragg condition

Volume holograms will be the main focus of study in this work as they can diffract 100 % of light in a single direction, and can mimic traditional refractive lens devices, unlike thin and reflection holograms.

For a volume hologram to efficiently diffract a number of conditions must be met. These conditions depend on both the properties of the hologram itself and the light probing it.

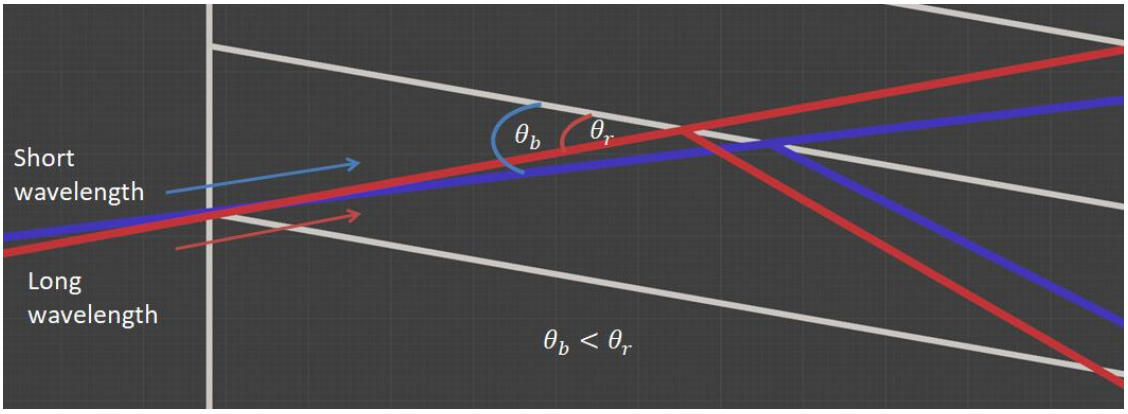

Figure 2-18: Volume hologram probed at the Bragg angle for 2 different wavelengths.

The above figure shows a short and long wavelength propagating through a volume hologram at their respective Bragg angles. The nature of how these beams propagate with respect to each other is dependent on the properties of the hologram.

Returning to *figure 2-14*, the spatial frequency (f) of a hologram is the number of fringes that fit within a certain distance and is typically given in lines per mm. It is the inverse of the spatial period (Λ).

$$f = \frac{\sin\theta_1 - \sin\theta_2}{\lambda} \quad (2.2)$$

Where f is the spatial frequency of the hologram, θ_1 and θ_2 are angles relative to the normal of the recording plane (orientation of the recording material relative to the interference wavefronts) and λ is the wavelength of the recording beam. If θ_1 and θ_2 are not of equal value with opposite signs then the hologram will have a slant $\theta_s$which can be found by calculating the bisector of θ_1 and θ_2. [47]

Looking at equation 2.2, the angles required to reproduce a fixed spatial frequency at different wavelengths can be calculated. This is illustrated in *figure 2-18* and shows the spatial separation of different wavelengths for a particular hologram. This situation shows two wavelengths probing a hologram at their respective Bragg angle. Kogelnik's

equations show how the reconstructed beam is affected by a change in probe angle at a fixed wavelength and a change in wavelength with a fixed probe angle. [47]

The diffraction efficiency η of a volume hologram can be found using equation 2.3.

$$\eta = \left[\frac{Sin(V^2 + \xi^2)^{\frac{1}{2}}}{\left(1 + \frac{\xi^2}{V^2}\right)^{\frac{1}{2}}} \right]^2 \quad (2.3)$$

V is an on Bragg parameter that determines the diffraction efficiency based on the properties of the hologram and the probing light. ξ is a term that quantifies the deviation from the Bragg condition; it does this for both an angular deviation and wavelength deviation. [47]

V represents the phase modulation caused by a periodic modulation of refractive index at the Bragg angle θ_b. Assuming the Bragg condition is met, a phase modulation of $\frac{\pi}{2}$ will give a diffraction efficiency of 100 %, further modulation would cause the object beam to couple back into the reference beam (an effect called over-modulation) and thus reduce the on-Bragg efficiency of the hologram. For an unslanted grating:

$$V = \frac{\pi n_1 T}{\lambda \cos\theta_b} \quad (2.4)$$

Where λ is the wavelength of the light diffracted by the grating, n_1 is the refractive index modulation; a measure of the change in refractive index across the fringes of the hologram, T is the thickness of the hologram and $\theta_b$is the Bragg angle. [47]

ξ represents the factor by which deviation from the Bragg angle affects diffraction efficiency. Where $\Delta\theta$ is the deviation from the Bragg angle. k is the grating vector and is equal to $\frac{2\pi}{\Lambda}$. Λ is the spatial period and T is the grating thickness. Deviating from the

Bragg angle changes the path of the light as it travels through the volume of the material such that the condition for constructive interference may no longer be met. When considering a fixed spatial frequency, thicker volumes exaggerate this effect leading to highly angularly selective holograms; whereas thinner holograms have fewer boundaries at which this phase difference can accumulate and so are less angularly selective. The deviation from the perfect matching conditions, ξ due to angular deviation is given by:

$$\xi = \Delta\theta \frac{kT}{2} \quad (2.5)$$

ξ is also used to describe the chromatic selectivity expressed through wavelength deviation from a central wavelength at the Bragg angle.

$$\xi = \frac{\Delta\lambda k^2 T}{8\pi n_0 \cos\theta_B} (2.6)$$

Where $\Delta\lambda$ is the wavelength deviation, n_0 is the average refractive index and θ_B is the Bragg angle.

This term ξ for the Bragg mismatch introduced by angular and wavelength deviation is related to diffraction efficiency through equation 2.3. ξ effectively measures the phase deviation that occurs when the Bragg condition is not met, one is at a fixed wavelength where a change in angle introduces the deviation. The other is at a fixed angle where a change in the wavelength introduces the deviation. [47, 48]

When probed at the Bragg angle ξ equation 2.3 is reduced to zero and the equation becomes:

$$\eta = Sin^2 \left[\frac{\pi n_1 T}{\lambda \cos\theta_b}\right] \quad (2.7)$$

The required refractive index modulation for a hologram given a thickness T and diffraction efficiency η at a particular wavelength λ when probed at the Bragg angle is given in equation 2.7. If a diffraction efficiency close to 100% is to be achieved while simultaneously reducing the thickness of the hologram there must be an increase in the refractive index modulation.

With this picture of volume holographic gratings in mind it is important to consider the conditions required for a hologram to be in the volume regime, as opposed to the thin regime. For this we consider two factors.

2.6.5 Volume regime:

Holograms operate as volume holograms when the Q parameter [49] is >10. Q is given by equation 2.8.

$$Q = \frac{2\pi\lambda T}{n_0 \Lambda^2} \quad (2.8)$$

Q is dependent on the wavelength of the probing beam λ, the hologram thickness T, the average refractive index of the material n_0 and the square of the period of the grating Λ. The Q factor is a convenient term to use practically, as it is a quick way to determine an appropriate thickness to remain in the Bragg regime for a specific spatial frequency. However, it can break down for certain values of V (equation 2.4) ($V > 3$). The Q parameter is applicable in cases when the refractive index modulation is relatively low. When the refractive index modulation is large the a different criterion is more appropriate – the Rho factor [49].The Rho factor determines the regime of operation of a hologram based on the spatial period and refractive index modulation of the hologram shown in equation 2.9.

$$\rho = \frac{\lambda^2}{\Lambda^2 n_0 n_1} \quad (2.9)$$

Values of Rho equal to or greater than 10 indicate that a hologram is operating in the volume regime. Its value is given by the spatial period Λ, the refractive index modulation n_1, at a wavelength λ and an average refractive index n_0

The Rho factor is a more appropriate description of the boundary between the Raman-Nath and Bragg regime in the cases when the refractive index modulation is large. Using it practically in the same way as Q described above would require modelling of the grating using Kogelnik's coupled wave theory; a more accurate description but less simple to use as more steps are required to calculate RIM [49].

2.6.6 Conclusion:

The theory discussed in this section can be used to calculate the limits of the operational regimes of holographic lenses, as well as their angular selectivity and diffraction efficiency. This information is crucial in the development of a well optimised holographic concentrator; quantities such as angular selectivity can be minimised given material properties such as RIM.

The mathematics of the fundamental function of holograms allows for the changing and optimisation of individual qualities to steer holographic devices towards more effective concentrators. The next section models holographic gratings using the mathematics outlined in this chapter. The variables that effect angular selectivity and diffraction efficiency are examined, and the qualities needed from recording materials to make effective concentrators determined.

2.7 References:

[1] Ge/GaAs/InGaP Triple-Junction Solar Cells for Space Exploration Sanat Pandey Department of Electrical and Computer Engineering University of Illinois at Urbana-Champaign, Urbana, IL 61801, USA (Completed 21st April 2019)

[2] Darbe, Sunita, et al. “Simulation and Partial Prototyping of an Eight-Junction Holographic Spectrum-Splitting Photovoltaic Module.” *Energy Science & Engineering*, vol. 7, no. 6, 2019, pp. 2572–2584., https://doi.org/10.1002/ese3.445.

[3] Papež, Nikola, et al. “Overview of the Current State of Gallium Arsenide-Based Solar Cells.” *Materials*, vol. 14, no. 11, 2021, p. 3075., https://doi.org/10.3390/ma14113075.

[4] K. Janzer, et al. “Influence of Orbit and Thermal Design Parameters on the Temperature Behaviour of CubeSats – Implications for Thermal Analysis and Thermal Hardware Demands” ICES, 2020

[5] Warmann, Emily C., et al. “An Ultralight Concentrator Photovoltaic System for Space Solar Power Harvesting.” *Acta Astronautica*, vol. 170, 2020, pp. 443–451., https://doi.org/10.1016/j.actaastro.2019.12.032.

[6] Needell, David R., et al. “Ultralight Luminescent Solar Concentrators for Space Solar Power Systems.” *2019 IEEE 46th Photovoltaic Specialists Conference (PVSC)*, 2019, https://doi.org/10.1109/pvsc40753.2019.8981161.

[7] Debije, Michael G., and Paul P. Verbunt. “Thirty Years of Luminescent Solar Concentrator Research: Solar Energy for the Built Environment.” *Advanced Energy Materials*, vol. 2, no. 1, 2011, pp. 12–35., https://doi.org/10.1002/aenm.201100554.

[8] Sark, Wilfried G.J.H.M., et al. “Luminescent Solar Concentrators - a Review of Recent Results.” *Optics Express*, vol. 16, no. 26, 2008, p. 21773., https://doi.org/10.1364/oe.16.021773.

[9] Van Sark, Wilfried GJHM, et al. “Upconversion in Solar Cells.” *Nanoscale Research Letters*, vol. 8, no. 1, 2013, https://doi.org/10.1186/1556-276x-8-81.

[10] Singh, Amit Pratap, and Indresh Yadav. “A Review on the Axis Tracking Used for Solar PV Application.” *IOP Conference Series: Materials Science and Engineering*, vol. 1116, no. 1, 2021, p. 012063., https://doi.org/10.1088/1757-899x/1116/1/012063.

[11] Zhang, Keke, et al. “A Two-Dimensional Solar Tracking Stationary Guidance Method Based on Feature-Based Time Series.” *Mathematical Problems in Engineering*, vol. 2018, 2018, pp. 1–12., https://doi.org/10.1155/2018/3420649.

[12] Poulek, V, and M Libra. “A Very Simple Solar Tracker for Space and Terrestrial Applications.” *Solar Energy Materials and Solar Cells*, vol. 60, no. 2, 2000, pp. 99–103., https://doi.org/10.1016/s0927-0248(99)00071-9.

[13] Zhang, Deming. “One-Axis Tracking Holographic Planar Concentrator Systems.” *Journal of Photonics for Energy*, vol. 1, no. 1, 2011, p. 015505., https://doi.org/10.1117/1.3590943.

[14] Chemisana, Daniel, et al. “Holographic Lenses for Building Integrated Concentrating Photovoltaics.” *Applied Energy*, vol. 110, 2013, pp. 227–235., https://doi.org/10.1016/j.apenergy.2013.04.049.

[15] Chrysler, Benjamin D., and Raymond K. Kostuk. “Volume Hologram Replication System for Spectrum-Splitting Photovoltaic Applications.” *Applied Optics*, vol. 57, no. 30, 2018, p. 8887., https://doi.org/10.1364/ao.57.008887.

[16] Collados, M. Victoria, et al. “Holographic Solar Energy Systems: The Role of Optical Elements.” *Renewable and Sustainable Energy Reviews*, vol. 59, 2016, pp. 130–140., https://doi.org/10.1016/j.rser.2015.12.260.

[17] Sherif, Hosam, et al. “Characterization of an Acrylamide-Based Photopolymer for Data Storage Utilizing Holographic Angular Multiplexing.” *Journal of Optics A: Pure and Applied Optics*, vol. 7, no. 5, 2005, pp. 255–260., https://doi.org/10.1088/1464-4258/7/5/007.

[18] Lee, Jeong-Hyeon, et al. “Holographic Solar Energy Concentrator Using Angular Multiplexed and Iterative Recording Method.” *IEEE Photonics Journal*, vol. 8, no. 6, 2016, pp. 1–11., https://doi.org/10.1109/jphot.2016.2634699.

[19] Naydenova, Izabela, et al. “Photopolymer Holographic Optical Elements for Application in Solar Energy Concentrators.” *Holography - Basic Principles and Contemporary Applications*, 2013, https://doi.org/10.5772/55109.

[20] Bianco, G., et al. “Photopolymer-Based Volume Holographic Optical Elements: Design and Possible Applications.” *Journal of the European Optical Society: Rapid Publications*, vol. 10, 2015, https://doi.org/10.2971/jeos.2015.15057.

[21] David Jurbergs, Friedrich-Karl Bruder, Francois Deuber, Thomas Fäcke, Rainer Hagen, Dennis Hönel, Thomas Rölle, Marc-Stephan Weiser, Andy Volkov, "New recording materials for the holographic industry," 2009 Proc. SPIE 7233, Practical Holography XXIII: Materials and Applications, 72330K

[22] Branigan, Emma, et al. “Direct Multiplexing of Low Order Aberration Modes in a Photopolymer-Based Holographic Element for Analog Holographic Wavefront Sensing.” *Environmental Effects on Light Propagation and Adaptive Systems IV*, 2021, https://doi.org/10.1117/12.2599912.

[23] Mikulchyk, Tatsiana, et al. “Investigation of the Sensitivity to Humidity of an Acrylamide-Based Photopolymer Containing N-Phenylglycine as a Photoinitiator.”

Optical Materials, vol. 37, 2014, pp. 810–815., https://doi.org/10.1016/j.optmat.2014.09.012.

[24] Yetisen, Ali K., et al. "Photonic Hydrogel Sensors." *Biotechnology Advances*, vol. 34, no. 3, 2016, pp. 250–271., https://doi.org/10.1016/j.biotechadv.2015.10.005.

[25] Mikulchyk, Tatsiana, et al. "N-Isopropylacrylamide-Based Photopolymer for Holographic Recording of Thermosensitive Transmission and Reflection Gratings." *Applied Optics*, vol. 56, no. 22, 2017, p. 6348., https://doi.org/10.1364/ao.56.006348.

[26] Collados, M. Victoria, et al. "Holographic Solar Energy Systems: The Role of Optical Elements." *Renewable and Sustainable Energy Reviews*, vol. 59, 2016, pp. 130–140., https://doi.org/10.1016/j.rser.2015.12.260

[27] Naydenova, I., et al. "Holographic recording in nanoparticle-doped photopolymer" *SPIE Proceedings*, 2006, https://doi.org/10.1117/12.676503.

[28] Martin S, Leclere P, Renotte Y, Toal V, Lion Y. "Characterization of an Acrylamide-Based Dry Photopolymer Holographic Recording Material." *Optical Engineering*, vol. 33, no. 12, 1994, p. 3942., https://doi.org/10.1117/12.186423.

[29] Zhao, Guoqiang, et al. "The Effect of Three Electron Donors on the Initiator System Efficiency of Photopolymer Film Photosensitized by Methylene Blue." *Materials & Design*, vol. 120, 2017, pp. 186–192., https://doi.org/10.1016/j.matdes.2017.01.093.

[30] Gong Q, Wang S, Huang M, Dong Y, Gan F. "Effects of dyes and initiators on the holographic data storage properties of photopolymer" Proceedings Volume 5966,

Seventh International Symposium on Optical Storage Zhanjiang, China, Proc. SPIE, 5966, 59660P 2005

[31] Ortuño, M., et al. “Pyrromethene Dye and Non-Redox Initiator System in a Hydrophilic Binder Photopolymer.” *Optical Materials*, vol. 30, no. 2, 2007, pp. 227–230., https://doi.org/10.1016/j.optmat.2006.10.029.

[32] Bruder, Friedrich-Karl, et al. “The Chemistry and Physics of Bayfol® HX Film Holographic Photopolymer.” *Polymers*, vol. 9, no. 12, 2017, p. 472., https://doi.org/10.3390/polym9100472.

[33] Waldman, David A., et al. “Crop Holographic Storage Media for Optical Data Storage Greater than 100 Bits/Mm2.” *SPIE Proceedings*, 2003, https://doi.org/10.1117/12.513614.

[34] Galli, Paola, et al. “Cyclic Allylic Sulfide Based Photopolymer for Holographic Recording Showing High Refractive Index Modulation.” *Journal of Polymer Science*, vol. 59, no. 13, 2021, pp. 1399–1413., https://doi.org/10.1002/pol.20210192.

[35] Silver-Halide Recording Materials H. I. Bjelkhagen Topics in Applied Physics, vol 20. "Holographic Recording Materials" ed H. M. Smith

[36] Chang, B. J., and C. D. Leonard. “Dichromated Gelatin for the Fabrication of Holographic Optical Elements.” *Applied Optics*, vol. 18, no. 14, 1979, p. 2407., https://doi.org/10.1364/ao.18.002407.

[37] Corriu, R.; N. T. Anh.; *Molecular chemistry of sol-gel derived nanomaterials*. Wiley 2009.

[38] Levy, D.; Zayat, M.; *The Sol-Gel Handbook*, Wiley-VCH 2015, Weinheim, Germany.

[39] Carretero, L., et al. “Acrylamide-N,n'-Methylenebisacrylamide Silica Glass Holographic Recording Material.” *Optics Express*, vol. 12, no. 8, 2004, p. 1780., https://doi.org/10.1364/opex.12.001780.

[40] Schnoes, Melinda G., et al. “Photopolymer-Filled Nanoporous Glass as a Dimensionally Stable Holographic Recording Medium.” *Optics Letters*, vol. 24, no. 10, 1999, p. 658., https://doi.org/10.1364/ol.24.000658.

[41] Gomez-Romero, P.; Sanchez, C.; Functional hybrid Materials, WILEY-VCH 2004.

[42] Mikulchyk, Tatsiana, et al. “Synthesis of Fast Curing, Water-Resistant and Photopolymerisable Glass for Recording of Holographic Structures by One- and Two-Photon Lithography.” *Advanced Optical Materials*, vol. 10, no. 6, 2022, p. 2102089., https://doi.org/10.1002/adom.202102089.

[43] Mikulchyk, Tatsiana, et al. “Characterisation of Holographic Recording in Environmentally Stable Photopolymerisable Glass.” *Applied Sciences*, vol. 12, no. 12, 2022, p. 5969., https://doi.org/10.3390/app12125969.

[44] Collados, M. Victoria, et al. “Holographic Solar Energy Systems: The Role of Optical Elements.” *Renewable and Sustainable Energy Reviews*, vol. 59, 2016, pp. 130–140., https://doi.org/10.1016/j.rser.2015.12.260.

[45] Knight, RD *Physics for scientists and engineers a strategic approach with modern physics* third edition page 709 Pearson, 2014. England.

[46] Magnusson, R., and T. K. Gaylord. “Diffraction Efficiencies of Thin Phase Gratings with Arbitrary Grating Shape.” *Journal of the Optical Society of America*, vol. 68, no. 6, 1978, p. 806., https://doi.org/10.1364/josa.68.000806

[47] Hariharan, P. *Basics of Holography*. Cambridge University Press, 2002.

[48] KOGELNIK, HERWIG. “Coupled Wave Theory for Thick Hologram Gratings.” *Landmark Papers on Photorefractive Nonlinear Optics*, 1995, pp. 133–171., https://doi.org/10.1142/9789812832047_0016.

[49] Moharam, M. G., and L. Young. “Criterion for Bragg and Raman-Nath Diffraction Regimes.” *Applied Optics*, vol. 17, no. 11, 1978, p. 1757., https://doi.org/10.1364/ao.17.001757.

3 Modelling of holographic structures for use in solar concentrators:

With the capabilities of available holographic recording materials understood, the theoretical limits of what holographic gratings are capable of can be examined. An effective solar concentrator should have a high diffraction efficiency and low angular selectivity. This chapter looks at the variables that affect these characteristics of diffraction gratings and examines the conditions that provide the optimal results for solar concentration. The calculations and concepts introduced in this chapter are novel to the best of the author's knowledge.

The properties of holographic devices are heavily influenced by the hologram's spatial frequency and thickness as they affect the angular and wavelength Bragg selectivity. Using equations 2.3, 2.4 and 2.5 from the previous chapter a Bragg angular selectivity curve can be generated and the required refractive index modulation for achieving 100% diffraction efficiency determined, given inputs of spatial period, diffraction efficiency and thickness. As the figure below demonstrates, for a fixed spatial frequency a thinner grating will be less angularly selective. *Figure 3-1* compares Bragg selectivity curves for gratings with 25 and 50 microns thickness (spatial frequency of 800 l/mm probed at 532 nm) and the difference in FWHM of the two curves is clear.

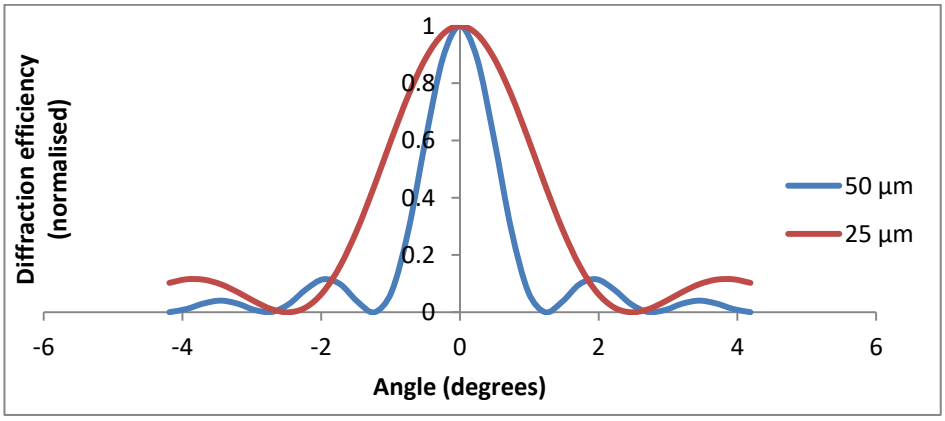

Figure 3-1: Bragg selectivity curves of gratings with a spatial frequency of 800 l/mm probed at 532 nm.

In general, we can conclude that the thinner the grating, the better the performance over a wide range of angles. However, it is also important for solar concentrating holographic optics to be in the volume regime so that 100 % diffraction efficiency can be achieved. In order to determine the appropriate conditions to meet this, the Q and Rho factor must be also considered.

3.1 Q Factor criterion

Though thinner gratings may lead to less angularly selective Bragg curves, a hologram cannot become infinitely thinner without transitioning from the volume to the thin regime. Using the Q factor, the regime of operation of a hologram can be determined based on its spatial frequency and thickness; with a Q factor greater than 10 indicating operation in the volume regime.

For a fixed spatial frequency, increasing the thickness of a hologram will increase the Q factor. The thinnest, least angularly selective holograms will therefor exist on the edge of the thin and volume regime boundaries at Q = 10.

Figure 3-2 shows how the angular selectivity can change in different conditions of thickness and spatial frequency while maintaining a constant Q-factor of 10.

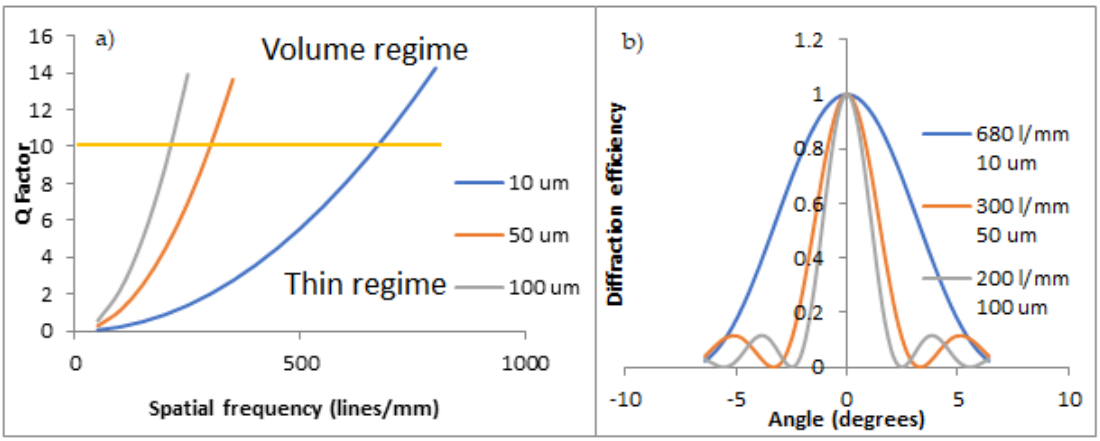

Figure 3-2: a) Q factor calculated at different grating thickness and spatial frequency values. b) Angular selectivity curve at three different grating thicknesses and spatial frequencies with a Q factor of 10.

The Bragg curves in *figure 3-2 b*) show how the angular selectivity is dependent on spatial frequency and thickness while maintaining a Q-factor of 10; displaying lower angular selectivity at higher spatial frequencies and lower thicknesses. Knowing this, we can say that for systems where no solar tracking is available it is better to aim for higher spatial frequencies with lower thicknesses. *Figure 3-3* demonstrates that raising the refractive index modulation enables the use of a hologram with reduced thickness which in turn enables a larger working angular range, but also indicates the lower spatial frequency limits associated with ensuring a single diffracted beam at each thickness.

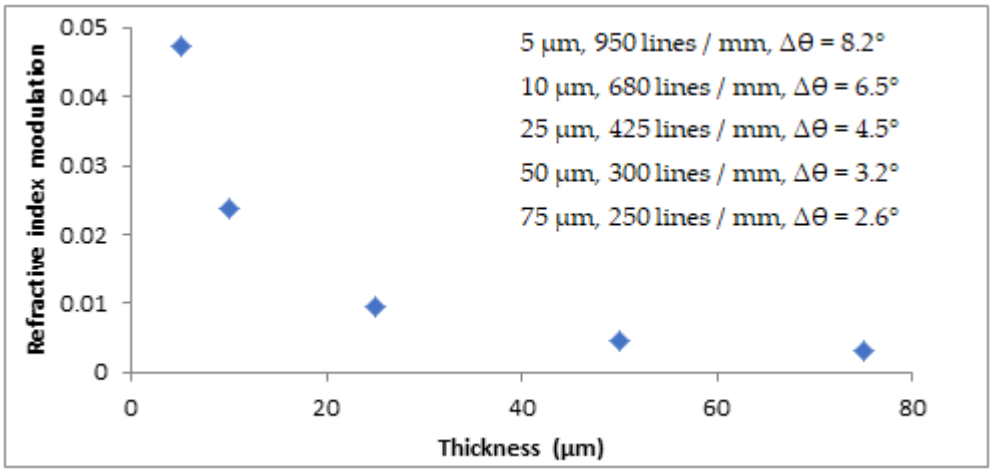

Figure 3-3: Refractive index modulation required at different layer thickness for achieving 100% diffraction efficiency, showing the spatial frequencies required at that thickness for Q=10 along with the resulting full width half max angle (Δθ) of Bragg angular selectivity curve

This illustrates one of the challenges facing holographic concentrators, novel materials capable of large refractive index modulations will allow for thinner less angularly selective holograms.

There is another factor that must be considered: the refractive index modulation of the hologram. In order to achieve high diffraction efficiency in thinner layers a larger refractive index modulation is required.

3.2 Rho Factor criterion

Another method of determining the regime of operation is to look at the Rho factor. *Figure 3-4* shows how the value of the Rho factor changes with spatial frequency at different values of refractive index modulation.

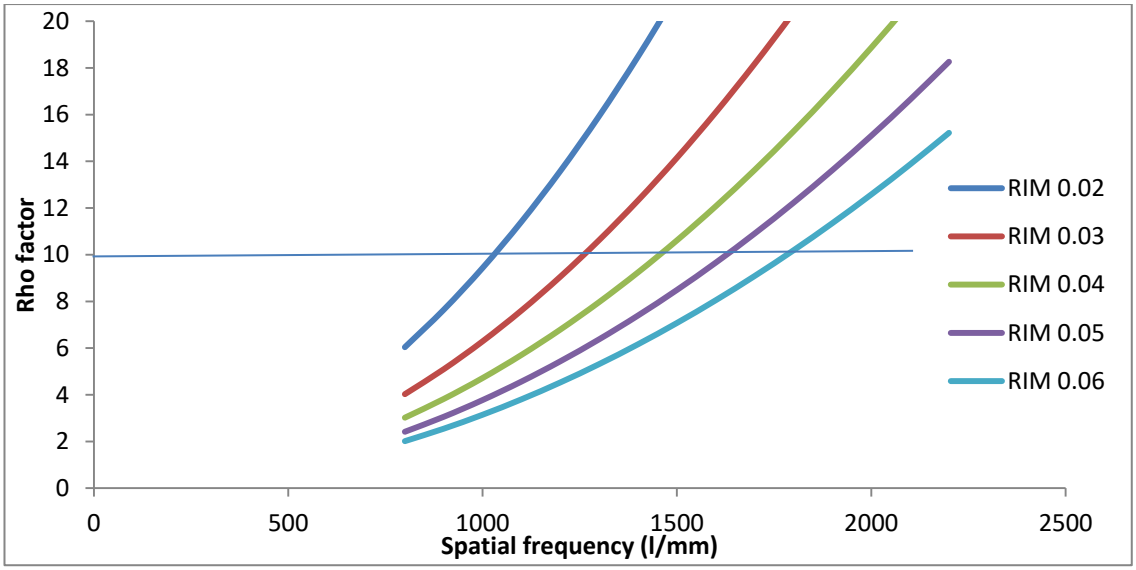

Figure 3-4: Rho factor for various RIMs and spatial frequencies at 532 nm.

The Rho factor can be used to find the minimum spatial frequency value in the volume regime for a material with a specific RIM. This information can be used to determine the lower limits of spatial frequency a holographic lens.

3.3 Chromatic Dispersion

One phenomenon that arises at higher spatial frequencies is an exaggerated chromatic dispersion. *Figure 3-5* shows the angular separation of two beams of different wavelength as it passes through a grating with a fixed spatial frequency at their respective Bragg angles.

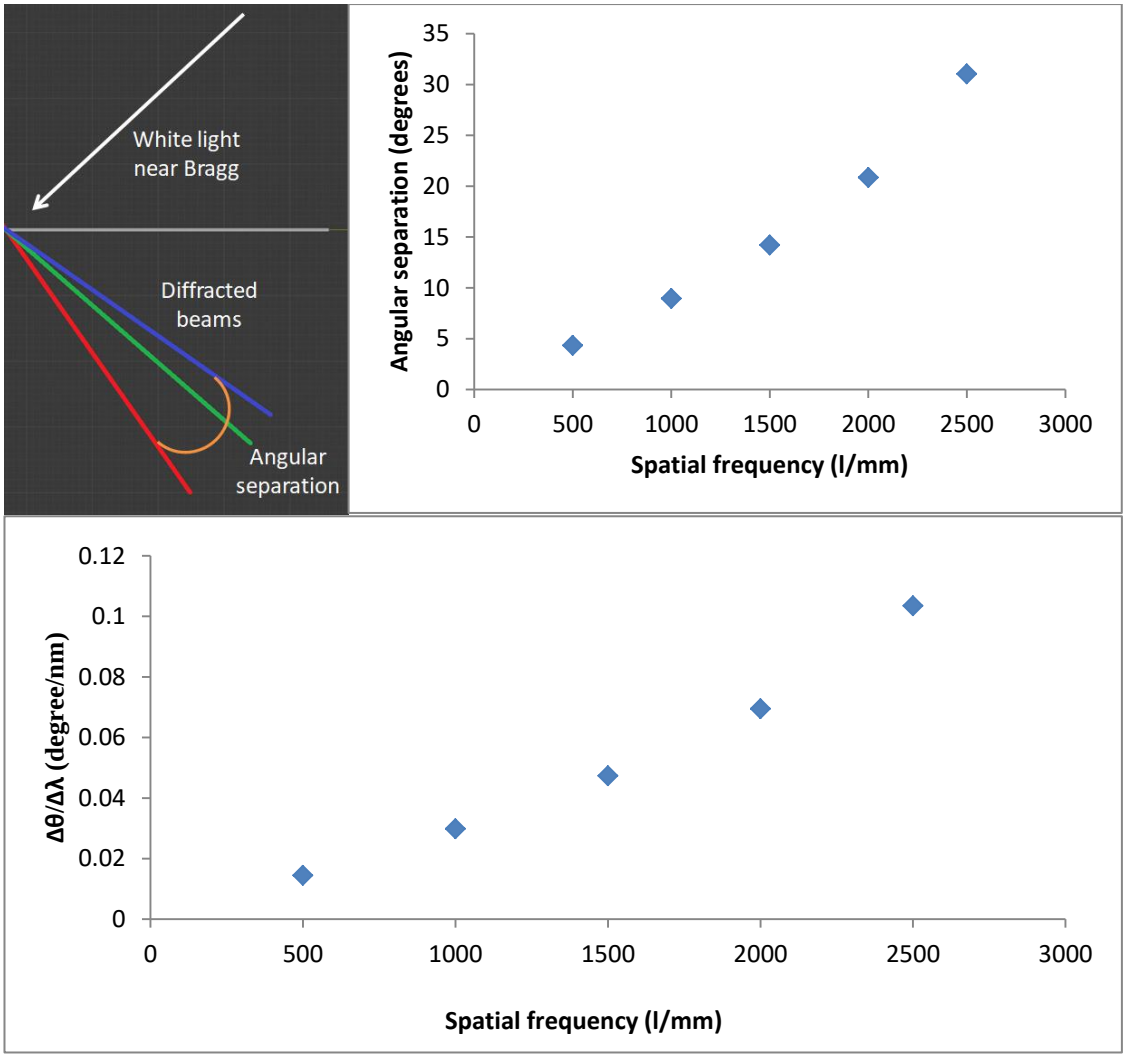

Figure 3-5: Angular separation of beam paths from 400 nm and 700 nm probe wavelengths at different spatial frequencies, presented as angular separation and dispersion.

The angular separation between the two wavelengths beams becomes significantly larger at higher spatial frequencies. This introduces some design challenges or opportunities for solar concentration applications and is important to consider during device design.

3.4 Holographic lenses

When dealing with a holographic lens, where one beam crosses the volume of the material at several different angles across the aperture of the lens, a locally varying spatial frequency can be expected across the aperture/width of the hologram.

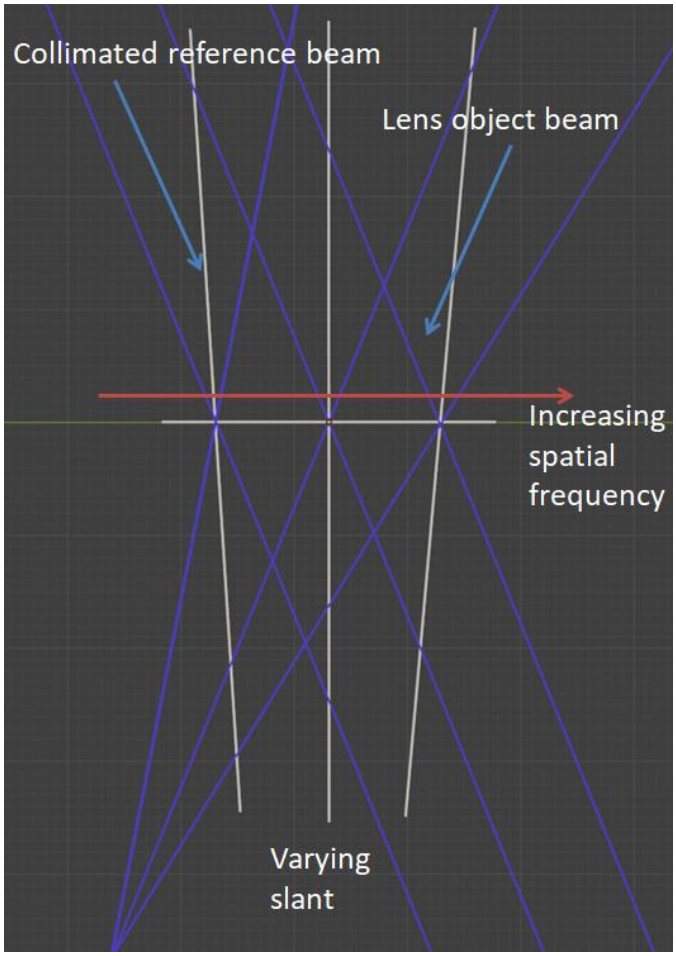

Figure 3-6: Propagation of the beams recording a holographic lens

For a holographic lens recorded with a collimated reference beam and concentrating lens object beam, there will be a variation of spatial frequency and slant across the holographic lens. This gives rise to some design challenges when optimising for low angular and chromatic selectivity; a desirable quality in holographic lenses designed for solar concentration.

A low angular selectivity allows light to be diffracted efficiently from a broad angle range. In the context of solar concentration this reduces the need for solar tracking [1] and allows additional light to be coupled from diffuse sources.

3.5 Conclusions:

The importance of achieving high RIM to make more effective holographic solar concentrators with low thickness and low angular selectivity is understood. This must be done while staying in the volume regime of operation and so the Q and Rho factor must be considered. This modelling has implications in the design of holographic concentrators and can influence device design across the field [2-9]. The next chapter looks at chemical changes made to an acrylamide based photopolymer with the aim of increasing its RIM.

3.6 References:

[1] Collados, M. Victoria, et al. “Holographic Solar Energy Systems: The Role of Optical Elements.” *Renewable and Sustainable Energy Reviews*, vol. 59, 2016, pp. 130–140., https://doi.org/10.1016/j.rser.2015.12.260.

[2] Zhang, Deming. “One-Axis Tracking Holographic Planar Concentrator Systems.” *Journal of Photonics for Energy*, vol. 1, no. 1, 2011, p. 015505., https://doi.org/10.1117/1.3590943.

[3] Chemisana, Daniel, et al. “Holographic Lenses for Building Integrated Concentrating Photovoltaics.” *Applied Energy*, vol. 110, 2013, pp. 227–235., https://doi.org/10.1016/j.apenergy.2013.04.049.

[4] Chrysler, Benjamin D., and Raymond K. Kostuk. “Volume Hologram Replication System for Spectrum-Splitting Photovoltaic Applications.” *Applied Optics*, vol. 57, no. 30, 2018, p. 8887., https://doi.org/10.1364/ao.57.008887.

[5] Collados, M. Victoria, et al. “Holographic Solar Energy Systems: The Role of Optical Elements.” *Renewable and Sustainable Energy Reviews*, vol. 59, 2016, pp. 130–140., https://doi.org/10.1016/j.rser.2015.12.260.

[6] Sherif, Hosam, et al. “Characterization of an Acrylamide-Based Photopolymer for Data Storage Utilizing Holographic Angular Multiplexing.” *Journal of Optics A: Pure and Applied Optics*, vol. 7, no. 5, 2005, pp. 255–260., https://doi.org/10.1088/1464-4258/7/5/007.

[7] Lee, Jeong-Hyeon, et al. “Holographic Solar Energy Concentrator Using Angular Multiplexed and Iterative Recording Method.” *IEEE Photonics Journal*, vol. 8, no. 6, 2016, pp. 1–11., https://doi.org/10.1109/jphot.2016.2634699.

[8] Naydenova, Izabela, et al. “Photopolymer Holographic Optical Elements for Application in Solar Energy Concentrators.” *Holography - Basic Principles and Contemporary Applications*, 2013, https://doi.org/10.5772/55109.

[9] Bianco, G., et al. “Photopolymer-Based Volume Holographic Optical Elements: Design and Possible Applications.” *Journal of the European Optical Society: Rapid Publications*, vol. 10, 2015, https://doi.org/10.2971/jeos.2015.15057.

4 Photopolymer refractive index modulation improvements:

Refractive index modulation is a major factor in producing effective solar concentrating devices. This chapter presents improvements to the RIM of an acrylamide based photopolymer as well as improvements to recording times through chemical alteration of the photopolymer.

4.1 Introduction:

The chemical composition of the photopolymer material is responsible for its recording properties. Changing the ratios of one compound to another can have significant effects on the photopolymer's performance. This chapter presents an optimisation of the chemical composition of the photopolymer in order to achieve the largest refractive index modulation. Changes to the concentration of the acrylamide monomer were made; this was found to have effects on both the recording time and the final refractive index modulation. An optimal concentration was determined in order to maximise both recording time and refractive index modulation.

This photopolymer consisted of an acrylamide monomer with a bis-acrylamide cross linker suspended in a polyvinyl alcohol (PVA) matrix. Martin et al reports on the effect of monomer concentration on reaction rate and refractive index modulation [1]. It states that higher concentrations of monomer should lead to higher reaction rates and refractive index modulation. Erythrosine B was chosen as the sensitising dye. Triethanolamine (TEA) was used as the initiator molecule.

4.2 Materials and methods

First a PVA stock solution (9% wt) was prepared by dissolving 10 g of PVA in 100 ml of deionized water under constant stirring at 50ºC. The solution was then poured through filter paper. A dye stock solution was also prepared by dissolving 0.11 g of Erythrosine B in 100 ml of deionized water

The photopolymer was prepared by mixing 4.38 ml of the PVA solution, 1 ml of the dye solution, 0.5 ml of TEA initiator, 0.05 g of N, N' Methylene bis-acrylamide cross-linker and acrylamide. Four masses of acrylamide were used to prepare different solution concentrations, 0.15 g, 0.20 g, 0.25 g, and 0.3 g. These masses produced solution with an acrylamide concentration of 0.355, 0.474, 0.592 and 0.711 M respectively. The figure below shows how the various concentrations affect the mass ratios of each chemical.

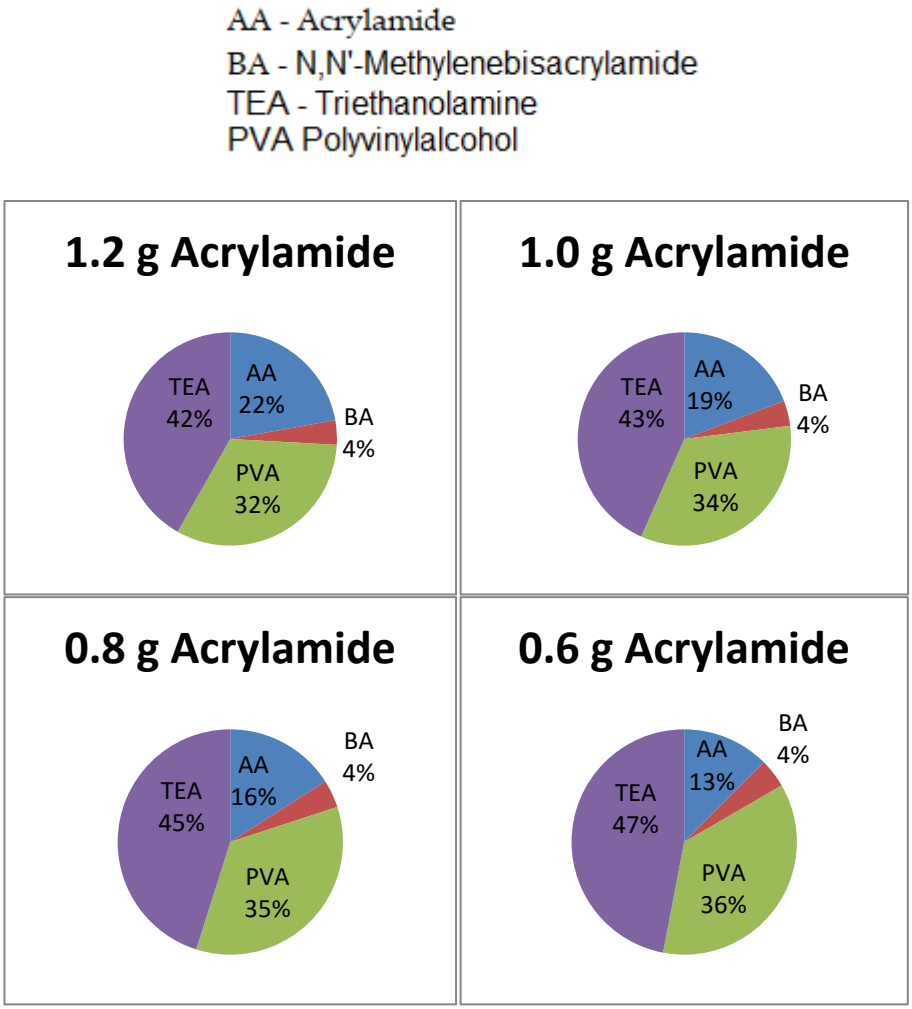

Figure 4-1: Mass ratios of photopolymer compositions with varying acrylamide concentration.

4.3 Experimental set up

The samples were recorded at 800 lines/mm with a combined beam intensity of approximately 5 mW/cm^2. The details of the recording process are outlined below.

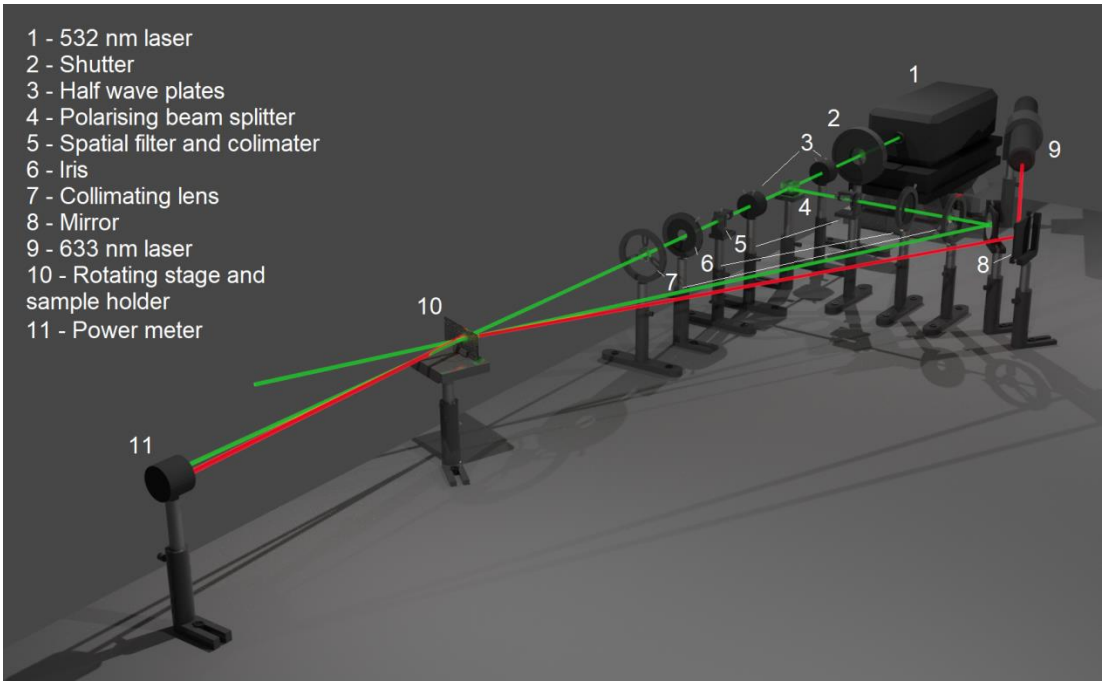

Figure 4-2: Optical set up for transmission hologram recording

The set up in *figure 4-2* was used to record transmission *holographic* gratings in the samples. After opening a shutter, the 532nm beam passes through a half wave plate followed by a polarising beam splitter. One beam is spatially filtered, collimated and directed towards the sample using a mirror. The other beam travels through another half wave plate, then spatially filtered and collimated. This system allows the intensity of both beams to be controlled and made equal. The two beams meet at the sample where the holographic recording takes place. The 633 nm beam is on Bragg and goes on to a power meter where the grating formation is tracked in real time using a computer. The angle between the two recording beams was 24.6° resulting in an interference pattern with spatial frequency of 800 lines/mm.

4.4 Experimental Results

The effect of the acrylamide concentration on refractive index modulation was investigated.

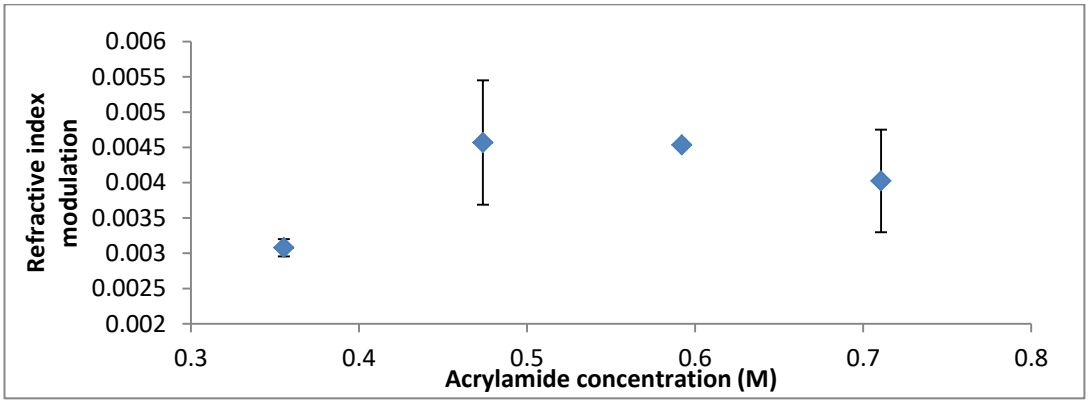

Figure 4-3: Refractive index modulation vs acrylamide concentration in 45 micron thick layers with a recording intensity of 5 mW/cm²

An acrylamide concentration of 0.59 M proved to have the largest refractive index modulation on average. This concentration would be used for all further photopolymer studies.

The effects of the acrylamide concentration on the growth rate were also examined. The figure below shows how initial growth rate, where diffraction efficiency increases linearly, changes with acrylamide concentration.

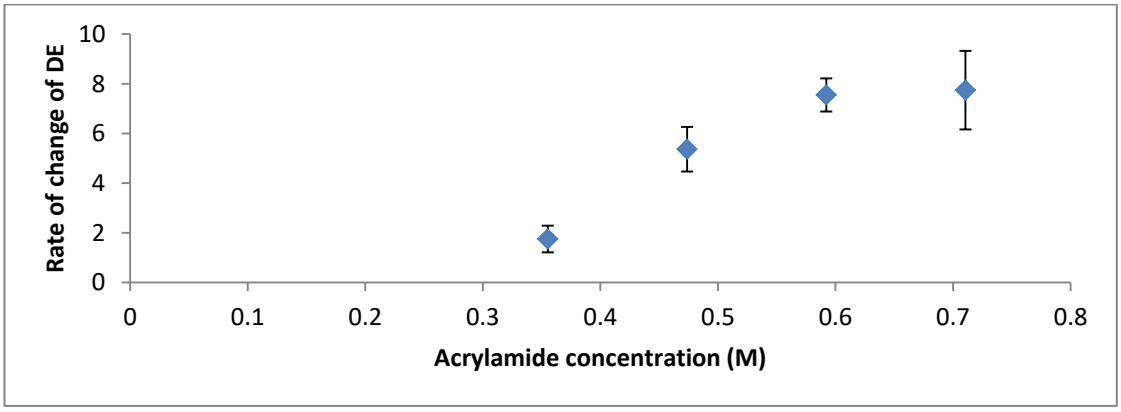

Figure 4-4: Initial growth rate vs acrylamide concentration in 45 ±5 micron thick layers examined with a recording intensity of 5 mW/cm²

The growth rate appears to plateau at an acrylamide concentration of 0.592 M, after which increasing the concentration results in no further growth. The consistent growth curves and high refractive index modulation made the 0.592 M solution the ideal concentration for further tests where the effects of different initiators in the photopolymer composition were examined.

The changes to the acrylamide concentration led to an increase of refractive index modulation of 45%. The rate of formation of the holographic gratings was also increased by a factor of 4.3 when compared to the standard formulation.

4.5 Investigation of the effect of TEA and MDEA Initiators:

Two different initiators TEA and MDEA are used in this study, which have similar chemical structures, but different sizes (*figure 4-5*). A third molecule, diethylmethanolamine (DMEA) was used, however layers made with this molecule dried poorly, likely due to the high vapour pressure.

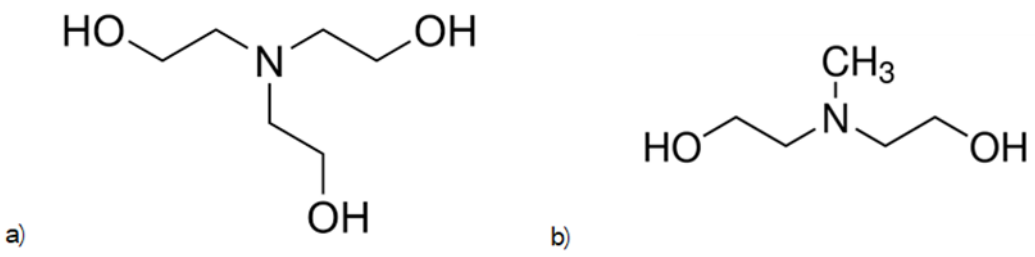

Figure 4-5: Structure of the studied initiators. a) TEA and b) MDEA.

A comparison between the refractive index modulation and diffraction grating growth rates for MDEA and TEA based photopolymer is presented in *figure 4-6*.

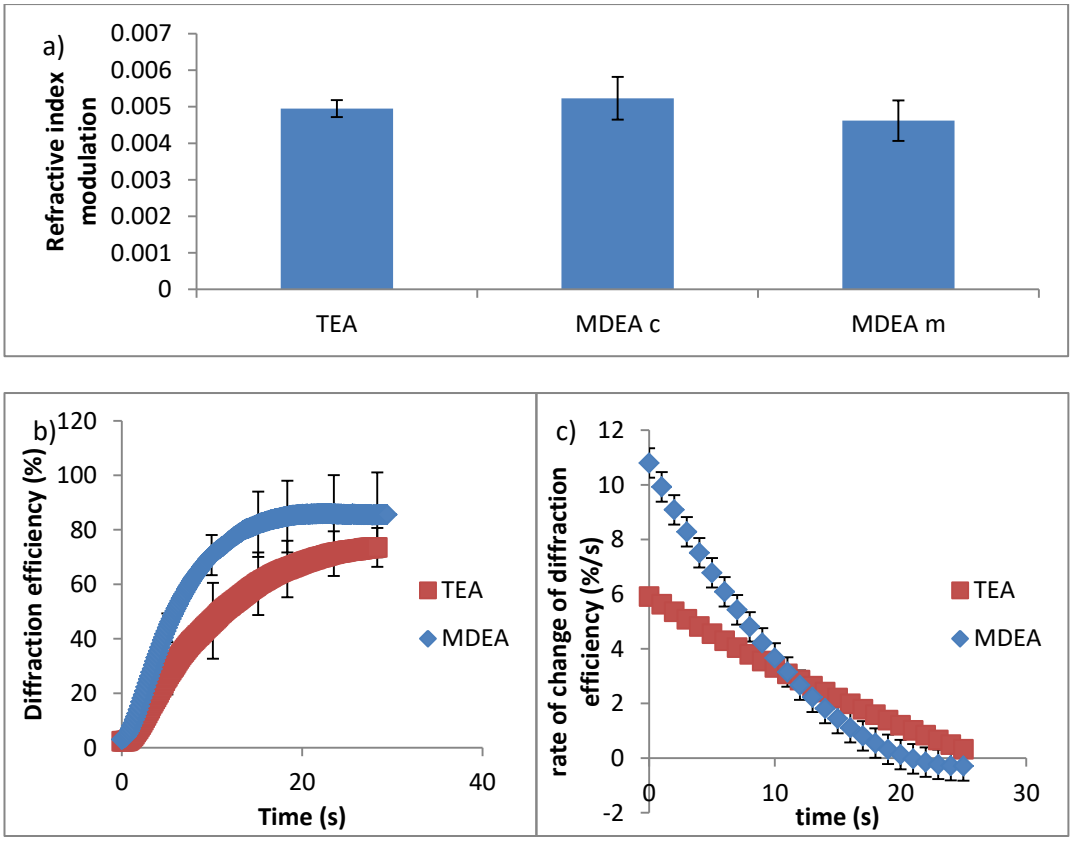

Figure 4-6: Refractive index modulation for each initiator composition. TEA, MDEA (same molar concentration), MDEA (same mass), from left to right (top) b) Growth curves (bottom left) and their rate of change of diffraction efficiency for TEA and MDEA with same molar concentration (bottom right).

The TEA and MDEA perform similarly in terms of refractive index modulation. In terms of growth rate *figure 4-6 b and c* show that the MDEA reaches saturation before the TEA. This faster growth can likely be attributed to two things: molecule size and number of hydrogen bonds. MDEA is a smaller molecule; this could make diffusion through the polymer matrix easier. MDEA also has one less alcohol functional group than TEA; this reduces the number of potential hydrogen bonds it could form in the matrix, which would otherwise slow the rate of diffusion.

4.5.1 Initiator comparison at different layer thicknesses:

Firstly, it is important to note the quality of the photopolymer layers when prepared with different initiators. TEA and MDEA layers dried normally and formed uniform

layers. DMEA however, due to its high vaper pressure, evaporated and formed non-uniform layers capable of only limited holographic recording. Therefore, only TEA and MDEA will be compared.

A comparison between the refractive index modulation was made at several different thicknesses in TEA and MDEA based photopolymer. These can be compared in the figure below:

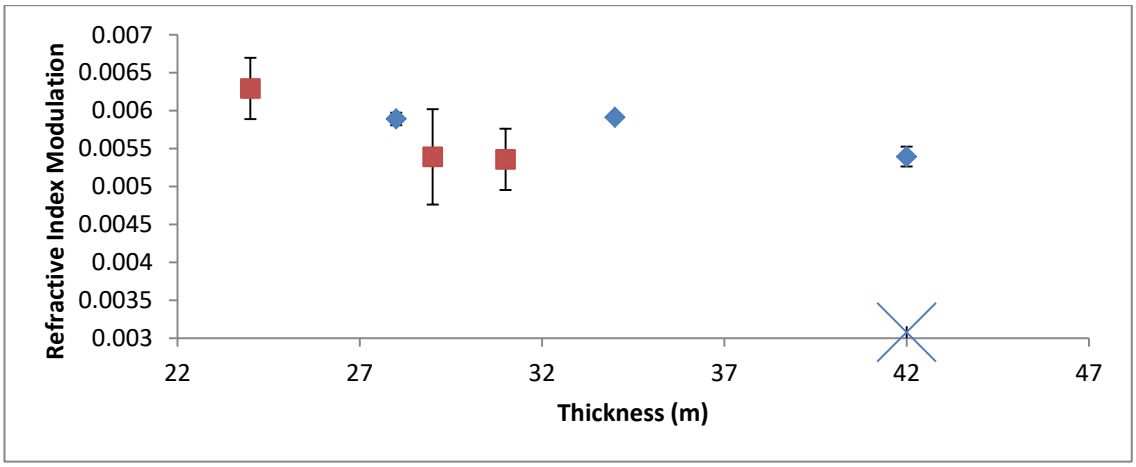

Figure 4-7: Refractive index modulation in layers of different thicknesses with TEA (red) and MDEA (blue) as initiator.

The figure above shows there is practically no difference in refractive index modulation between the layers containing the different initiators, this is true across a range of thicknesses. On average the MDEA based photopolymer has a 2.7% higher refractive index modulation.

This similarity in refractive index modulation makes MDEA as viable as TEA as an initiator with the added bonus of increased growth rates at higher thicknesses. The point marked by the X shows the refractive index modulation of the photopolymer before acrylamide optimisation in TEA based photopolymer at a thickness of 42 microns.

4.5.2 Effect on grating formation rates:

The rate of formation of holographic gratings was determined at different thicknesses of photopolymer. The difference in this rate can be seen in *figure 4- 8* below. The point marked by the X shows the original formulation's rate of formation at a thickness of 42 microns before any acrylamide optimisation.

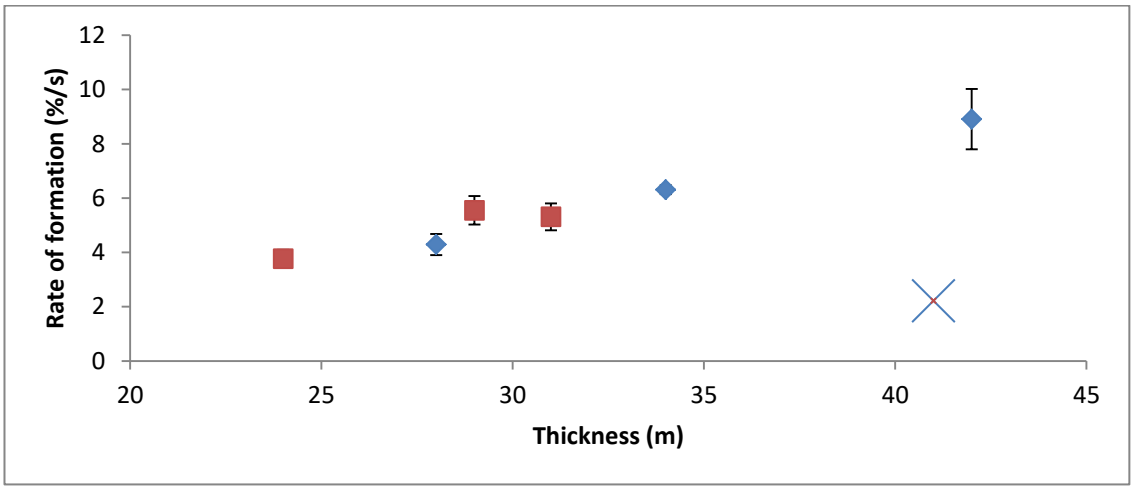

Figure 4-8: Rate of formation of holographic gratings using TEA (red) and MDEA (blue) as initiator.

When looking at the rate of change of grating formation rates across thicknesses, MDEA based photopolymer's growths rates increase 1.37 times more than TEA based photopolymer does as thickness increases. This means MDEA based photopolymer performs similarly to TEA at low thicknesses, however, the thicker the MDEA based photopolymer is the better it will perform in comparison to TEA.

4.5.3 Investigation of the effect of exposure to UV light on the diffraction efficiency of the gratings:

For each set of samples the refractive index modulation was calculated before and after degradation. The robustness factor is the ratio of the post-UV exposure value of the refractive index modulation to the original value of refractive index modulation. The

degradation factor was determined for each sample and can be compared in *figure 6-9* below.

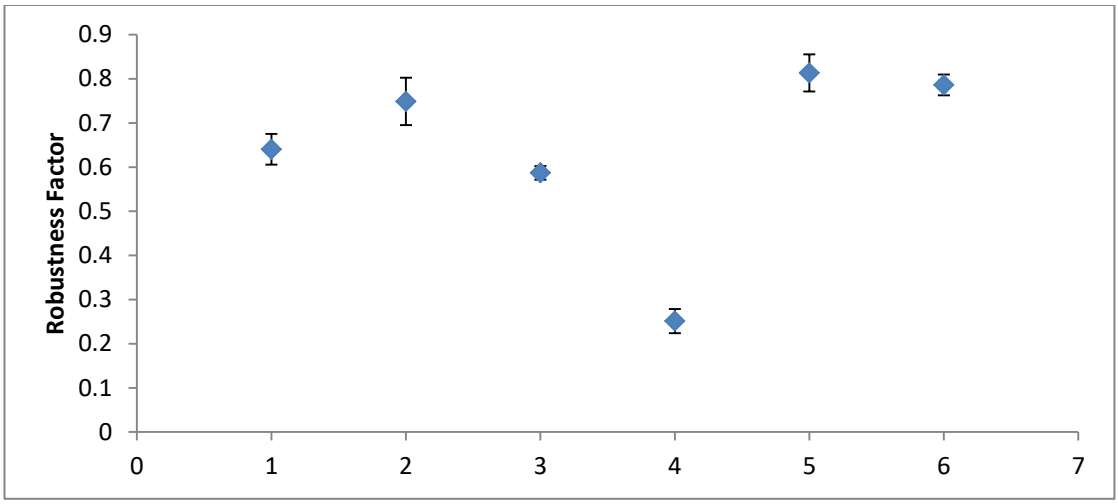

Figure 4-9: The degree of robustness of each set of samples. 1 - TEA Uncovered, 2 - TEA Melinex, 3 - TEA UV Protective layer, 4 - MDEA Uncovered, 5 - MDEA Melinex, 6 - MDEA UV Protective layer.

In general, samples coated with Melinex degraded less than other samples, with both the TEA and MDEA based samples degrading to between 0.7 and 0.85 their original values. The UV protective plastic performed no better than the Melinex. The uncovered TEA based sample performed within a similar range to the coated samples. The uncovered MDEA sample however degraded almost completely. In each case, this was repeated for 3 samples.

4.6 Conclusions

The research conducted confirms that variations in the concentration of acrylamide drastically affect the properties of photopolymer and optimises it for this formulation. Both the refractive index modulation and the time to record can be improved by working with an optimal amount of acrylamide. Using an acrylamide concentration of 0.592 M the largest refractive index modulation achieved in TEA initiated photopolymer was 6.8×10^{-3}. On average, the refractive index modulation was

increased by 50% over compositions containing 0.6 times less acrylamide. The rate of grating formation was increased by a factor of 4.3 at higher acrylamide concentrations.

MDEA which has a similar chemical composition to TEA were found to further improve the recording time of holograms. MDEA showed a 25% decrease in recording times compared to photopolymer initiated with TEA. The increased recording rate in MDEA based photopolymer over TEA based photopolymer is likely due to its smaller molecular size, which enables faster mass transport.

When MDEA and TEA are compared at different thicknesses MDEA was shown to out-perform TEA at higher thicknesses.

When subjected to UV radiation both MDEA and TEA holograms were found to degrade to some degree. Uncovered MDEA initiated samples underwent the largest decrease in refractive index modulation, reducing their diffraction efficiency to 0.25 of their original value post exposure. The covered MDEA samples, however, were some of the best-performing samples. This large difference in the performance of covered and uncovered samples was not observed with the TEA samples.

Increased RIM, chemical stability and faster recoding time benefits many holographic devices and concentrators [2-12]

Though improvements to the photopolymer's RIM and recording time were made as well as measures to improve the materials UV resistance other novel materials may prove more effective with the right development. This next chapter presents the development of a novel sol-gel recording material. Chemical changes and post processing techniques have proved to make the material more suitable for solar concentration applications.

4.7 References

[1] Martin, S. (1995). *A new photopolymer recording material for holographic applications: photochemical and holographic studies towards an optimized system*. Doctoral thesis. Technological University Dublin pg 123. doi:10.21427/D7DP4B

[2] Zhang, Deming. "One-Axis Tracking Holographic Planar Concentrator Systems." *Journal of Photonics for Energy*, vol. 1, no. 1, 2011, p. 015505., https://doi.org/10.1117/1.3590943.

[3] Chemisana, Daniel, et al. "Holographic Lenses for Building Integrated Concentrating Photovoltaics." *Applied Energy*, vol. 110, 2013, pp. 227–235., https://doi.org/10.1016/j.apenergy.2013.04.049.

[4] Chrysler, Benjamin D., and Raymond K. Kostuk. "Volume Hologram Replication System for Spectrum-Splitting Photovoltaic Applications." *Applied Optics*, vol. 57, no. 30, 2018, p. 8887., https://doi.org/10.1364/ao.57.008887.

[5] Collados, M. Victoria, et al. "Holographic Solar Energy Systems: The Role of Optical Elements." *Renewable and Sustainable Energy Reviews*, vol. 59, 2016, pp. 130–140., https://doi.org/10.1016/j.rser.2015.12.260.

[6] Sherif, Hosam, et al. "Characterization of an Acrylamide-Based Photopolymer for Data Storage Utilizing Holographic Angular Multiplexing." *Journal of Optics A: Pure and Applied Optics*, vol. 7, no. 5, 2005, pp. 255–260., https://doi.org/10.1088/1464-4258/7/5/007.

[7] Lee, Jeong-Hyeon, et al. "Holographic Solar Energy Concentrator Using Angular Multiplexed and Iterative Recording Method." *IEEE Photonics Journal*, vol. 8, no. 6, 2016, pp. 1–11., https://doi.org/10.1109/jphot.2016.2634699.

[8] Naydenova, Izabela, et al. “Photopolymer Holographic Optical Elements for Application in Solar Energy Concentrators.” *Holography - Basic Principles and Contemporary Applications*, 2013, https://doi.org/10.5772/55109.

[9] Bianco, G., et al. “Photopolymer-Based Volume Holographic Optical Elements: Design and Possible Applications.” *Journal of the European Optical Society: Rapid Publications*, vol. 10, 2015, https://doi.org/10.2971/jeos.2015.15057.

[10] Mikulchyk, Tatsiana, et al. “Synthesis of Fast Curing, Water-Resistant and Photopolymerisable Glass for Recording of Holographic Structures by One- and Two-Photon Lithography.” *Advanced Optical Materials*, vol. 10, no. 6, 2022, p. 2102089., https://doi.org/10.1002/adom.202102089.

[11] Mikulchyk, Tatsiana, et al. “Characterisation of Holographic Recording in Environmentally Stable Photopolymerisable Glass.” *Applied Sciences*, vol. 12, no. 12, 2022, p. 5969., https://doi.org/10.3390/app12125969.

[12] Branigan, Emma, et al. “Direct Multiplexing of Low Order Aberration Modes in a Photopolymer-Based Holographic Element for Analog Holographic Wavefront Sensing.” *Environmental Effects on Light Propagation and Adaptive Systems IV*, 2021, https://doi.org/10.1117/12.2599912.

5 Development and characterisation of sol-gel material for holographic recording

5.1 Introduction

The previous chapter showed improvements to RIM and faster recording times; qualities that are beneficial to minimising angular selectivity and mass production respectively. A solar concentrator intended for either terrestrial or space-based applications must be able to endure in their intended environment. For this reason environmental stability and physical robustness is an important quality for a holographic solar concentrator to have. A photosensitive sol-gel has proven to be robust and stable in several environments; however to improve its effectiveness in solar concentrating applications improvements to the RIM must be made as its value lies in a range of 8.9×10^{-4} to 3.2×10^{-3} in samples with thicknesses ranging from 255 to 30 μm [1]. Reducing the thickness while maintaining high diffraction efficiency through improved RIM would make this sol-gel a more appropriate candidate for holographic solar concentration.

Experiments characterising and modifying sol gel holographic recording materials were carried out to optimise it in the context of solar concentrators. These experiments had two major goals, to improve understanding of the holographic recording mechanism in the sol gel and to increase the refractive index modulation.

5.2 Materials and methods

5.2.1 Photosensitive sol-gel preparation:

The photosensitive sol-gel was synthesised by employing a four-step process using two hybrid precursors: a trialkoxyorganosilane (3-trimethoxysilylpropyl methacrylate) and a zirconium complex prepared from the chelation of zirconium (IV) propoxide and methacrylic acid as described in details in [1]. A typical synthesis includes 15 grams

(6.04×10^{-2} mol) of 3-trimethoxysilylpropyl methacrylate is mixed in a glass container with 0.8 grams (4.44×10^{-2} mol) of aqueous nitric acid solution (0.1 M) for 45 minutes. At the same time 0.727 grams (2.218×10^{-3} mol) of zirconium (IV) propoxide is mixed with 0.13 grams (1.567×10^{-3} mol) of methacrylic acid and is also stirred for 45 minutes. After both solutions have been prepared they are then mixed together along with 1.08 grams (6×10^{-2} mol) of deionised water for 24 hours. This forms the base of the sol-gel and is illustrated in *figure 5-1*.

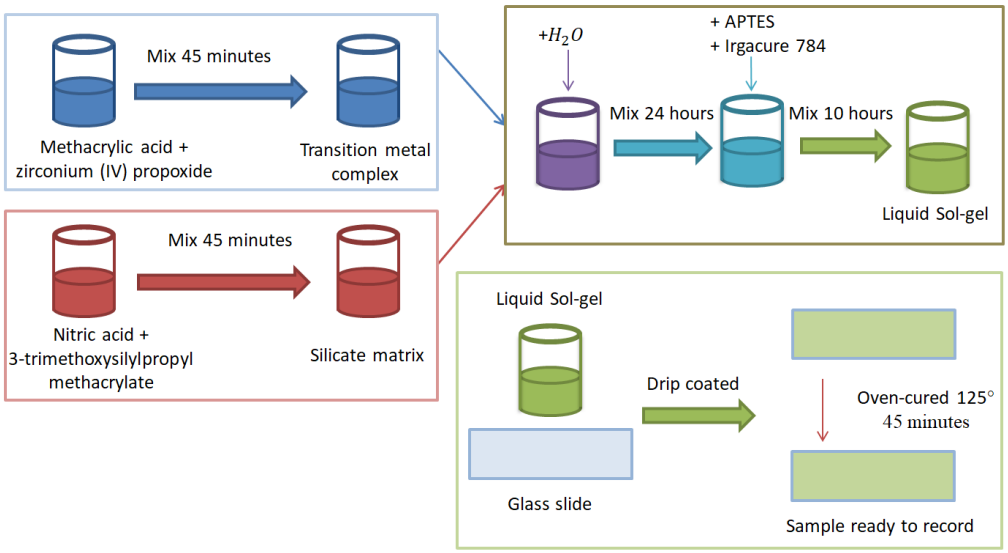

Figure 5-1: Illustration of the photosensitive sol-gel layer preparation procedure.

After the base is made, (3-Aminopropyl)triethoxysilane (APTES) is added to improve the condensation of the hybrid nanoparticles during the gelation process and reduce the gelation time. Along with APTES, a photoinitiator Bis(eta.5-2,4-cylcopentadien-1-yl)-bis(2,6-difluoro-3-(1H-pyrrol-1-yl)-phenyl) titanium (Irgacure 784) is added to introduce photosensitivity in the blue-green wavelength region. Practically, this involved mixing 0.225 grams of APTES(3.608×10^{-3} mol), 0.025 grams (1.81×10^{-4}

mol) of Irgacure 784, 2 ml (2.617×10^{-2} mol) of Isopropanol and 5 grams of base. This is mixed for 24 hours.

5.2.2 Sol-gel layer preparation:

Photosensitive layers are prepared by coating glass slides (76 mm x 26 mm) using a drip coating method. A pipette is used to measure 150-1000 ml of solution to achieve dry layer thicknesses of 15-100 μm respectively. The samples are then put in an oven (Binder, model ED56) and cured at 125 °C for 45 minutes. The obtained dry layers are ready for recording.

5.2.3 Holographic recording set up:

Holographic recording of volume phase transmission gratings was performed using a standard two-beam holographic recording geometry. Two lasers, either a 532 nm NDYAG laser or a 476 nm argon ion laser, were used as a light source in the holographic recording. The 532 nm recording arrangement is illustrated in *figure 4-2*. The recording in the blue wavelength region was carried out with a similar set-up using the 476 nm line of an Argon ion laser.

After the electronic shutter, the laser beam passes through a half wave plate followed by a polarising beam splitter, which allows easy adjustment of the beam ratio, to ensure high contrast in the interference pattern. The beam reflected by the polarising beam splitter is then spatially filtered, passed through an aperture and collimated before being reflected towards the photosensitive material in the sample holder. The other beam passes through another half wave plate to ensure both beams are in the same polarisation state (s-polarised), and then undergoes the same spatial filtering and collimation. Both beams overlap and interfere at the sol-gel sample in a sample holder with a spot size of 1 cm^2. A power meter records the power of a diffracted beam from a 633 nm probe beam (a wavelength to which the material is not sensitive). The data is

sent to a computer and real time growth curves are generated as the grating is being recorded. A rotation stage on which the sample holder is mounted allows the same detector to also be used to generate Bragg selectivity curves. It should be noted that the diffraction efficiency figures were all obtained using an s-polarised 633 nm probe beam. In many real-world applications however, the incident light is unpolarised. Diffraction efficiencies for unpolarised light will remain within 5% lower than that for s-polarised light, given that the spatial frequency of the grating is lower than 1000 l/mm. In addition, the modelling in this chapter has been carried out for s-polarised light. For p-polarised components of the incident light, the phase term would be reduced by the cosine of twice the Bragg angle [2] and can be readily modelled. For large Bragg angles, such as those for coupler elements, a p-polarised probe beam can experience a significant drop in efficiency for a given refractive index modulation. For the results reported here (1000 and 500 l/mm gratings probed at 633 nm) the difference has been modelled and measured experimentally and is limited to a few percent.

5.2.4 UV-Vis characterisation of the recording layers

A UV-Vis spectrum of dry photosensitive sol-gel layers on a glass substrate was obtained using a Perkin Elmer Lambda 900 UV/Vis/NIR Spectrometer to determine sensitivity at wavelengths between 325 and 800 nm in steps of 1 nm.

5.2.5 Thermal Processing

The heat treatment of photosensitive sol-gel samples was carried out using a fan assisted oven (Binder, model ED56). This was used for dry layer preparation as detailed in section 7.2.2, and for post recording heat treatment.

5.3 Experimental results:

5.3.1 Characterisation of the sol-gel layers for holographic recording

Since absorption of the recording light by the photosensitive layer is a crucial first step in the recording process, tuning the recording wavelength to better suit the absorption

characteristics of the material is a key route to improved sensitivity. The UV-Vis spectrum of a photosensitive sol-gel layer was taken to determine its absorption at different laser recording wavelengths (*Figure 5-2 a*)).

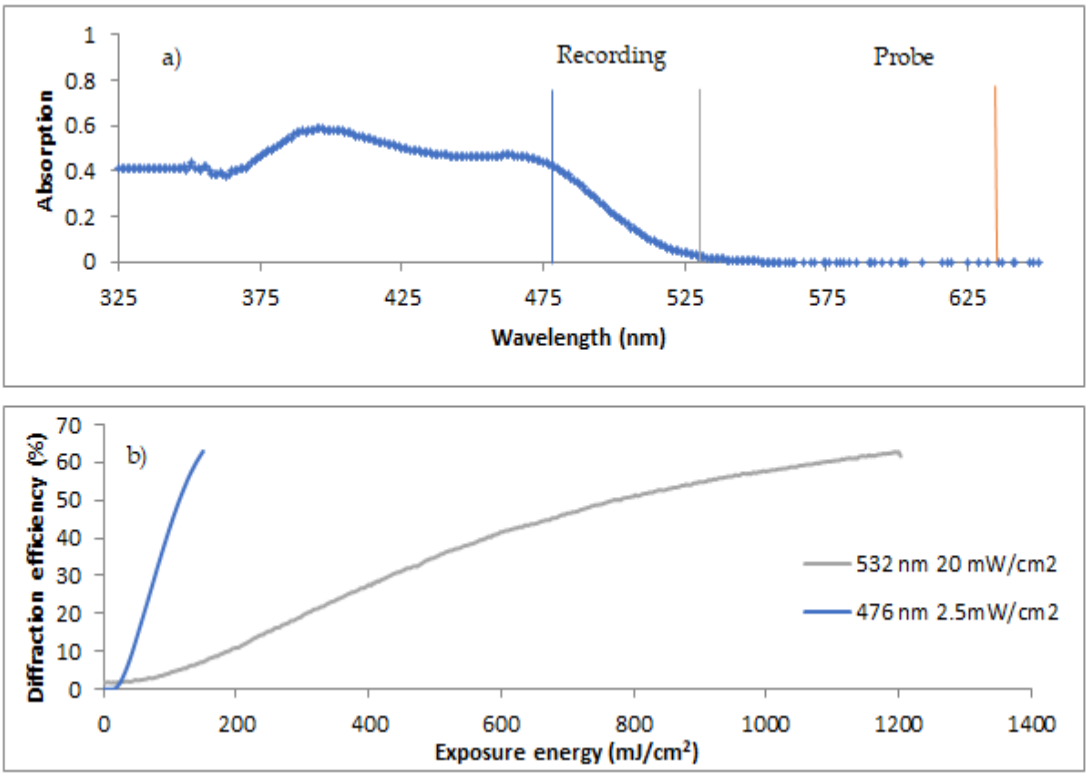

Figure 5-2: UV-Vis absorption spectrum of photosensitive sol-gel layers (after oven curing outlined in figure 7-1) noting recording wavelengths of 532 and 476 nm, and probe wavelength of 633 nm; b) Diffraction efficiency growth curves of transmission gratings with spatial frequency of 500 l/mm recorded at 532 nm and 476 nm with an intensity of 20 mW/cm^2 and 2.5 mW/cm^2 , respectively; thicknesses for 476 nm and 532 nm recordings are 80 and 100 µm respectively.

The sol-gel absorption at 476 nm is 0.435, approximately 18 times higher than 0.023 for 532 nm. Although the recording processes are complex and absorption is only the first step, this information is useful when comparing the recording at the two different wavelengths and for determining the equivalent intensity to achieve equal photonic absorption independent of the wavelength used.

Figure 5-2 b) shows typical grating growth as a function of exposure energy for recording in green (532nm) and in blue (476nm) wavelength region. The difference in

exposure energy required for 50% diffraction efficiency, (785 mJ/cm^2 for 532 nm vs. 114 mJ/cm^2 for 476 nm) confirms that the material absorbs much more efficiently at 476 nm; we can see an approximately 7-fold increase in sensitivity under these conditions. The final diffraction efficiency achieved was not significantly increased for any given layer thickness, however, the capacity to record with 7-8 times less intensity could confer a significant advantage in mass production.

5.3.2 Determination of the RIM and its dependence on thickness of the layers at 500/1000 l/mm:

In order to find the upper limits of the RIM achievable with the photosensitive sol-gel, many holograms were recorded at both 532 and 476 nm at 500 and 1000 l/mm spatial frequencies and across a range of thicknesses from 18 to 380 µm. To avoid ambiguity, the Bragg selectivity curves of all samples were analysed and only values from samples that have not been over-modulated are included. The RIM achieved for individual samples was calculated by using equation 2.3 and presented in *figure 5-3*.

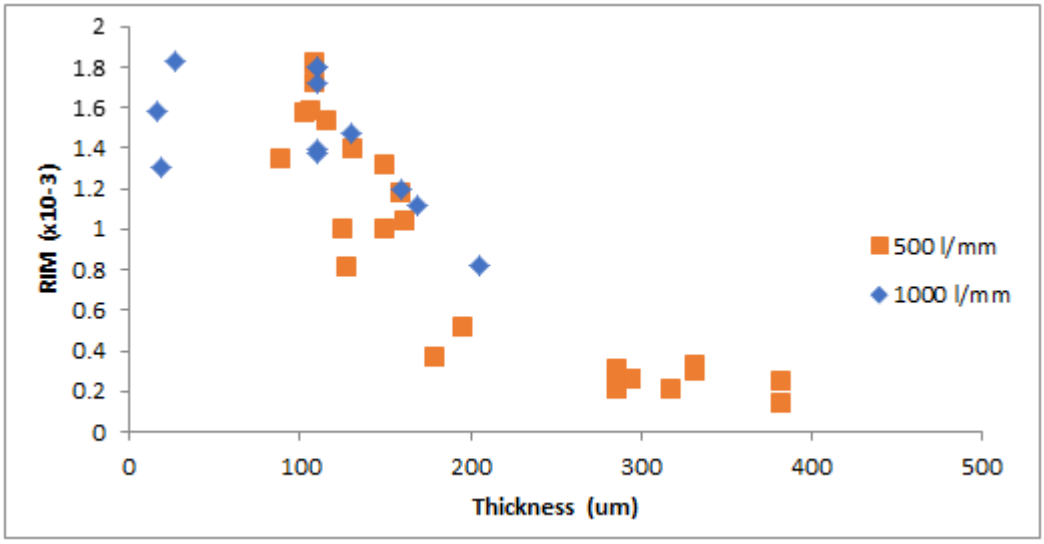

Figure 5-3: Maximum RIM achieved for individual samples with different thicknesses and recorded at spatial frequencies of 500 and 1000 l/mm.

In order to determine the RIM the sol-gel can achieve with this recording method, several more holograms were recorded in sample thicknesses below 100 µm. A 100

second recording time with a 476 nm laser and an intensity of 2.5 mW/cm^2 was used. An average RIM of $1.4 \times 10^{-3} \pm 1 \times 10^{-4}$ was achieved in layers with a thickness of 92 $\pm$ 11 μm over 9 samples.

A few samples were recorded at a lower thickness than the others (15-25 μm), in order to determine if the RIM would continue to increase when layer thickness is below 100 μm. However, no increase in RIM was found at these thicknesses.

5.4 Effect of Zirconium concentration:

As mentioned above, a study of the zirconium concentration's effect on recording characteristics is of interest due to its effect on layer density. The addition of 2 – 9 times more zirconium(and methacrylic acid) to the sol-gel has proved to have a multitude of effects. One that is immediately observable is the exaggeration of an inhibition period at the beginning of holographic recording.

5.4.1 Effect of zirconium concentration on grating growth and RIM:

Four example growth curves with different zirconium concentrations are shown in *Figure 5-4 a).* As seen from *figure 5-4 a),* there is a period where, despite the recording beams illuminating the sol-gel, zero-growth of the diffraction efficiency is observed. This inhibition period depends on the zirconium concentration, and it is longer for higher zirconium concentrations. *figure 5-4 b)* shows the data for a wider range of concentrations and shows how the inhibition time changes linearly with zirconium concentration in this range.

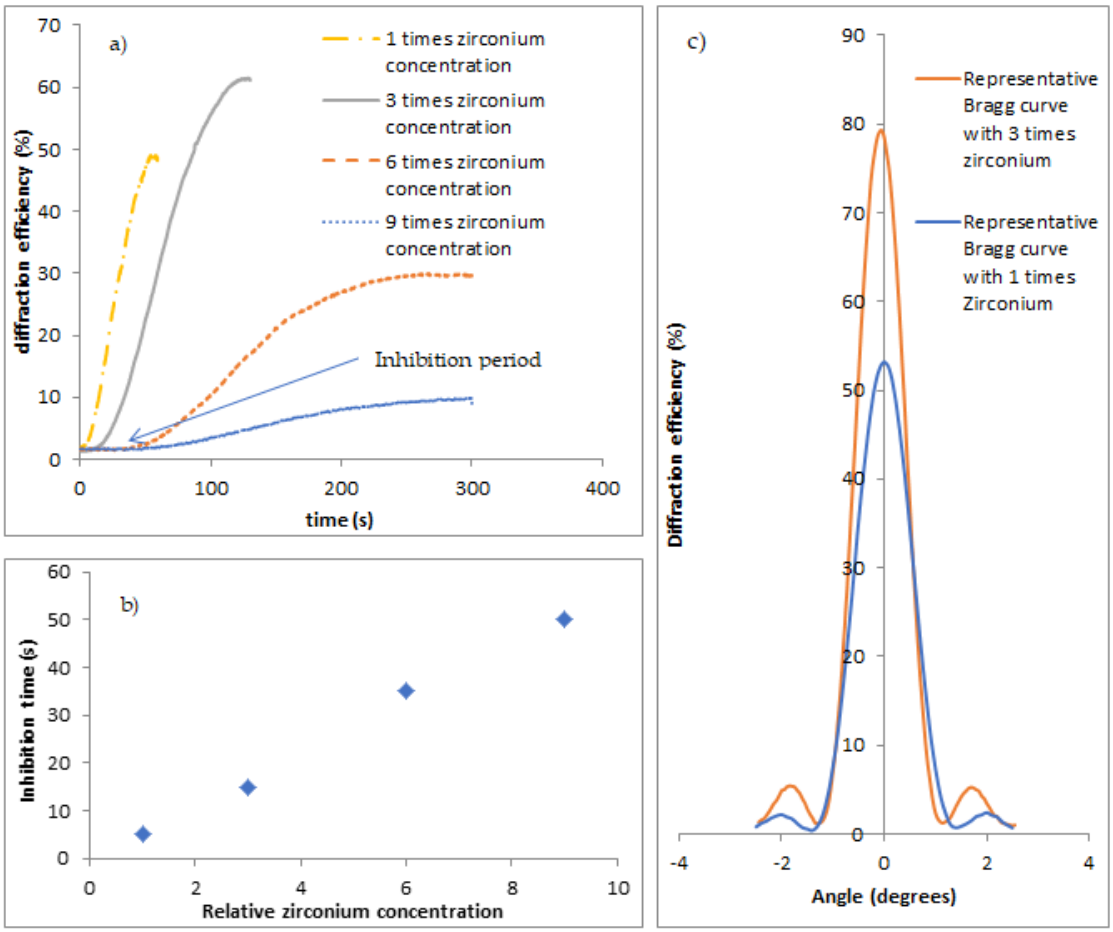

Figure 5-4: a) Real time diffraction efficiency growth curve for gratings recorded in photosensitive sol-gel with a 1, 3, 6 and 9 times increase in zirconium concentration (20 mW/cm^2, 532 nm, 1000 l/mm layer thickness ≈100 μm); b) Inhibition time vs relative zirconium concentration. c) Representative Bragg curves for samples with 3 times zirconium concentration compared with the standard concentration (1 times). Samples recorded at 500 l/mm, 476 nm wavelength, 2.5 mW/cm^2 total recording intensity, 100 seconds exposure, ~80 μm thickness.

For the highest concentration of zirconium, recording times of 5 minutes are required to reach the maximum diffraction efficiency. The overall sensitivity can be compared by measuring the time it takes to reach 10 % diffraction efficiency: 300 seconds for 9 times the zirconium concentration compared to 6 seconds for reference (unmodified, 1 times) concentration.

It should be noted that the addition of zirconium greater than 3 times the initial concentration increases the brittleness of the dry layers to a point where recording

becomes ineffective. It was observed that layers with 3 times or less the initial zirconium concentration remain sufficiently plastic to form good stable layers. This physical change to the hardness of the material due to higher zirconium concentration may be a contributing factor to the observed inhibition times; along with the increased density that comes with high zirconium concentrations, it is possible mass transport becomes more limited.

Several holographic gratings were recorded in order to determine the average RIM achieved when using 3 times the normal zirconium concentration. Two representative Bragg curves from the two thickness regimes chosen are shown in *figure 5-4 c)*. The average RIM achieved over 23 samples in layers with 3 times the zirconium concentration at 500 l/mm was $1.9 \times 10^{-3} \pm 1 \times 10^{-4}$. This is a 36 % increase over samples recorded with the standard zirconium concentration.

One possible reason for the differing recording times could be the change in sample transparency with zirconium concentration.

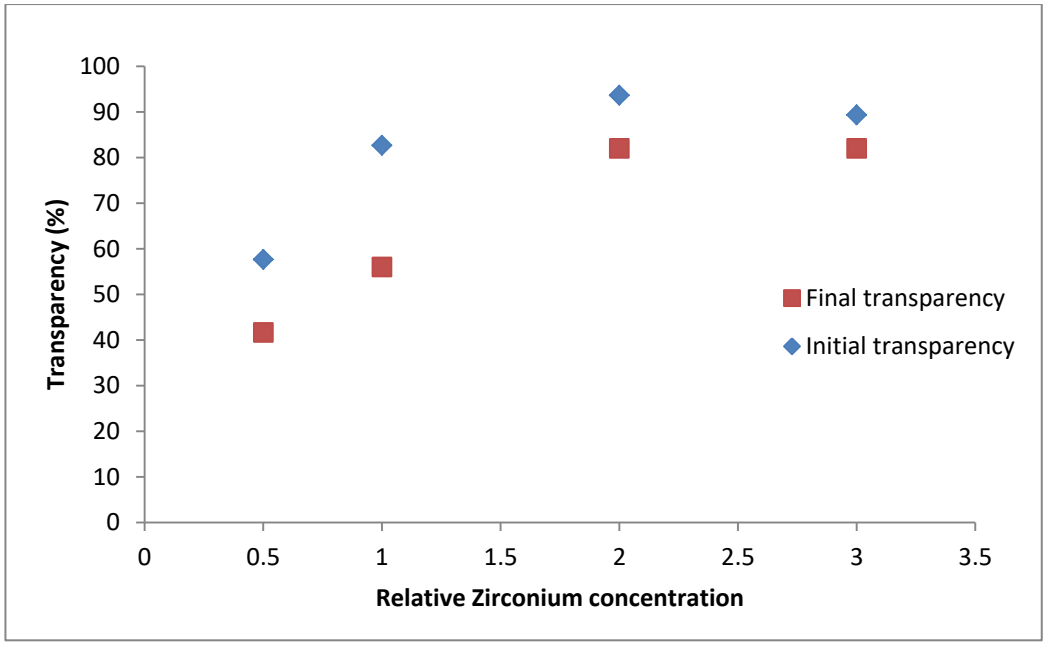

Figure 5-5: Initial and final material transparency at 532 nm. Final transparency achieved after 300 s exposure at 20 mW/cm^2 average sample thickness 94 μm.

As the zirconium concentration increases the transparency increases. This increase in transparency leads to a reduced "transparency change" compared to lower zirconium concentrations when exposed to the same intensity light for a period of time. It is possible that this reduced absorption plays a role in the increased inhibition and recording times when using higher zirconium concentrations.

5.5 Thermal treatment after a short exposure time:

It was observed that sol-gel samples exposed to the recording pattern for short periods ($\sim$ 10 seconds) would continue to develop in the absence of light. This dark process is shown in *figure 5-6 a)*, where after the initial exposure for 10 seconds the grating's diffraction efficiency increases from approximately 3% to between 40-90% within 1800 seconds. This process on its own does not produce better results in terms of the final RIM; reaching values of $1.0 \times 10^{-3} \pm 1 \times 10^{-4}$ i.e. less when compared to fully exposed gratings. However, it does point towards the existence of processes with slower dynamics and their contribution to the recording process. It should be noted that this

effect is most prominent in samples with the standard concentration of zirconium and less noticeable in higher zirconium concentration layers. This also points towards a light-driven process with fast dynamics (at these exposure conditions), followed by a dark process with relatively slower dynamics. Since the dark process was not observed as strongly in samples with additional zirconium, all experiments involving the dark process were carried out with the reference (1 times) zirconium concentration.

Figure 5-6. a) shows a real time growth curve of a sol-gel sample developing through the dark process and *figure 5-6 b)* shows the effect of thermal treatment during this period.

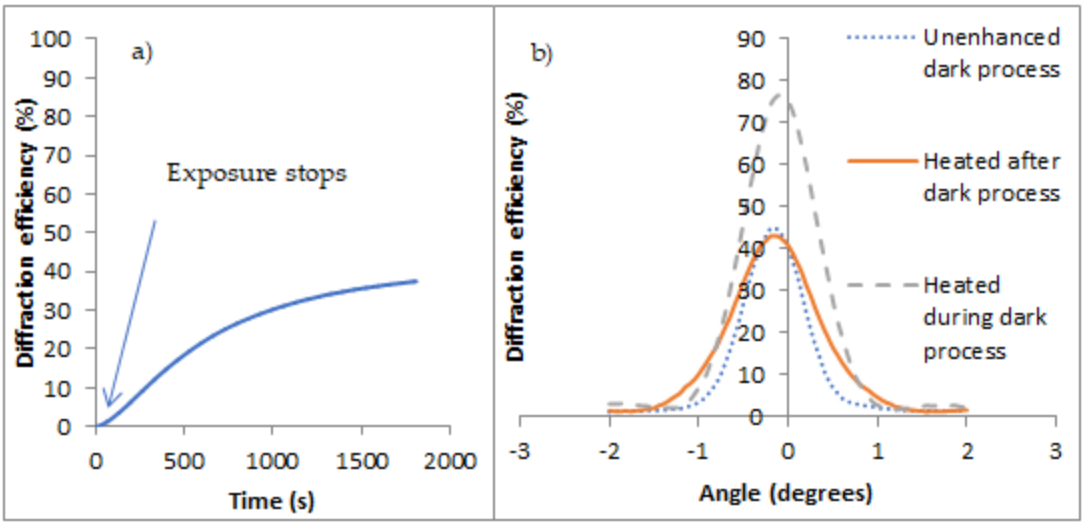

Figure 5-6: a) Growth curve of grating recorded using 10 seconds initial exposure, 476 nm, 2.5 $mW/cm2$ total recording intensity, dark process observed after the recording light is switched off; b) Bragg curves of thermally treated grating after the dark process had completed (solid), the grating heated during the dark process (dashed), and the grating with no heat treatment (dotted). Recorded at 532 nm, 1000 l/mm, 20 $mW/cm2$, heat treatment at $90°C$

A few processes could be behind this dark process. The refractive index modulation may be increasing due to a continuation of chain polymerisation initiated during exposure, diffusion/ mass-transport of material as a result of the concentration difference set up by the consumption of material in the bright fringes; indeed, the dark

process may be some combination of these effects., It was hypothesised that an increased temperature could assist in some chemical or physical process, as condensation reactions can be driven by catalysis and/or thermally [3]. So, it is possible that the thermal treatment of the sol-gel after recording may promote further condensation and a denser species and/or speed up diffusion, both of which could improve the RIM. The length of time it takes for the dark process to complete under these conditions made it practical to also examine the effect of temperature on the process observed in *figure 5-6a).*

Samples were heat treated immediately after recording (during the dark process) for 30 minutes at different temperatures (60-110°C) with a control sample that was heated after the dark process had already completed. *Figure 5-6 b)* shows how only the sample heated during the dark process experienced an increase to its diffraction efficiency. Samples heated above 80°C during the dark process showed consistent improvement to the RIM compared to unheated samples. No notable difference was observed between samples heated at 80, 90 or 110 degrees (table 1).

Table 5-1: Max RIM achieved by heating during dark process at different temperatures

Temperature (°C)	RIM
60	0.0018
70	0.0017
80	0.0031
90	0.0032
110	0.0034

Numerous samples were recorded at 500 l/mm and were heated immediately after exposure for 10 s. The average RIM of these samples was $2.6 \times 10^{-3} \pm 5 \times 10^{-4}$ with thicknesses of 65 ±16 μm. Some of these samples became over-modulated as a result, so in order to determine the true limit to the RIM, the sample thickness was reduced and the spatial frequency increased to 1000 l/mm in order to stay in the volume regime.

For the thinner samples recorded at 1000 l/mm the RIM had an average value of $3.3 \times 10^{-3} \pm 4 \times 10^{-4}$ in layers with an average thickness of 45 $\pm$ 13 μm. This represents an average increase due to heating of a factor of 2.4. The highest single value of RIM achieved was 4.2×10^{-3}. This was measured in a sample heated at 90 degrees for 30 minutes during the dark process after 10 s exposure to a 532 nm laser at 20 mW/cm^2. The spatial frequency of recording was 1000 l/mm. This method produced the highest RIM of all methods.

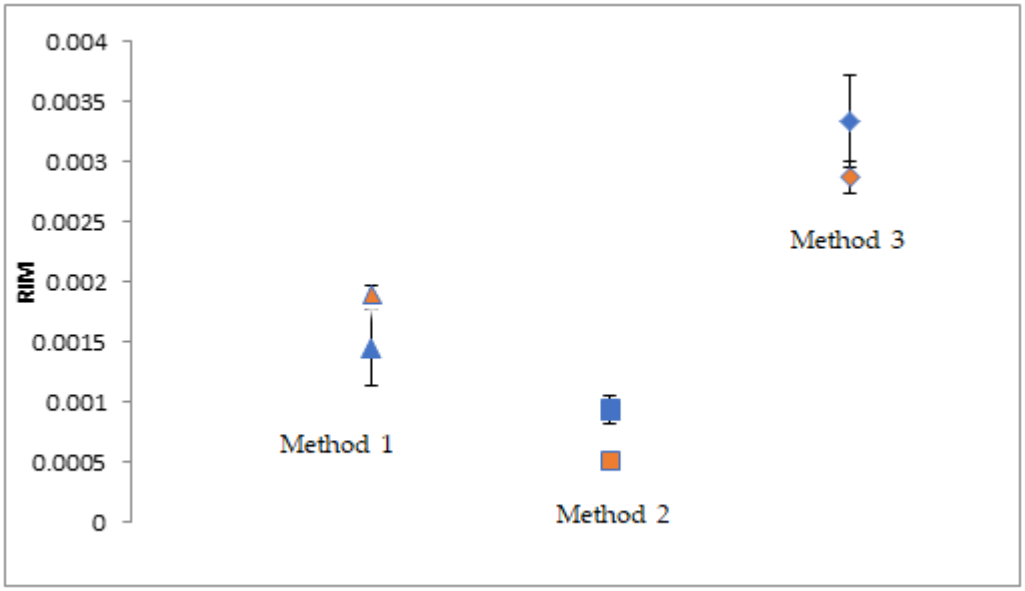

Figure 5-7: Average RIM values achieved by each method of holographic recording as shown in Table 1. 1: Exposed to laser until full saturation of the diffraction efficiency growth, 2: Short exposure then allowed to complete dark process after, 3: Short exposure then thermally enhanced dark process at 90°C, blue points for unmodified zirconium concentration and red points for 3 times zirconium concentration.

A summary of the RIM achieved using different methods is presented in *Figure 5-7.*

Table 5-2: Description of the recording conditions for samples in figure 5-7.

Method.	Details of the sample
1	Exposed to laser until diffraction efficiency peaked (between 60-100 second exposure) (1000 lines / mm)
2	Exposed for 10 seconds and allowed to self-develop for 30 minutes (1000 lines / mm)
3	Exposed for 10 seconds and allowed to self-develop for 30 minutes at 90 degrees (1000 lines / mm)

5.6 Recording mechanism

5.6.1 Mass transport and the thermal process

Holograms with a range of spatial frequencies were recorded using both a 476 nm and 532 nm laser with a total beam intensity of 2.5 mW/cm^2 and 20 mW/cm^2 respectively, with a recording time of 10 seconds. Given the absorption of the material at 476 nm and 532 nm the same number of photons should be absorbed. After recording they were immediately placed in an oven with a temperature over 90 °C. The purpose of these experiments is to investigate the effect of spatial frequency on the dark process thermal post processing.

Compiling the data from all the heated samples at different spatial frequencies a trend emerges as shown in *figure 5-8.*

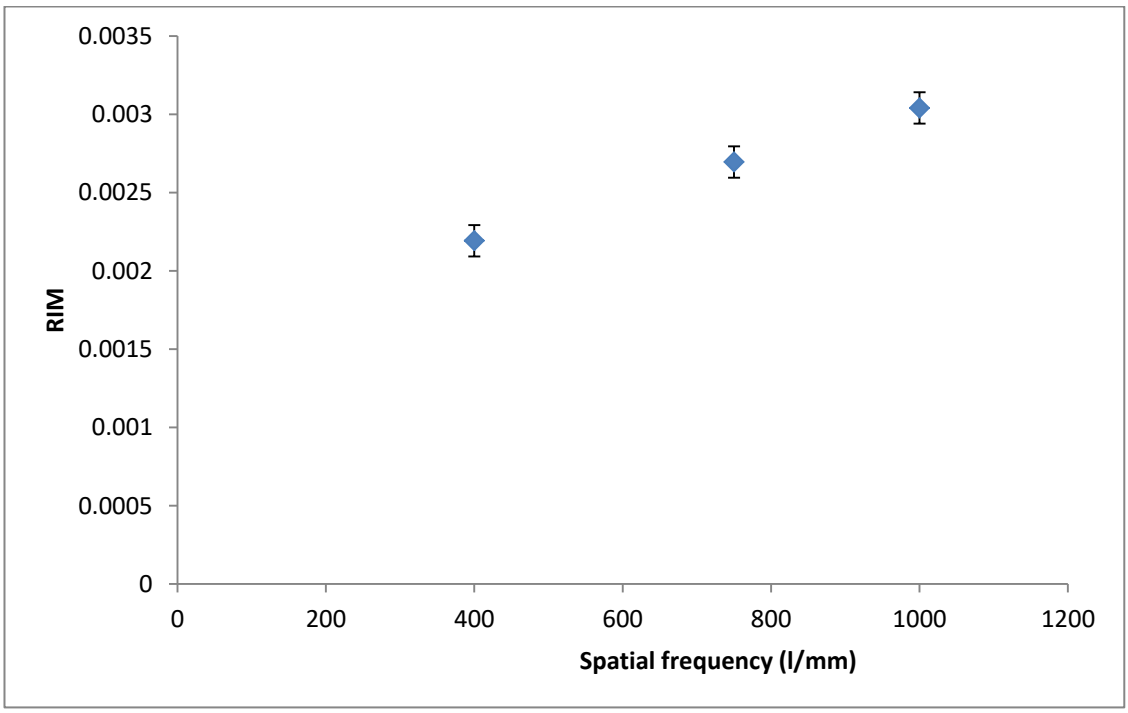

Figure 5-8: Aggregate data of all heated samples (temperature above 90° C, recorded at 476 nm or 532 nm) showing decreased RIM with decreasing spatial frequency.

One possible reason for the reduced effect of temperature curing on RIM at smaller spatial frequencies is the increased diffusion distance particles may have to undergo

with larger fringe spaces. This may indicate that the thermal post processing has an effect on the mass transport of material.

5.6.2 Recording time and RIM

Holograms were recorded in the same conditions as outlined in 7.6.1 with the exception of a varying recording time. Five holograms were recorded for each recording time. Holograms were exposed to the beam for 10, 20, 30, and 40 seconds. After recording they were immediately placed in the oven over 90° C for 30 minutes. All holograms were recorded at 532 nm.

This experiment is intended to investigate how adding more photons to the reaction affects the RIM and the dark process. *figure 5-9* shows the average RIM of the 5 samples for each recording time.

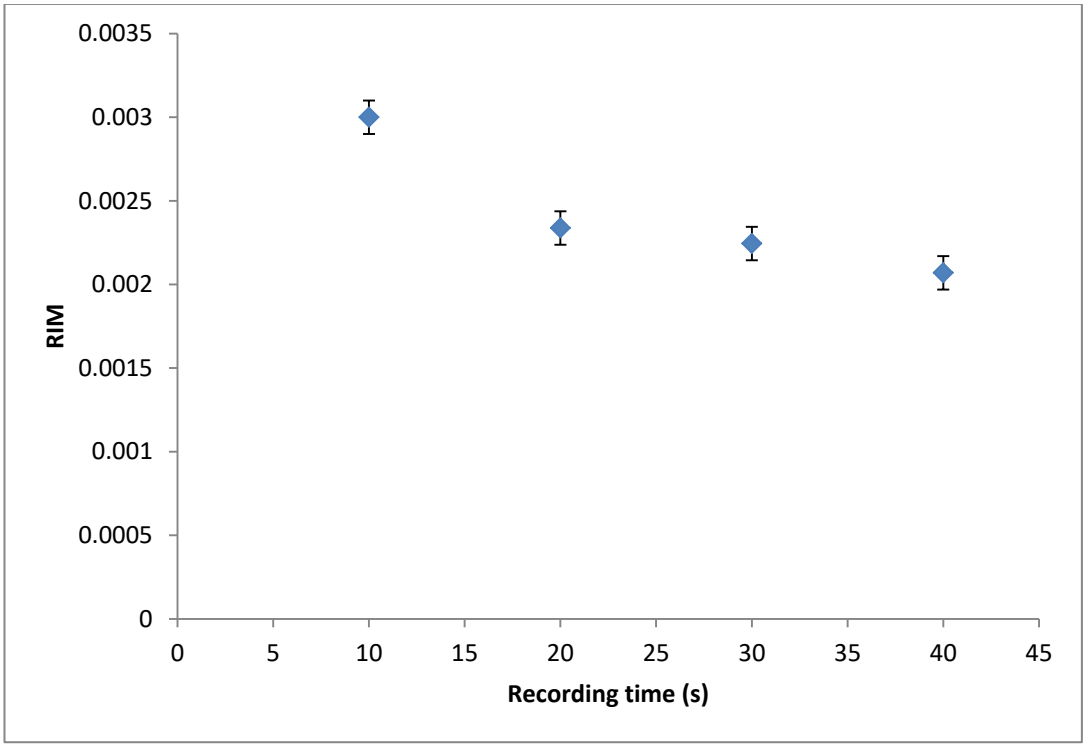

Figure 5-9: RIM vs initial beam exposure time

There is a slight downward trend with RIM as the exposure time increases. It is possible that the additional photons may accelerate the chemical reaction within the sol gel, limiting the mass transport that can take place.

5.7 Discussion:

The average RIM value has been improved using different methods. Producing holograms by exposing the sol-gel sample to the recording beams until the maximum diffraction efficiency was reached produced an average refractive index modulation of $1.4 \times 10^{-3} \pm 1 \times 10^{-4}$. Adding three times the amount of zirconium improved this value by 36% to $1.9 \times 10^{-3} \pm 1 \times 10^{-4}$. This improvement may be in part due to the denser sol-gel matrix that comes with increased zirconium concentrations. The relationship between zirconium concentration and material density is explored by Cullen et al where it is shown that low zirconium concentrations lead to the formation of materials with lower densities. [4]

Thermally treating sol-gel samples during the dark process at 90°C for 30 minutes produced the highest RIM samples with an average value of $3.3 \times 10^{-3} \pm 4 \times 10^{-4}$ at 1000 l/mm, a factor of three improvement compared to unbaked samples. When this method of heating during the dark process is used on samples with 3 times the zirconium concentration, the effect of the heating on the RIM was slightly reduced achieving a value of $2.8 \times 10^{-3} \pm 1 \times 10^{-4}$. It should also be noted that when comparing the RIM achieved during the dark process without thermal treatment (method 2) the sample with the higher zirconium concentration had lower RIM compared with samples with less zirconium. This can be explained by diffusion and/or polycondensation occurring after initial exposure. If diffusion contributes to the dark process, then the denser matrix that occurs when zirconium concentration is higher may

hinder any mass transport through the pores of the matrix. The fact that sol-gel with higher zirconium concentration shows smaller RIM increase during the dark process could also indicate that polycondensation is a contributor to the dark processes, since a more rigid structure (or sol-gel with higher zirconium concentration) has lower potential for densification of the network due to thermal curing.

The relative merits of the physical and chemical changes in improving RIM are shown in *figure* 5-7 and Table 5-3 summarizes all the processes investigated here.

Table 5-3: Summary of Results.

Change /improvement	Sensitivity/grating growth rate	RIM	Comment
Decreased the recording wavelength from green to blue	Increased 8 fold	Unchanged	
Increased Zirconium concentration	Decreased	Increased 30-40%	
Post-exposure thermal treatment	Reduced exposure time to 1/10th	Final RIM improved by a factor of 2.4	Heating immediately after exposure

5.8 Conclusions:

To conclude, a number of different methods have been explored, to the best of authors knowledge for the first time with this sol-gel material, to improve its holographic recording properties and make it suitable for fabrication of HOEs for outdoor applications. An increase of the sensitivity by an order of magnitude was achieved by recording at a wavelength better matched to the material absorption spectrum. The refractive index modulation was improved by a factor of 2.4 by post-recording thermal treatment.

Heat treatment adds a production step to the process, but offers the promise of both shorter light exposure *and* significantly higher final RIM.

The average RIM value of $1.4 \times 10^{-3} \pm 1 \times 10^{-4}$ using typical holographic exposure methods has been improved to $3.3 \times 10^{-3} \pm 4 \times 10^{-4}$ using the thermal treatment method alone. A combination of different aspects of the above processes may improve this further to achieve the target RIM of 4×10^{-2}, as may a more detailed study of the recording dynamics and heating conditions.

5.9 Implications and prospects

The work presented here is of course not an exhaustive study of all possible options or combinations, but it does provide a template and additional knowledge for tailoring the characteristics of this robust, durable, high optical quality material to suit desired specific applications. For example, chemical formulation changes (Zirconium increase) can be used in most applications to achieve a higher RIM but at the cost of grating growth rate. This may better suit applications such as solar collectors [6][7] where RIM is crucial but a slower production rate is tolerable, compared to low cost sensing devices [8-10], where lower RIM can be tolerated but high mass production rate is needed to drive down cost. The suitability of highly environmentally stable materials [1] for application in holographic sensors may seem counterintuitive, but in fact the insensitivity to variations in environmental humidity and temperature make it an ideal matrix to be functionalised for detection of a target analyte, without interference form the environmental conditions.

Better matching between recording wavelengths and the photosensitive material absorption properties very significantly increases the grating growth rate and improves production rates. This can be particularly useful in applications such as HOE TIR couplers [11] where the short wavelength enables recording without prisms; however,

short wavelength lasers tend to be significantly more expensive at present, and the final RIM reached does not seem to be improved by recording in blue.

In order to fully realise the potential for holograms to function as solar concentrators a high value of RIM is required. This next chapter presents the characterisation of a high RIM cyclic allylic sulphide based recording material and practical concentration tests with PV cells and a solar simulator.

5.10 References

[1] Mikulchyk, Tatsiana, et al. “Synthesis of Fast Curing, Water-Resistant and Photopolymerizable Glass for Recording of Holographic Structures by One- and Two-Photon Lithography.” *Advanced Optical Materials*, vol. 10, no. 6, 2022, p. 2102089., https://doi.org/10.1002/adom.202102089.

[2] Baldry, I. K., et al. “Volume Phase Holographic Gratings: Polarization Properties and Diffraction Efficiency.” *Publications of the Astronomical Society of the Pacific*, vol. 116, no. 819, 2004, pp. 403–414., https://doi.org/10.1086/383622.

[3] Oubaha, M.; *Introduction to Hybrid Sol-Gel Materials,* Volume 3, World Scientific Reference of Hybrid Materials. World Scientific Publishing Co. Singapore

[4] Cullen, M.; O'Sullivan, M.; Kumar, A.M.; The role of the hydrolysis and zirconium concentration on the structure and anticorrosion performances of a hybrid silicate sol-gel coating. *Journal of Sol-Gel Science and Technology* **2018**, *86*(3), pp 553-567.

[5] Cullen, M., et al. “The Role of the Hydrolysis and Zirconium Concentration on the Structure and Anticorrosion Performances of a Hybrid Silicate Sol-Gel Coating.” *Journal of Sol-Gel Science and Technology*, vol. 86, no. 3, 2018, pp. 553–567., https://doi.org/10.1007/s10971-018-4657-3.

[6] Marín-Sáez, Julia, et al. “Characterization of Volume Holographic Optical Elements Recorded in BAYFOL HX Photopolymer for Solar Photovoltaic Applications.” *Optics Express*, vol. 24, no. 6, 2016, https://doi.org/10.1364/oe.24.00a720.

[7] Chrysler, Benjamin D., and Raymond K. Kostuk. “Volume Hologram Replication System for Spectrum-Splitting Photovoltaic Applications.” *Applied Optics*, vol. 57, no. 30, 2018, p. 8887., https://doi.org/10.1364/ao.57.008887.

[8] Branigan, Emma, et al. “Direct Multiplexing of Low Order Aberration Modes in a Photopolymer-Based Holographic Element for Analog Holographic Wavefront Sensing.” *Environmental Effects on Light Propagation and Adaptive Systems IV*, 2021, https://doi.org/10.1117/12.2599912.

[9] Yetisen, Ali K., et al. “Holographic Sensors: Three-Dimensional Analyte-Sensitive Nanostructures and Their Applications.” *Chemical Reviews*, vol. 114, no. 20, 2014, pp. 10654–10696., https://doi.org/10.1021/cr500116a.

[10] Naydenova, I.; Holographic sensors. Optical Holography. Edited by Pierre-Alexandre Blanche, Elsevier Inc, 2020, ISBN: 978-0-12-815467-0

[11] Fernández, R., et al. “Holographic Waveguides in Photopolymers.” *Optics Express*, vol. 27, no. 2, 2019, p. 827., https://doi.org/10.1364/oe.27.000827.

6 Characterisation of High RIM Photopolymer

Low angular selectivity and high diffraction efficiency are desirable qualities in holographic solar concentrators. As demonstrated by the theoretical modelling presented in chapter 5, to achieve this, a high refractive index modulation is required. This chapter presents the characterisation of a high RIM photopolymer and a test of its performance as a holographic lens in a solar simulator.

6.1 Introduction to the ring opening photopolymer.

The photopolymer studied in this chapter has a ring opening photo polymerisation mechanism with a cyclic allylic sulphide (CAS) based monomer dispersed in a cellulose acetate butyrate binding matrix. Galli et at report a high RIM of 0.03 – 0.05 [1, 2].

The high RIM of this photopolymer material indicates that it could be very well suited for use as a solar concentrator, however the material must be characterised at a range of spatial frequencies in order to determine whether an appropriate holographic lens can be designed. As shown in chapter 5 a holographic lens is a diffractive device made up of a range of spatial frequencies, that is why to ensure homogeneous diffraction efficiency of the final device it is necessary to study the response of the material to different spatial frequencies.

6.2 Sample preparation.

The development and preparation of the photopolymer used in this chapter is detailed in the experimental section of the literature [2] and is summarised here.

“CAB (cellulose acetate butyrate (CAB-531-1)), MDTOA (7-methylene-1,5-dithiacyclooctan-3-yl acetate), PETMP (pentaerythritol tetrakis(3-mercaptopropionate)) and the plasticizer (Citrofol AHII) were dissolved in butyl acetate using the concentrations reported in Table 8-1. The photoinitiator I784 (Irgacure 784)(Bis(2,6-difluoro-3-[1-hydropyrrol-1-yl]phenyl)titanocene) was then added to the formulation.

The solution was stirred for at least 4 h and sonicated to remove air bubbles before deposition" [2]

Table 6-1: Chemical composition of photopolymer [2]

Photopolymer formulation	Sample	Component (mass, mg)				
		MDTOA	PETMP	CAB	Plasticizer	I784
MDTOA/PETMP/I784 MDTOA/thiol 1:1	8[a]	126	70.8	250	100	100

The study details the use of multiple concentrations of monomer MDTOA, the version used in this study is 19.5% wt (shown in table 8-1) and is capable of achieving refractive index modulations of 0.0346 when thermally treated. [2] Further details of the chemical process to make the monomer are included here. [3]. The figure below is a summary of the synthesis process in used to make the monomer in papers [2, 3].

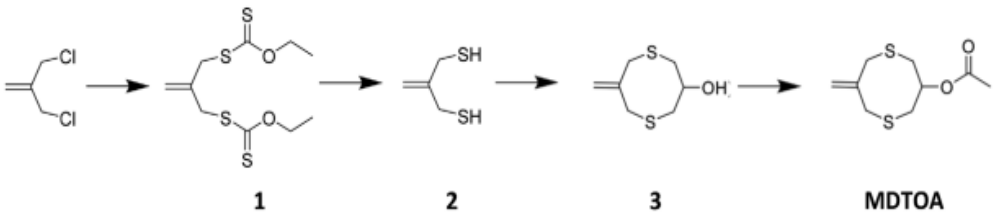

Figure 6-1: Summary of monomer synthesis [2].

This photopolymer's refractive index modulation is enhanced when thermally treated after holographic recording. This is due to high temperatures aiding in the mass transport of writing material. After holographic recording the samples were thermally treated in an oven at 120 degrees for 2.5 hours a process that was optimised by Galli et al in their paper [2].

The samples used in this chapter were spin coated and have a thickness of 5 ± 2 μm (determined through the fitting of Bragg curves).

Holograms were probed with different polarisation states to better understand how unpolarised sunlight would diffract through the holographic lenses. This is necessary as s and p polarised light diffract through gratings at different efficiencies [4].

6.3 Experimental:

6.3.1 Holographic recording set up

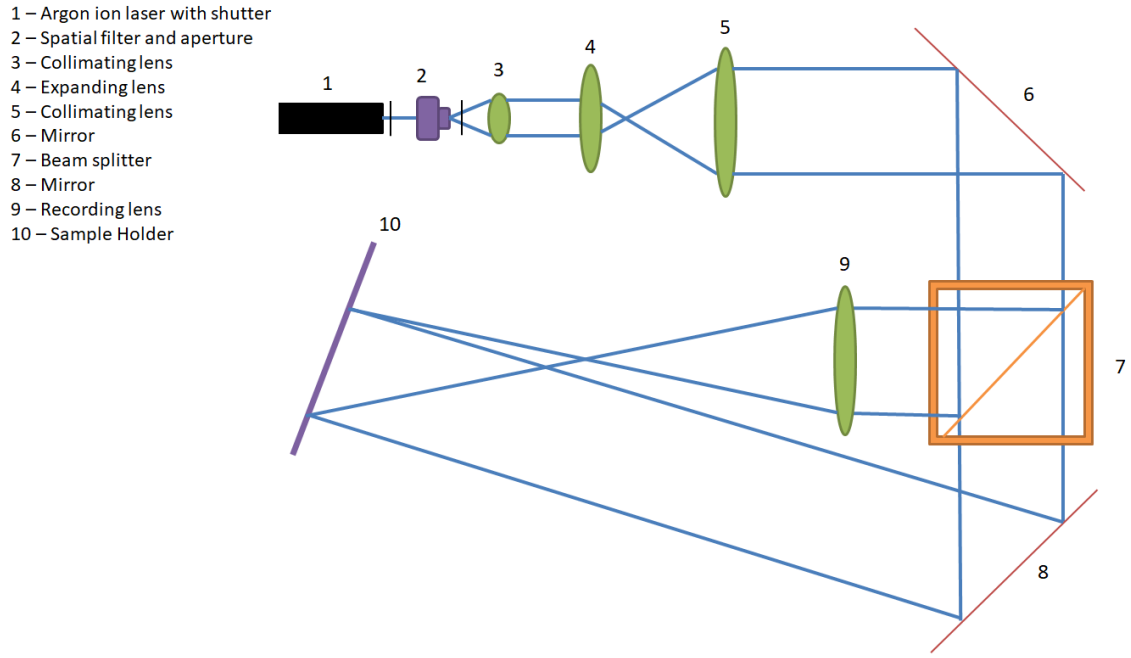

Figure 6-2: Holographic lens recording set up

The recording of holographic transmission gratings and holographic lenses was done through the interference of two beams from an argon ion laser at 476 nm. The beam passes through an electronic shutter before being spatially filtered and collimated. The beam then passes through an aperture and beam splitter where it is then expanded to have a diameter of 2 cm. The collimated beam is then reflected into a beam splitter where it splits into two equidistant mirrors (in order to maintain ensure that the beams path difference is less than the laser coherence length). From here the beams are directed onto a sample, the mirrors can be adjusted to record in transmission mode at

different spatial frequencies. A neutral density filter is added when necessary to equalise the beam intensity. To record holographic lenses a 5 cm focal length achromatic doublet is added to one beam path. The sample holder can be adjusted by rotation to record slanted gratings.

Either 532 nm NDYAG laser or a 633 nm laser beams are used to probe the recorded transmission holographic gratings and holographic lenses. The 532 nm laser beam passes through a half wave plate followed by a polarising beam splitter and another half wave plate. In order to probe in S and P polarised states the second half wave plate can be inserted or removed to change polarisation states.

6.3.2 PV Cell IV curves

In order to evaluate and compare the performance of different holographic lenses as solar concentrators a solar cell was coupled with the holographic lenses in a solar simulator.

An Ossila Source measure unit – X200 was used to measure the IV curves from a solar cell which were generated by rotating the holographic lens and solar cell (1 X 2 cm) which sits inside the focal length of the holographic lens through a series of angles in front of the solar simulator. Direct light was blocked from reaching the PV cell so only light diffracted from the holographic lens would reach it.

6.4 Results:

A characterisation of the material was carried out at several spatial frequencies in order to experimentally determine the RIM at different spatial frequencies and to verify the regime of operation of the holographic gratings.

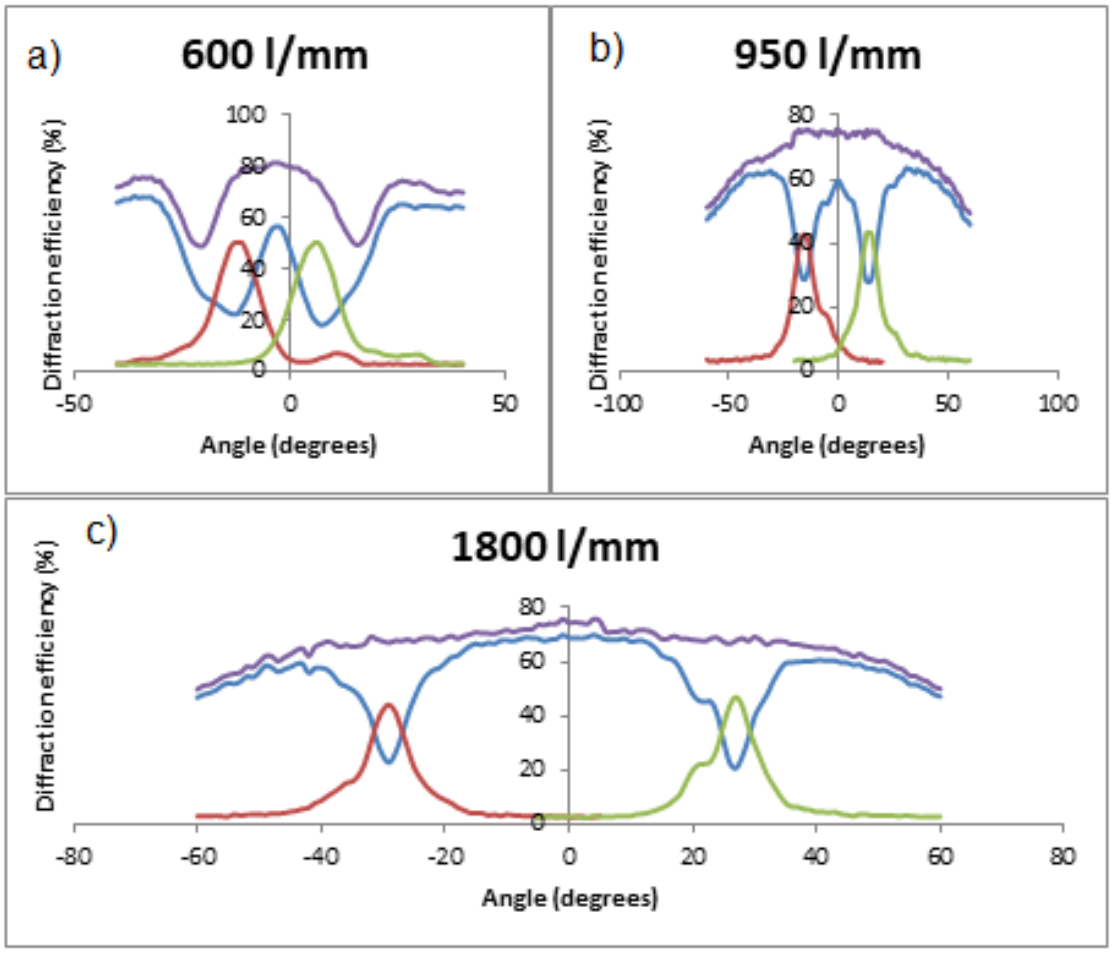

Figure 6-3: Bragg angular selectivity curves for spatial frequency test (probed at 532 nm). Zero order curve (blue), first order curves (red and green), zero and first order summed (purple).

Firstly, the regime of operation can be determined visually by observing multiple orders simultaneously when probing the sample, this can also be shown quantitatively by summing the intensities of light diffracted in the first order Bragg curves with the intensity of the zero order light. When summed, a smooth curve changing only as reflection losses increase would indicate that all light is going to the first order. Examples are included in *figure 6-3* in each graph the purple line is the sum of the fist and zero order light at each angle. The smooth curves in *figure 6-3 b)* and *c)* indicate that all the light diffracted from the zero order is detected in the first order. The purple line in *figure 6-3 a)* however, indicates there is light going into other diffraction orders,

and the conditions for volume diffraction are not present in this sample. The average RIM of the samples was 0.027 ± 0.010 in layers with thickness 5 ± 2 μm, these values were found by matching the experimental Bragg selectivity curves to modelled counterparts. An average of the refractive index modulation across all recorded spatial frequencies was taken as there was no statistical difference between them.

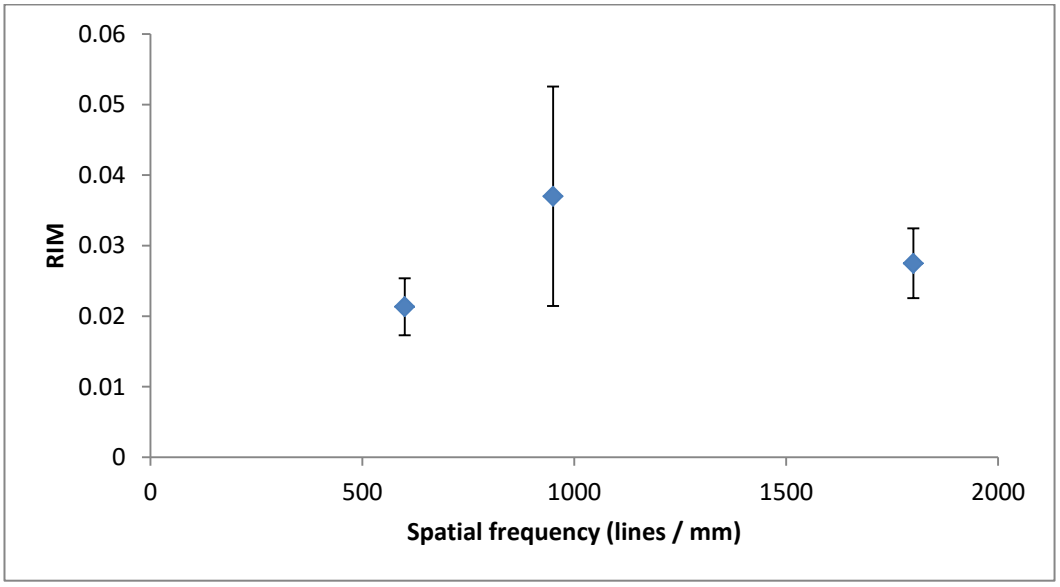

Figure 6-4: Distribution of RIM across recorded spatial frequencies.

Looking back to the model in *figure 3-4*, we would expect this material to enter the volume regime somewhere between 1000 and 1200 l/mm for this RIM. This is reflected in the Bragg curves in *figure 6-3*, with the 950 l/mm sample teetering on the edge of thin and volume regime. *Figure 6-4* shows that the value of RIM is independent of spatial frequency.

With the lower limit to the spatial frequency for this material determined from its RIM, an appropriate holographic lens can be designed that operate entirely in the volume regime. A 5 cm focal length lens with a central spatial frequency of 1500 l/mm and an upper and lower spatial frequency of 1700 and 1100 l/mm at the respective lens edges was recorded. The lens diameter was 2 cm.

Given the unpolarised and polychromatic nature of sunlight, Bragg curves were taken with S and P polarised beams at 532 nm. This gives a more complete picture of how the holographic lenses redirect sunlight.

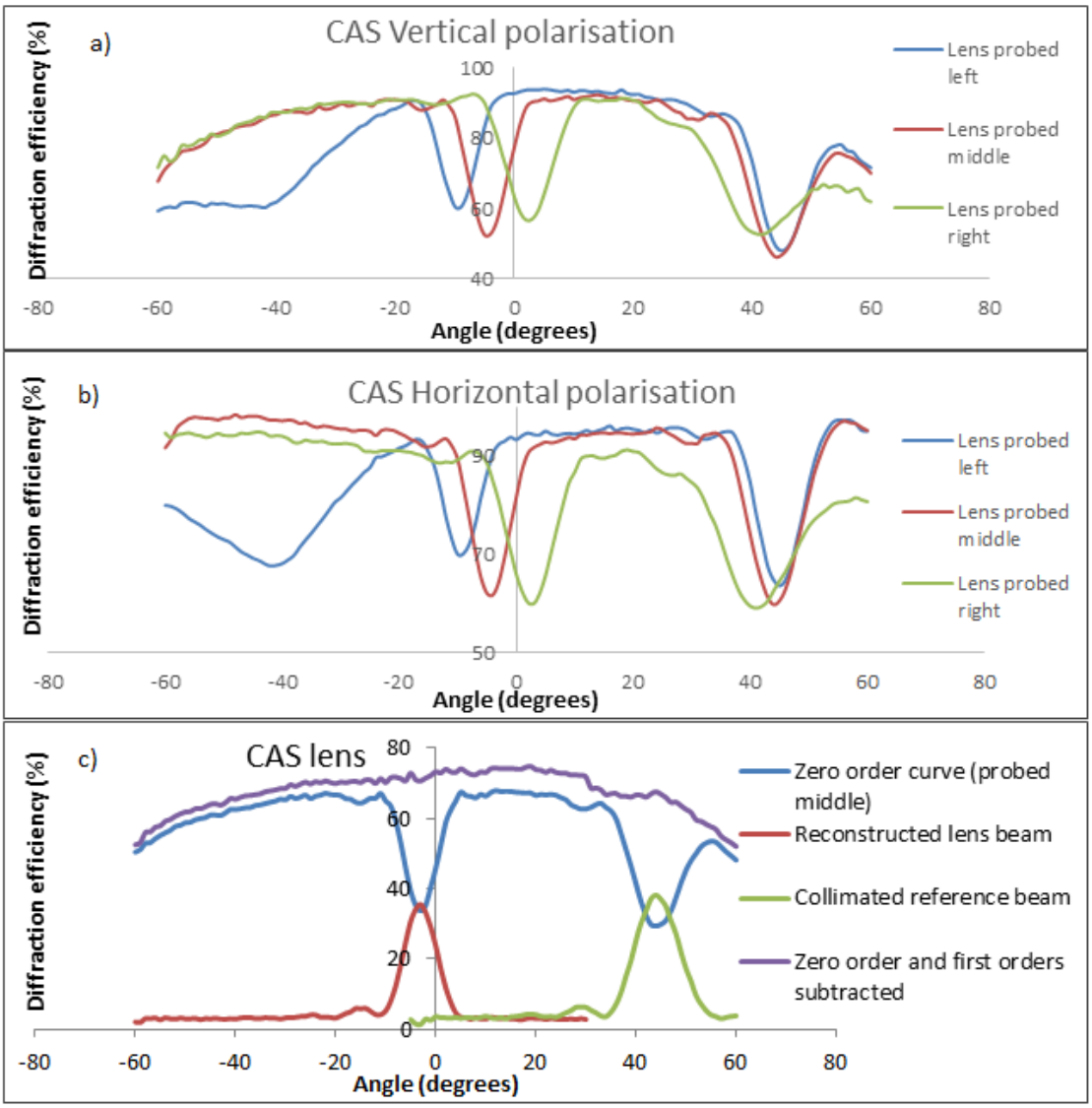

Figure 6-5: a) Zero order Bragg selectivity curves of CAS lens probed with vertically polarised light in the left, middle and right of lens. b) Zero order Bragg selectivity curves of CAS lens probed with horizontally polarised light in the left, middle and right of lens. c) Zero order curve (blue), first order curves (red and green), zero and first order summed (purple). All probed at 532 nm.

At these values of spatial frequency and thickness there is a small difference in diffraction efficiency when probed with S and P polarisation states of light; the difference is on the order of about 10 % with vertically polarised light diffracting more light.

To obtain spatial frequency and slant information for the holographic lens zero order Bragg curves were taken at both edges and the middle of the lens (-1, 0, +1,0 cm $\pm 0.1\ cm$). The RIM and thickness information was found by fitting the Bragg curve (probed in the middle of the lens) and matching it to a model of Bragg angular selectivity curves using equations 2.3, 2.4 and 2.5. The slant and spatial frequency information was calculated from the zero order Bragg curves by finding the difference in Bragg angle positions.

Table 6-2: Information on CAS lens taken experimentally from Bragg curves

Probe area	SF (l/mm) ($\pm 50\ l/mm$)	Slant in air. (degrees) (± 1 °)	RIM (from fit) (± 0.0005)	Thickness (from fit) (μm) (± 0.2 μm)
L	1650	17		
M	1450	19	0.029	4
R	1150	22		

The minimum spatial frequency of the lens is near 1100 l/mm putting it near the volume regime for its calculated RIM of 0.029 and a Rho value of 8. The lens is therefor at its minimum angular selectivity values with a full width half max of 10 degrees (probed in middle) for the given RIM and material thickness.

In order to see the complete benefits of a small angular selectivity for solar concentration the lens recorded in CAS was compared in a solar simulator to a lens recorded in a Covestro photopolymer with identical properties including diffraction efficiency but with more angular selectivity (from thicker layers 10 μm). The figure below shows the Covestro lens probed at 532 nm with vertically and horizontally polarised light.

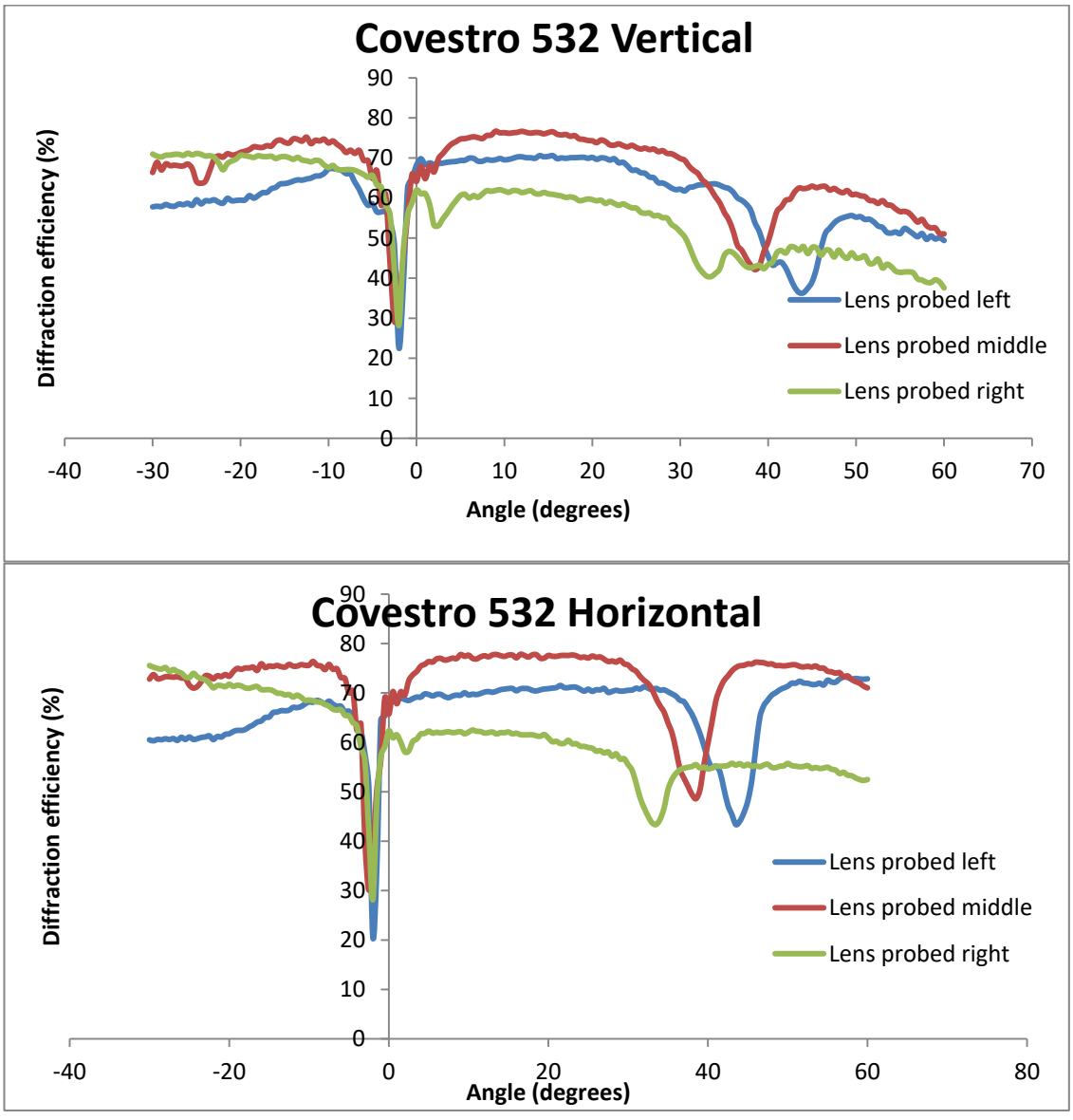

Figure 6-6: Zero order Bragg selectivity curves probed with S and P polarised light at 532 nm for Covestro lens.

Table 6-3: Information on Covestro lens taken experimentally from Bragg curves

Probe area	SF (l/mm) ($\pm 50\ l/mm$)	Slant in air. (degrees) (± 1 °)	RIM (from fit) (± 0.0005)	Thickness (from fit) (μm) (± 0.2 μm)
L	1450	23		
M	1300	20	0.014	9
R	1150	17		

6.5 Solar simulator

A test to quantify how the both the CAS and Covestro lenses would perform in sunlight was carried out (as described previously). An example IV curve is presented with the peak current values generated by the CAS lens at different angles.

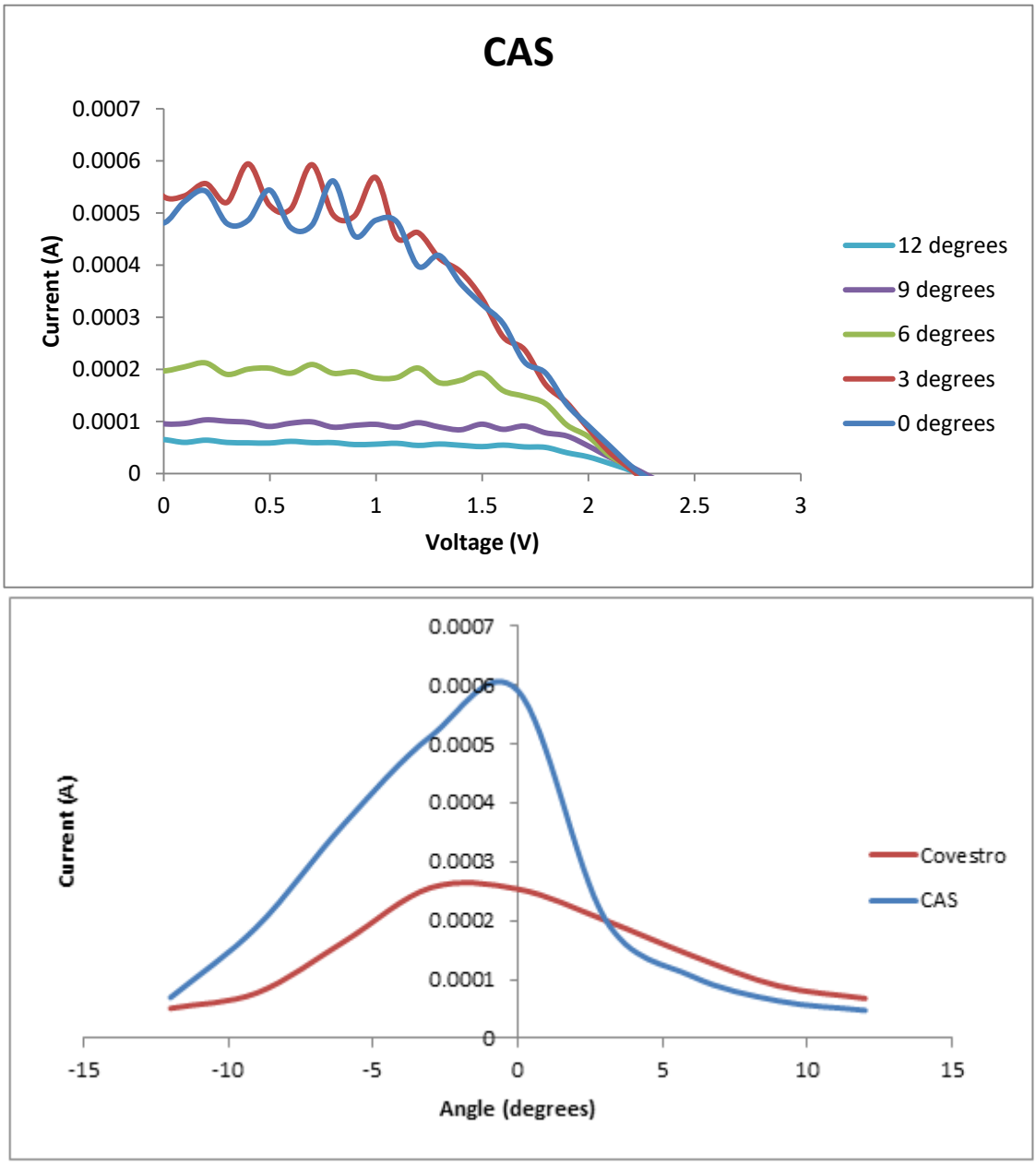

Figure 6-7: Example IV curve and current value achieved in PV cell at a range of angles in CAS and Covestro lens.

Despite having equal values of diffraction efficiency, the lens with lower angular selectivity (CAS) had a higher current value when on Bragg than the alternate lens. Calculating the area under each curve the CAS works out to be 0.00627 and the Covestro 0.00361 amp degrees, meaning the CAS lens is coupling almost double the light of the Covestro lens.

This is likely because more disperse light is coupled from the solar simulator. This gives holograms with low angular selectivity a twofold advantage of being more effective solar trackers and coupling more disperse light and sending it to the PV cell.

6.6 Conclusion:

The photopolymer was characterised at a thickness of 5 ± 2 μm at various spatial frequencies for the purposes of experimentally determining the appropriate conditions to make volume holographic gratings in this material. An important determining factor for this was the RIM which had an average value of 0.027 ± 0.010 from the characterisation tests. Holograms recorded in layers this thin will have low angular selectivity – an important factor for holographic solar concentrators. However this low angular selectivity is useless without the high RIM this material offers to drive the diffraction efficiencies to high values and allows it to operate in the volume regime. When comparing lenses of equal diffraction efficiency but differing angular selectivity, the less selective lens coupled double the light as the more selective lens. This has major implications for their use in solar concentration as less selective lenses have the twofold advantage of passive tracking and more light coupling.

With a combination of modelling of the Rho factor and experimental results a holographic lens was carefully designed and recorded for minimal angular selectivity. When compared against a lens with identical properties with the exception of angular selectivity an approximate threefold increase to the PV cells performance was measured when probed on Bragg. This result highlights the effect that low angular selectivity gratings can have in practical solar concentrating environments, and the benefits that a high RIM material can offer. This does not come without its limitations as in order to remain in the volume regime high spatial frequencies are required which could limit device design.

With the high values of RIM achieved in many novel self-processing materials, the modelling employed here could help shape lens devices optimising for low angular selectivity and high RIM. The high RIM achieved in the photopolymer studied in this chapter, combined with its stable performance across multiple spatial frequencies makes it a good candidate for holographic lenses [1, 2, 5-13].

High refractive index modulation and thin layers have proven to make for effective holographic lenses, their low angular selectivity allowing the coupling of more light and enabling more effective passive solar tracking. However some issues inherent to holographic gratings arise when recording at higher spatial frequencies, the next section will explore holographic chromatic dispersion and potential holographic solutions to correct it.

6.7 References:

[1] Bianco, Andrea, et al. “New Photosensitive Systems for Volume Phase Holography.” *SPIE Proceedings*, 2017, https://doi.org/10.1117/12.2264908.

[2] Galli, Paola, et al. “Cyclic Allylic Sulfide Based Photopolymer for Holographic Recording Showing High Refractive Index Modulation.” *Journal of Polymer Science*, vol. 59, no. 13, 2021, pp. 1399–1413., https://doi.org/10.1002/pol.20210192.

[3] Evans, Richard A., and Ezio Rizzardo. “Free-Radical Ring-Opening Polymerization of Cyclic Allylic Sulfides. 2. Effect of Substituents on Seven- and Eight-Membered Ring Low Shrink Monomers.” *Macromolecules*, vol. 33, no. 18, 2000, pp. 6722–6731., https://doi.org/10.1021/ma9917646.

[4] Baldry, I. K., et al. “Volume Phase Holographic Gratings: Polarization Properties and Diffraction Efficiency.” *Publications of the Astronomical Society of the Pacific*, vol. 116, no. 819, 2004, pp. 403–414., https://doi.org/10.1086/383622.

[5] Bruder, Friedrich-Karl, et al. “The Chemistry and Physics of Bayfol® HX Film Holographic Photopolymer.” *Polymers*, vol. 9, no. 12, 2017, p. 472., https://doi.org/10.3390/polym9100472.

[6] Zhang, Deming. “One-Axis Tracking Holographic Planar Concentrator Systems.” *Journal of Photonics for Energy*, vol. 1, no. 1, 2011, p. 015505., https://doi.org/10.1117/1.3590943.

[7] Chemisana, Daniel, et al. “Holographic Lenses for Building Integrated Concentrating Photovoltaics.” *Applied Energy*, vol. 110, 2013, pp. 227–235., https://doi.org/10.1016/j.apenergy.2013.04.049.

[8] Chrysler, Benjamin D., and Raymond K. Kostuk. “Volume Hologram Replication System for Spectrum-Splitting Photovoltaic Applications.” *Applied Optics*, vol. 57, no. 30, 2018, p. 8887., https://doi.org/10.1364/ao.57.008887.

[9] Collados, M. Victoria, et al. “Holographic Solar Energy Systems: The Role of Optical Elements.” *Renewable and Sustainable Energy Reviews*, vol. 59, 2016, pp. 130–140., https://doi.org/10.1016/j.rser.2015.12.260.

[10] Sherif, Hosam, et al. “Characterization of an Acrylamide-Based Photopolymer for Data Storage Utilizing Holographic Angular Multiplexing.” *Journal of Optics A: Pure and Applied Optics*, vol. 7, no. 5, 2005, pp. 255–260., https://doi.org/10.1088/1464-4258/7/5/007.

[11] Lee, Jeong-Hyeon, et al. “Holographic Solar Energy Concentrator Using Angular Multiplexed and Iterative Recording Method.” *IEEE Photonics Journal*, vol. 8, no. 6, 2016, pp. 1–11., https://doi.org/10.1109/jphot.2016.2634699.

[12] Naydenova, Izabela, et al. “Photopolymer Holographic Optical Elements for Application in Solar Energy Concentrators.” *Holography - Basic Principles and Contemporary Applications*, 2013, https://doi.org/10.5772/55109.

[13] Bianco, G., et al. “Photopolymer-Based Volume Holographic Optical Elements: Design and Possible Applications.” *Journal of the European Optical Society: Rapid Publications*, vol. 10, 2015, https://doi.org/10.2971/jeos.2015.15057.

7 Device Proof of Concept:

7.1 Introduction:

One noteworthy feature of the holographic lenses is the chromatic dispersion associated with them illustrated in chapter 4 and in the following example. The figure below shows how diffracted light from a white light source forms a focal point but the lateral position of the focus depends on the wavelength.

Figure 7-1: On Bragg collimated white light source diffracting through CAS lens.

The dispersion of the wavelengths could raise challenges for solar concentration or potentially provide opportunity. As discussed previously it's possible to tune the bandgap of gallium arsenide solar cells for particular wavelengths [1, 2]. However not all solar cells operate this way and so the chromatic dispersion only serves to reduce the concentration factor of the lens.

7.2 Holographic dispersion correction

In this section a holographic solution to correcting the dispersion is explored.

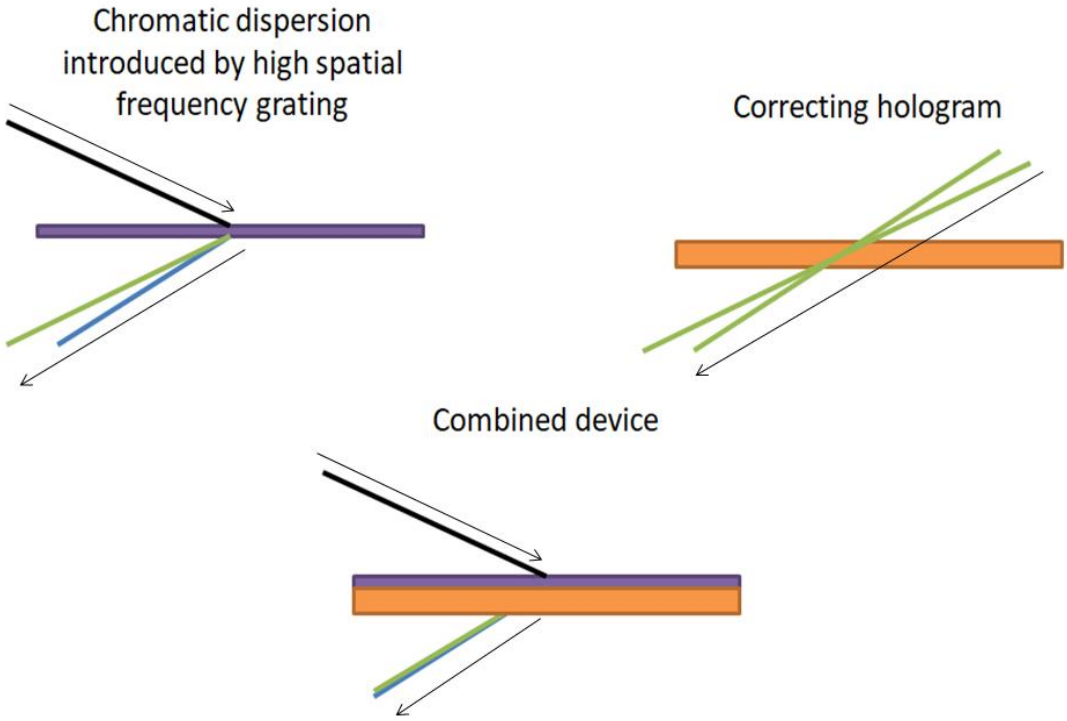

Figure 7-2: Chromatic dispersion of high spatial frequency grating corrected with hologram.

By measuring the difference in angle between two diffracting wavelengths, the dispersion between them can be corrected by recording a hologram using those angles as the angles of the object and reference waves. This is illustrated in the figure above. In theory this method can be used to correct dispersion for any hologram, however there are some practical limitations.

As explored already in the modelling section in *figure 3-5* chromatic dispersion is exaggerated at larger spatial frequencies. This means that as the spatial frequency of the hologram causing the chromatic dispersion increases so too must the spatial frequency of the correcting hologram. Furthermore because the spatial frequencies of the correcting holograms is in the order of 50-300 l/mm the angular separation as described previously would be on the scale of 1-3 degrees, in other words low spatial frequency holograms have low chromatic dispersion.

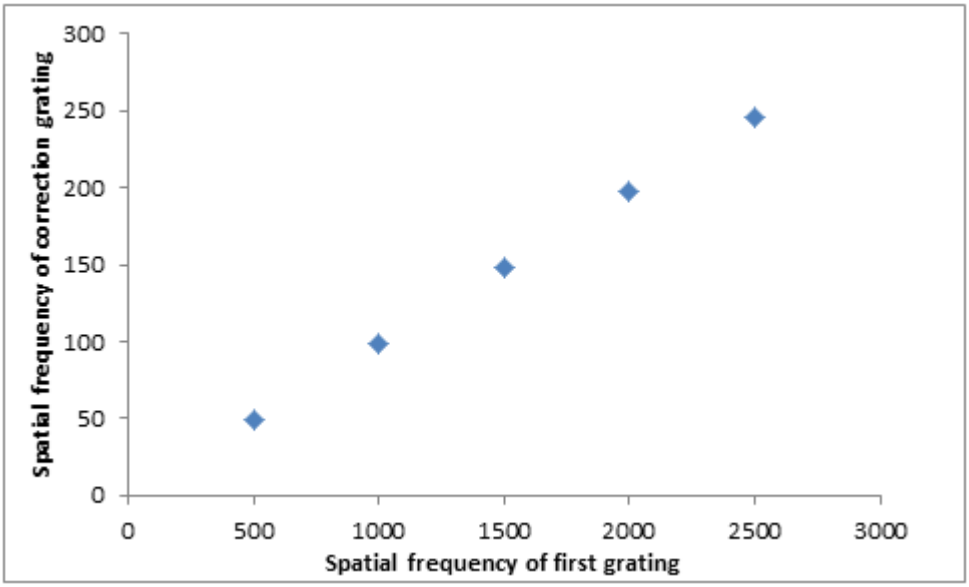

Figure 7-3: Spatial frequency of correction hologram required to superimpose 660 nm light onto 530 nm spot given the spatial frequency of the hologram that introduced the dispersion.

These values were calculated using equation 2.2 to find the difference in angle between a 660 and 530 nm beam, probed at their Bragg angle at a particular special frequency. The spatial frequency of the correction hologram was calculated using the same equation, using the angles calculated from the Bragg angle difference between the two wavelengths. It's advantageous for the correcting holograms to have a low angular and chromatic selectivity so that it can couple a broad range of wavelengths at different angles, which is useful in the context of solar concentration. For this reason each hologram should have a Q or Rho factor equal to 10, to keep it in the volume regime but minimise angular selectivity. Even with this limitation to the thickness of correcting holograms, their thickness can reach mm scale values which introduce some practical issues.

7.3 Experimental

An experiment was designed to demonstrate a proof of concept for a holographic chromatic dispersion corection device. The same set up described in *figure 7-2* was used

to record the transmission grating with the exception of the lens marked (9) being removed. A 1600 l/mm grating was recorded at 476 nm using and Argon ion laser. The location of the diffracted beam was marked on a piece of paper attached to a stable surface. The wavelength of the Argon ion laser was changed to 514 nm and the location of the new green diffracted spot was marked on the paper. With the spots for where the blue and green light fall marked, the set up was changed to record the correction grating. This was done using a series of mirrors and beam splitters, a simplified illustration is shown in *figure 7-4.* The recording and object beams were alligned with the two spots marked on the paper while also overlapping on the sample holder which had not changed position. The correction hologram was then recorded.

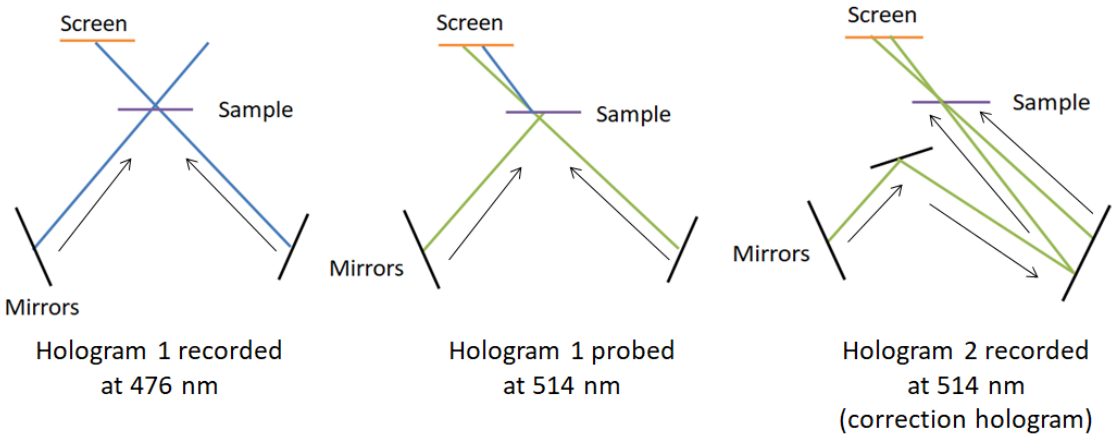

Figure 7-4: Simplified set up for chromatic dispersion correction device.

7.4 Results

With both holograms recorded the two were stuck together (using the natural adheason of the photopolymer). The device was then probed at 476 nm and 514 nm.

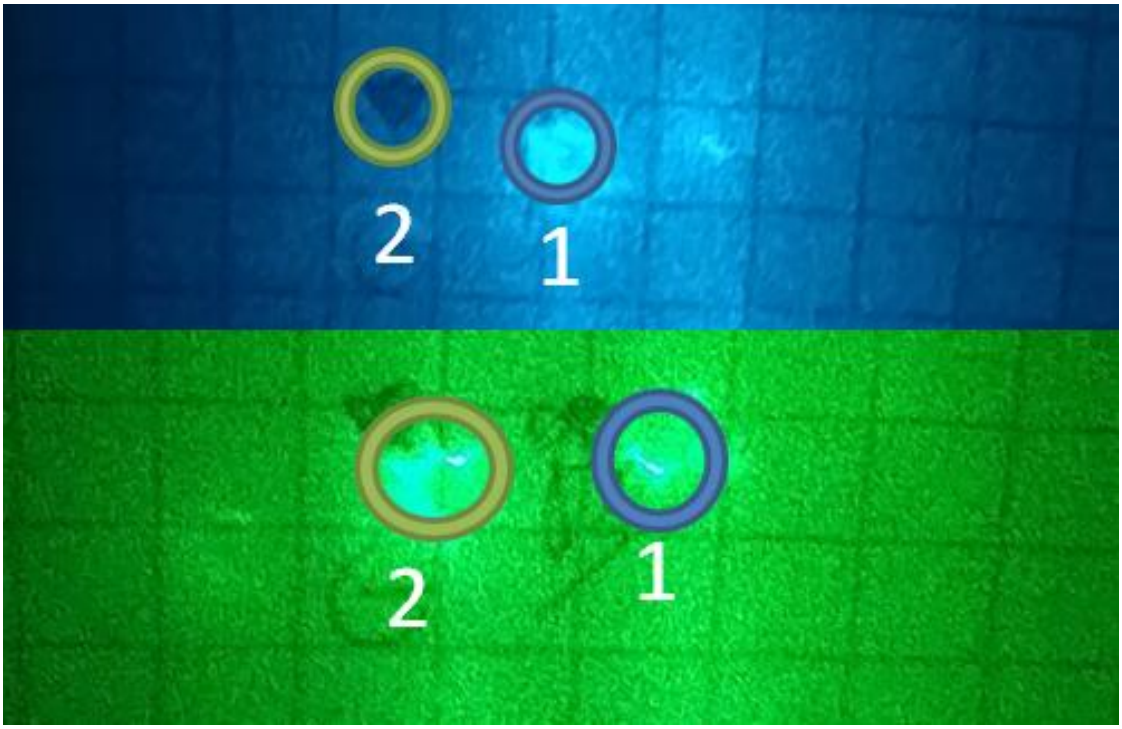

Figure 7-5: Diffracted beams from stacked grating probed at 476 nm and 514 nm.

The spots marked 1 and 2 on the figure above show where the blue and green light fall respectively when diffracting through the 1600 l/mm grating. When the full device is probed (the two stacked gratings) in blue, the beam path is unchanged. When probed in green however it can be seen in *figure 7-5,* that the light is being diffracted by the correction grating from spot 2 onto spot 1.

7.5 Challenges

This proof of concept experiment had some limitations. The correction grating had a thickness of 50 μm and with a spatial frequency of aproximately 150 l/mm was operating in the thin regime and had a diffraction efficiency of less than 1%. Attempts to make a correction hologram in the volume regime were made however with a thickness of 450 μm this only served to intoduce significant scater to the beam as shown in *figure 7-6.*

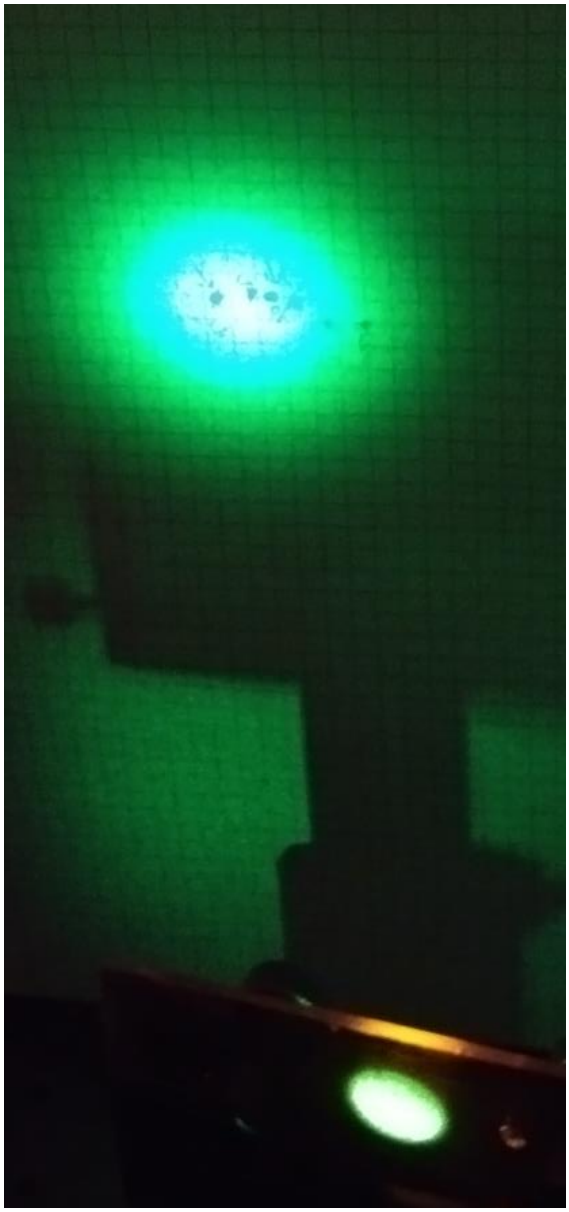

Figure 7-6: Diffraction through 450 μm correction hologram.

Addressing this issue would also require some material change to reduce scatter, which is beyond the scope of this proof of concept experiment. There are some further insights that can be drawn from the modeling and experimental results that can help shape the design of solar concentrating holographic devices.

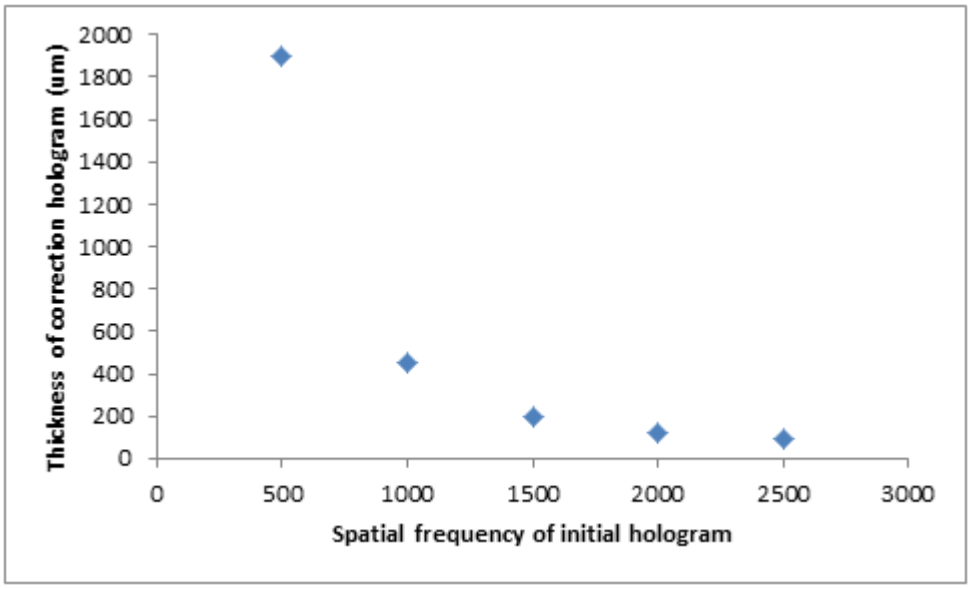

Figure 7-7: Spatial frequency of dispersion introducing hologram and the required thickness of the correction hologram given Q=10 (directing 660 nm light onto the 530 nm spot)

The above figure shows how the required thickness of a correction hologram in the volume regime changes with the spatial frequency of the hologram introducing the abberation. For spatial frequencies in the 2000 l/mm + the range of the thickness of the correcting hologram is in a regime where scatter is less likely to occur with layers less than 125 µm.

7.6 Solar concentrating device

Using what was learned from the proliminary experiments, a hypothetical holographic solar concentration device suitable for concentration onto a long thin strip of a PV cell is theorised. *Figure 7-8* illustrates a side view of such a PV cell with a series of transmission holograms above it (fixed spatial frequency not lenses). The figure is to scale, with accurate angles and distances.

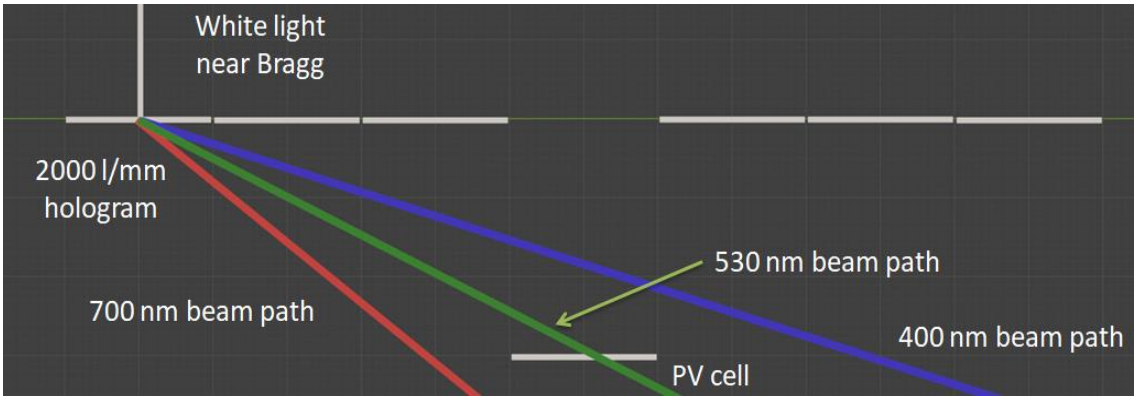

Figure 7-8: Chromatic dispersion from 2000 l/mm grating on PV cell in concentration device.

This first figure shows the extent of the chromatic dispersion for the outermost holographic cell of the device at 2000 l/mm. It's clear that many wavelengths that a gallium arsenide cell for example could absorb are directed beyond the PV cell target. This is less of an issue for holograms closer to the cell.

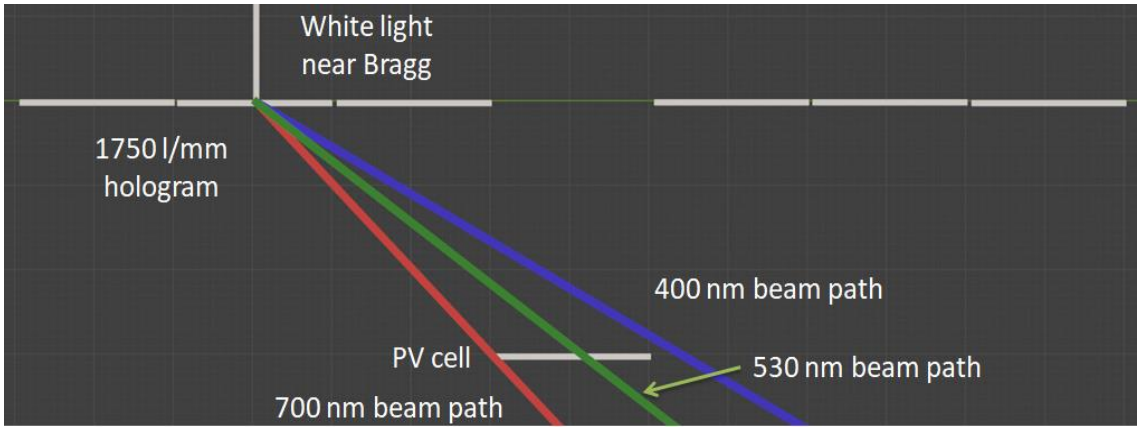

Figure 7-9: Chromatic dispersion from 1750 l/mm grating on PV cell in concentration device.

Far less of the light from the 1750 l/mm cell misses the target. The reason for this is twofold. One, the lower spatial frequency of the device reduces the angular spread of the wavelength paths. Two, the lower spatial frequency holographic cells are naturally closer to the PV cell; meaning the PV cell will intercept the cone of light sooner before it disperses further.

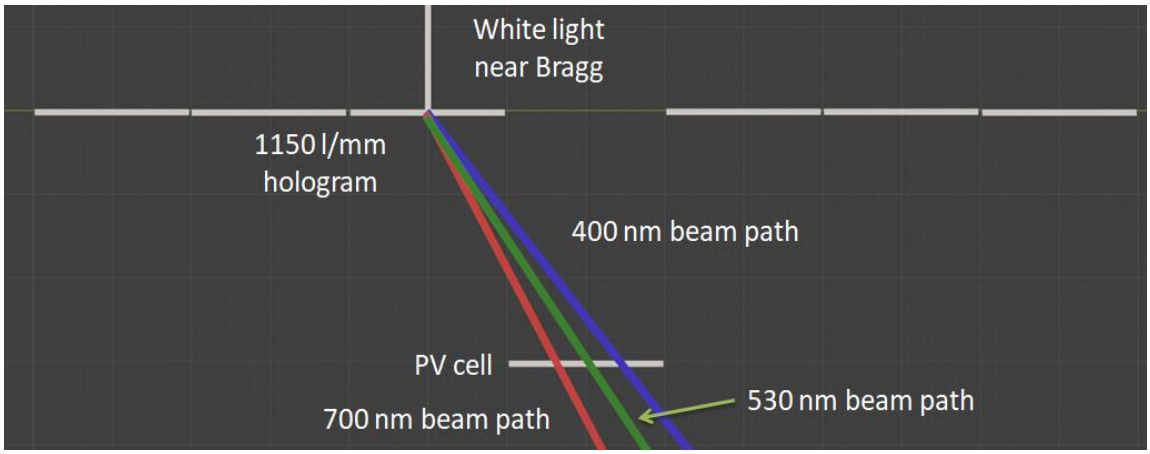

Figure 7-10: Chromatic dispersion from 1150 l/mm grating on PV cell in concentration device.

This effect becomes more exaggerated the closer a holographic cell gets to the PV cell, as shown in the figure above.

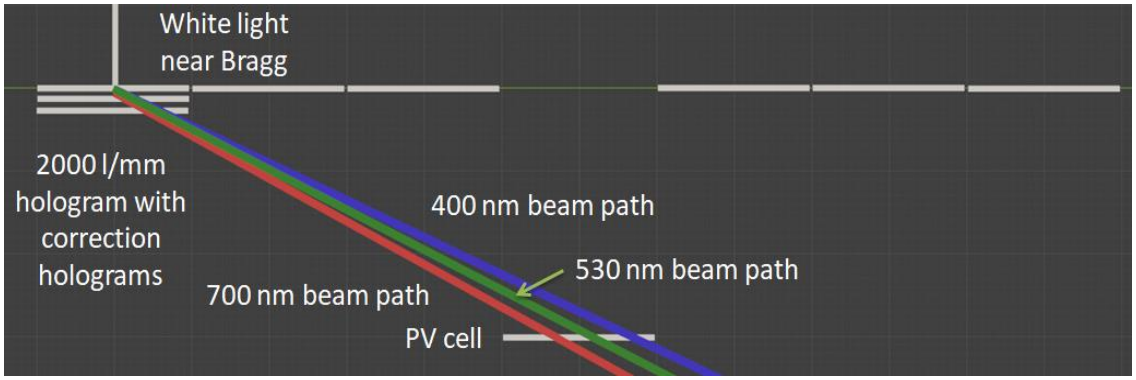

Figure 7-11: 2000 l/mm hologram with correction holograms in device.

Holograms closer to the PV cell do not need correction for their chromatic dispersion, this means only the larger spatial frequency cells on the outside of the device need correction. This is advantagous for one, because fewer holograms need correction. But importantly the holograms that do need correction have the wideest angular spread, meaning the correction holograms themselves will need thicknesses less than 125 μm as calculated previously. This eliminates the problem with scatter and also means the

correction devices will have relatively low angular selectivity due to their lower thicknesses.

7.7 Conclusion

There are some limitations associated with this kind of chromatic dispersion correction using holograms; namely the fact that the correction holograms are likely to be thicker than the hologram they are correcting if they are to be in the volume regime. This means there will be a noticable increase to the angular selectivity. This kind of device would be best suited to a system with solar tracking.

This device design makes use of holograms with a wide range of thicknesses and RIM values and could benefit from the unique qualities of a combination of materials discussed previosly in chapter 3 [3-15]. A device with this design has the potential to diffract close to 100% of light at wavelengths relevant to the absorpsion of a solar cell, making it as effective as a tradidional lens with none of the bulk or weight if employed correctly.

7.8 References

[1] Darbe, Sunita, et al. “Simulation and Partial Prototyping of an Eight-Junction Holographic Spectrum-Splitting Photovoltaic Module.” *Energy Science & Engineering*, vol. 7, no. 6, 2019, pp. 2572–2584., https://doi.org/10.1002/ese3.445.

[2] Chrysler, Benjamin D., and Raymond K. Kostuk. “Volume Hologram Replication System for Spectrum-Splitting Photovoltaic Applications.” *Applied Optics*, vol. 57, no. 30, 2018, p. 8887., https://doi.org/10.1364/ao.57.008887.

[3] David Jurbergs, Friedrich-Karl Bruder, Francois Deuber, Thomas Fäcke, Rainer Hagen, Dennis Hönel, Thomas Rölle, Marc-Stephan Weiser, Andy Volkov, "New

recording materials for the holographic industry," 2009 Proc. SPIE 7233, Practical Holography XXIII: Materials and Applications, 72330K

[4] Mikulchyk, Tatsiana, et al. "N-Isopropylacrylamide-Based Photopolymer for Holographic Recording of Thermosensitive Transmission and Reflection Gratings." *Applied Optics*, vol. 56, no. 22, 2017, p. 6348., https://doi.org/10.1364/ao.56.006348.

[5] Bianco, G., et al. "Photopolymer-Based Volume Holographic Optical Elements: Design and Possible Applications." *Journal of the European Optical Society: Rapid Publications*, vol. 10, 2015, https://doi.org/10.2971/jeos.2015.15057.

[6] Naydenova, I., et al. "Holographic recording in nanoparticle-doped photopolymer" *SPIE Proceedings*, 2006, https://doi.org/10.1117/12.676503.

[7] Martin S, Leclere P, Renotte Y, Toal V, Lion Y. "Characterization of an Acrylamide-Based Dry Photopolymer Holographic Recording Material." *Optical Engineering*, vol. 33, no. 12, 1994, p. 3942., https://doi.org/10.1117/12.186423.

[8] Zhao, Guoqiang, et al. "The Effect of Three Electron Donors on the Initiator System Efficiency of Photopolymer Film Photosensitized by Methylene Blue." *Materials & Design*, vol. 120, 2017, pp. 186–192., https://doi.org/10.1016/j.matdes.2017.01.093.

[9] Ortuño, M., et al. "Pyrromethene Dye and Non-Redox Initiator System in a Hydrophilic Binder Photopolymer." *Optical Materials*, vol. 30, no. 2, 2007, pp. 227–230., https://doi.org/10.1016/j.optmat.2006.10.029.

[10] Bruder, Friedrich-Karl, et al. "The Chemistry and Physics of Bayfol® HX Film Holographic Photopolymer." *Polymers*, vol. 9, no. 12, 2017, p. 472., https://doi.org/10.3390/polym9100472.

[11] Galli, Paola, et al. “Cyclic Allylic Sulfide Based Photopolymer for Holographic Recording Showing High Refractive Index Modulation.” *Journal of Polymer Science*, vol. 59, no. 13, 2021, pp. 1399–1413., https://doi.org/10.1002/pol.20210192.

[12] Carretero, L., et al. “Acrylamide-N,n'-Methylenebisacrylamide Silica Glass Holographic Recording Material.” *Optics Express*, vol. 12, no. 8, 2004, p. 1780., https://doi.org/10.1364/opex.12.001780.

[13] Schnoes, Melinda G., et al. “Photopolymer-Filled Nanoporous Glass as a Dimensionally Stable Holographic Recording Medium.” *Optics Letters*, vol. 24, no. 10, 1999, p. 658., https://doi.org/10.1364/ol.24.000658.

[14] Mikulchyk, Tatsiana, et al. “Synthesis of Fast Curing, Water-Resistant and Photopolymerisable Glass for Recording of Holographic Structures by One- and Two-Photon Lithography.” *Advanced Optical Materials*, vol. 10, no. 6, 2022, p. 2102089., https://doi.org/10.1002/adom.202102089.

[15] Mikulchyk, Tatsiana, et al. “Characterisation of Holographic Recording in Environmentally Stable Photopolymerisable Glass.” *Applied Sciences*, vol. 12, no. 12, 2022, p. 5969., https://doi.org/10.3390/app12125969.

8 Conclusions:

Several holographic recording materials have been characterised and modified for improvement in the context of solar concentration. Modelling of diffraction gratings has enabled the design of optimised holographic lenses and concentrating devices. The identification of relevant material improvements for solar concentration was identified through novel modelling. Physical and chemical changes to several holographic recording materials were made with the goal of improving the most important qualities identified by the modelling, namely RIM. A summary of the achievements and novelty of this research follows:

Modelling:

Modelling of HOEs has shown that in order to decrease angular selectivity while staying in the volume regime it is best to tend towards low thickness high spatial frequency gratings that require high RIM to achieve 100 % diffraction efficiency. Previously it was thought that low spatial frequency gratings provide better angular operational range. The conclusions from the in-depth analysis of the properties of volume holographic gratings provide a novel approach to the design of holographic solar concentrating devices. It highlights the limitations and potential of holographic concentration devices and offers possible solutions to the challenges. This novel method of modelling the qualities of HOEs on the edge of the volume regime at Rho = 10 has shown that the most effective lenses require high RIM, and tending toward high RIM will increase the effective dynamic range and concentration factor.

Acrylamide based photopolymer:

The RIM of an acrylamide based photopolymer was increased by 45 % and the grating formation rate was increased by a factor of 4.3 by altering the concentration of the

acrylamide monomer and crosslinker, a novel achievement in this material. Furthermore, a change of initiator from TEA to MDEA, studied for the first time in this work, significantly increased the rate of grating formation in thicker layers by a factor of 2.3. The increase in RIM of this photopolymer offers advantages to many holographic devices that require larger diffraction efficiencies in thinner layers. Furthermore. the improvements to the recording time have significant impact on the feasibility of the material to be used in mass production of holograms as reduced recording times can lead to increased output.

Sol-gel material:

The chemical composition of a photosensitive sol-gel material was altered with the aim of improving RIM and its possible application in solar concentrators was considered and studied for the first time. Multiplying the amount of zirconium in the sol gel by a factor of 3 improved the RIM by 36% from a value of $1.4 \times 10^{-3} \pm 1 \times 10^{-4}$ to $1.9 \times 10^{-3} \pm 1 \times 10^{-4}$. However, it was found out that a more effective thermal post processing technique improved RIM further to a value of $3.3 \times 10^{-3} \pm 4 \times 10^{-4}$. The employment of this post processing technique enhanced the RIM of the material to the highest achieved in a single grating recorded in this sol-gel material. One of the major advantages of the sol-gel material is in its robust nature. This physical stability enables it to be employed in environments where other photosensitive materials may be weathered, or react to changes to the environment such as humidity. Improving the RIM of this material enables higher diffraction efficiency, thinner devices to be utilised in environments where physical stability is important.

CAS photopolymer:

A cyclic allylic sulphide based photopolymer was characterised in low thickness layers at different spatial frequencies and holographic lenses optimised for low angular selectivity were recorded for the first time. The results from the spatial frequency study informed the design of the lens and particularly the spatial frequency range within which the lens operates in volume regime. These lenses were tested in a solar simulator and were compared to lenses with the same diffraction efficiency but recorded in thicker layers , thus having higher angular selectivity. The lower angular selectivity lenses were able to couple more light and performed better than the high selectivity lenses when studied with a solar simulator as a light source. This shows experimentally that the modelling of thinner less angularly selective devices has tangible benefits in practical holographic solar concentrating environments. It also highlights some of the challenges that holographic solar concentration faces such as chromatic dispersion.

Chromatic dispersion correction:

The groundwork for a chromatic dispersion correction device was laid out. Potential uses in a solar concentrating device were discussed along with the limitations of the technology based on practical experimental results and theoretical limits from modelling. A device design was illustrated and modelled as one possible example solution to the chromatic dispersion problem; without doubt there are a multitude of engineering solutions that could tackle these problems in the future.

8.1 Conclusions:

Improving the RIM of materials to maintain high diffraction efficiency with low angular selectivity has shown to be valuable in holographic solar concentrators. Less solar

tracking and more disperse light coupling reduce solar tracking complexity and increase device efficiency. RIM was improved significantly in both photopolymer and sol-gel materials; RIM was identified as an important factor in the modelling and so the experimental improvement of RIM in these materials brings them closer to practical use as an effective holographic solar concentrator. Developed to its conclusion, holographic concentrators could play a real role in microsatellite solar concentration. This work serves as a significant stepping stone towards that goal.

8.2 Future work:

Experimentally realising the device described in the previous section along with the encompassing material challenges could lay the groundwork for real holographic concentrators being tested and implimented on microsatellites. Maintaining a physically and chemically robust holographic recording material capable of thin layers and a high RIM would be the ultimate achievement for holographic solar concentration.

8.3 Dissemination:

Journal:

Rogers, B.; Martin, S.; Naydenova, I. Study of the Effect of Methyldiethanolamine Initiator on the Recording Properties of Acrylamide Based Photopolymer. *Polymers* 2020, *12*, 734

Rogers, B.; Mikulchyk, T.; Oubaha, M.; Cody, D.; Martin, S.; Naydenova, I. Improving the Holographic Recording Characteristics of a Water-Resistant Photosensitive Sol–Gel for Use in Volume Holographic Optical Elements. *Photonics* 2022, *9*, 636. https://doi.org/10.3390/photonics9090636

Keshri, S.; Rogers, B.; Murphy, K.; Reynolds, K.; Naydenova, I.; Martin, S. Development and Testing of a Dual-Wavelength Sensitive Photopolymer Layer for

Applications in Stacking of Hoe Lenses. *Applied Sciences*, vol. 11, no. 12, 2021, p. 5564., https://doi.org/10.3390/app11125564.

Mikulchyk, T.; Stoeva, P.; Kaworek, A.; Ouabha, M.; Rogers, B.; Martin, S.; Naydenova, I.; Characterisation of Holographic Recording in Environmentally Stable Photopolymerisable Glass. *Applied Sciences*, vol. 12, no. 12, 2022, p. 5969., https://doi.org/10.3390/app12125969.

Oral Presentations:

PIERS Rome 2019 Development of Holographic Solar Concentrator in Photopolymer with High Dynamic Range and Improved Photosensitivity

SPIE Photonics West San Diego 2020 Comparison of Sol-Gel and Photopolymer for use as a Recording Material for Holographic Lenses

Photonics Ireland 2021 Characterisation of Photosensitive Sol-gel Material for Optimised High Refractive Index Modulation in Thin Layers for the Development of Holographic Solar Concentrators

SPIE Strasbourg 2022 Development of Photosensitive Sol-gel Material for High Refractive Index Modulation using Thermal Treatment during Post Exposure Diffraction Efficiency Growth Process

Poster Presentations:

DIT 2019 Development of Holographic Recording Material for Fabrication of Solar Concentrators for Micro-Satellites

Spie Optics + Photonics 2019 San Diego Development of Photopolymer Material with Improved Dynamic Range and Sensitivity.

Conference:

Brian Rogers, Izabela Naydenova, Suzanne Martin, "Development of photopolymer material with improved dynamic range and sensitivity," Proc. SPIE 11081, Active Photonic Platforms XI, 110812G (5 September 2019); doi: 10.1117/12.2528715

8.3 Supplemental error calculation:

Table 8-1 and 8-2 error calculations:

Slant in air error was calculated using:

$$\Delta\theta = [(\Delta\theta_1)^2 + (\Delta\theta_2)^2]^{\frac{1}{2}}$$

Where $\Delta\theta_1$ and $\Delta\theta_2$ are the errors on the measured Bragg angles.

The spatial frequency error was calculated by taking the value for $\Delta\theta$ and inserting it into equation 2.2 to convert the angle error to a spatial frequency error. This overestimates the error; however, the value is small enough for this to not make an impact on the overall findings.

The RIM and thickness errors were calculated by simulations of the range of experimental curves possible based on the instrumental error of the angle and diffraction efficiency measurements.

All other errors were calculated based on the standard error from multiple samples.

RIM and Spatial frequency calculation:

RIM and spatial frequency were calculated in all occasions by matching the experimental curve to a theoretically modelled curve using equations 2.2 – 2.7.